ANALYSIS OF THE IMPACT OF INTEGRATING DISTRIBUTED ENERGY RESOURCES ON DISTRIBUTION SYSTEM RELIABILITY

REBEKA PASSOS GOMES

DISSERTAÇÃO DE MESTRADO
EM ENGENHARIA ELÉTRICA

DEPARTAMENTO DE ENGENHARIA ELÉTRICA

FACULDADE DE TECNOLOGIA

UNIVERSIDADE DE BRASÍLIA

Universidade de Brasília
Faculdade de Tecnologia
Departamento de Engenharia Elétrica

Analysis of the Impact of Integrating Distributed Energy Resources on Distribution System Reliability

Rebeka Passos Gomes

DISSERTAÇÃO DE MESTRADO SUBMETIDA AO PROGRAMA DE PÓS-GRADUAÇÃO EM ENGENHARIA ELÉTRICA DA UNIVERSIDADE DE BRASÍLIA COMO PARTE DOS REQUISITOS NECESSÁRIOS PARA A OBTENÇÃO DO GRAU DE MESTRE.

APROVADA POR:

Prof. Anésio de Leles Ferreira Filho, Ph.D, FT/UnB
(Orientador)

Prof. Elder Geraldo Domingues, Ph.D, IFG
(Coorientador)

Prof. Erika Pequeno dos Santos, Ph.D, INESC P&D Brazil
(Examinador externo)

Prof. Gabriel Santos Bolacell, Ph.D, INESC P&D Brazil
(Examinador externo)

Brasília/DF, novembro de 2024.

FICHA CATALOGRÁFICA

PASSOS, REBEKA

Analysis of the Impact of Integrating Distributed Energy Resources on Distribution System Reliability. [Brasília/DF] 2024.

xvii, 142p., 210 x 297 mm (ENE/FT/UnB, Mestre, Dissertação de Mestrado, 2024).

Universidade de Brasília, Faculdade de Tecnologia, Departamento de Engenharia Elétrica.

Departamento de Engenharia Elétrica

1. Battery storage
2. Distribution network
3. Islanding operation
4. Microgrid
5. Monte Carlo simulation
6. Photovoltaic generation
7. Reliability assessment

I. ENE/FT/UnB   II. Título (série)

REFERÊNCIA BIBLIOGRÁFICA

PASSOS, REBEKA (2024). Analysis of the Impact of Integrating Distributed Energy Resources on Distribution System Reliability. Dissertação de Mestrado, Publicação PPGENE.DM-823/25, Departamento de Engenharia Elétrica, Universidade de Brasília, Brasília, DF, 142p.

CESSÃO DE DIREITOS

Rebeka Passos

Universidade de Brasília (UnB)

Campus Darcy Ribeiro

Faculdade de Tecnologia - FT

Departamento de Engenharia Elétrica(ENE)

Brasília - DF CEP 70919-970

To my beloved husband, Davi, for being my soul and life partner.

AGRADECIMENTOS

A Deus, a quem dedico tudo o que sou e tenho. Ao longo dessa jornada, experimentei mais uma vez Seu cuidado e amor em minha vida.

Ao meu marido, por todo o apoio, incentivo e compreensão em cada passo desta jornada. Agradeço por não me deixar desistir, e por ser meu acalento e refúgio nos momentos de ansiedade e preocupação. Você é minha inspiração diária. Obrigada por tornar essa trajetória mais leve.

Aos meus pais, Pedro e Delma, que me ensinaram a lutar pelos meus sonhos e sempre me deram o amor e o apoio de que precisei. Estou aqui graças ao amor e à confiança que recebi desde a infância. Jamais esquecerei dos beijinhos na cabeça e das orações da minha mãe antes de enfrentar as madrugadas dedicadas a este trabalho, nem das mensagens de encorajamento do meu pai.

Às minhas irmãs e melhores amigas, Sarah e Fatinha, pela paciência e compreensão. A chegada do meu sobrinho querido, João Pedro, ao longo dessa jornada, trouxe ainda mais alegria para nossa família.

Ao meu orientador, Professor Anésio de Leles Ferreira Filho, e ao meu coorientador, Professor Elder Geraldo Domingues, por me guiarem pelos melhores caminhos e por todo o apoio, conselhos, compreensão e amizade ao longo desta jornada. Mesmo com as dificuldades inerentes ao tema, os senhores mantiveram sempre a confiança em meu trabalho, pelo que lhes sou profundamente grata.

Ao Professor Pedro César Cordeiro Vieira, que gentilmente dedicou seu escasso tempo para contribuir significativamente com esta dissertação. Sou imensamente grata pelo apoio, orientação e amizade ao longo desta trajetória. Este trabalho não seria possível sem sua colaboração.

À minha querida equipe da Head Energia, minhas amigas Andressa Farias, Fabiola Sena e Nathália Nóbrega, pelo apoio e incentivo essenciais para a concretização desta trajetória. Eu sequer acreditaria que poderia sonhar em viver essa experiência se não fosse o "empurrãozinho"de vocês.

À minha família e amigos, que zelaram por mim durante todo o percurso: meus tios, em especial Tia Enedelma e Tio Adelmo; meus sogros, Cátia e Wedes; e meus avós, Joaquim, Concita e Jovina.

Aos alunos do REILab da UnB, em especial Breno Menezes, pelo suporte.

Por fim, minha gratidão a todos que, de alguma forma, contribuíram para a realização deste projeto.

ABSTRACT

The reliability evaluation of microgrids presents greater challenges than traditional power systems, due to their more complex structure and operating modes. In this sense, this study presents a methodology to identify the technical impacts that microgrids composed of photovoltaic distributed generation and Battery Energy Storage Systems can cause in the evaluation of the reliability of distribution systems. The study utilized probabilistic simulations employing the Monte Carlo method. The algorithm was initially validated using a system with an established analytical solution. Subsequently, scenarios with different levels of photovoltaic generation (PV) and battery energy storage system (BESS) were simulated in a real Brazilian distribution network to evaluate their effects and identify those that bring the greatest benefits to system reliability. It was implemented a time-varying islanding operation, where the power supply areas of the islanding operation are dynamically changed according to the loads and the distributed energy resources (DERs) output. The code validation results revealed a maximum error of -4.10%, demonstrating the code's robustness and reliability. The results of applying the method in the case study show that, in scenarios with only the insertion of a PV system, the benefits in reliability, when varying the penetration level, are minimal for the microgrids and the complete feeder. Alternatively, changing the penetration of BESS influences the battery performance by ensuring a high and stable state of charge (SoC), which is crucial for minimizing instabilities and enhancing the distribution system's reliability in the context of PV integration. However, for penetrations exceeding 50%, there is minimal further variation in stability due to the stabilization of the State of SoC. The indices that assess the microgrid performance during time-varying islanding operations indicate an enhancement in the utilization of loads and available DER during failure scenarios, with negligible additional benefits of BESS at elevated penetration levels.

Keywords: Battery storage; Distribution network; Islanding operation; Microgrid; Monte Carlo simulation; Photovoltaic generation; Reliability assessment.

RESUMO

Título: Análise do Impacto da Integração de Recursos Energéticos Distribuídos na Confiabilidade de Sistemas de Distribuição

A avaliação da confiabilidade de microrredes apresenta desafios maiores do que os sistemas de energia tradicionais, devido à sua estrutura e modos operacionais mais complexos. Nesse sentido, este estudo apresenta uma metodologia para identificar os impactos técnicos que microrredes compostas por geração distribuída fotovoltaica (PV) e Sistema de Armazenamento de Energia em Baterias (BESS) podem provocar na avaliação da confiabilidade de sistemas de distribuição. O estudo utilizou simulações probabilísticas empregando o método de Monte Carlo. O algoritmo foi inicialmente validado usando um sistema com uma solução analítica estabelecida. Posteriormente, cenários com diferentes níveis de geração PV e BESS foram simulados em uma rede de distribuição real brasileira para avaliar seus efeitos e identificar aqueles que trazem os maiores benefícios para a confiabilidade do sistema. Foi implementada uma operação de ilhamento variável no tempo, onde as áreas de fornecimento de energia da operação de ilhamento são alteradas dinamicamente de acordo com as cargas e a saída dos Recursos Energéticos Distribuídos (RED). Os resultados da validação do código revelaram um erro máximo de -4,10%, demonstrando a robustez e a confiabilidade dos resultados. Os resultados da aplicação do método no estudo de caso mostram que, em cenários com apenas a inserção do sistema PV, os benefícios em confiabilidade, ao variar o nível de penetração, são mínimos para as microrredes e o alimentador completo. Alternativamente, mudar a penetração de BESS influencia o desempenho da bateria ao garantir um estado de carga (SoC) alto e estável, o que é crucial para minimizar instabilidades e aumentar a confiabilidade do sistema de distribuição no contexto da integração PV. No entanto, para penetrações que excedem 50%, há uma variação mínima adicional na estabilidade devido à estabilização do estado do SoC. Os índices que avaliam o desempenho da microrrede durante as operações de ilhamento com variação temporal indicam um aprimoramento na utilização de cargas e RED disponível durante cenários de falha, com benefícios adicionais insignificantes do BESS em níveis elevados de penetração.

Palavras-chave: Armazenamento de bateria; Avaliação de confiabilidade; Geração fotovoltaica; Microrrede; Operação de ilhamento; Simulação de Monte Carlo; Sistemas de distribuição.

TABLE OF CONTENTS

Table of contents i

List of figures v

List of tables vii

List of symbols x

Glossary xi

Chapter 1 – Introduction 1

1.1 Overview . . . 1
1.2 State of the Art . . . 4
1.3 Objectives . . . 8
1.4 Contributions . . . 8
1.5 Dissertation Organization . . . 9

Chapter 2 – Theoretical Background 10

2.1 Initial considerations . . . 10
2.2 Distributed Energy Resources (DER) . . . 10
2.2.1 Solar Photovoltaics (PV) modelling . . . 13
2.2.2 Battery Energy Storage Systems (BESS) modelling . . . 13
2.3 Microgrids . . . 14
2.3.1 Community Microgrids . . . 15
2.4 Reliability in Power Systems . . . 16
2.4.1 Impacts of Modern Power Systems . . . 17
2.5 Distribution System Adequacy Assessment . . . 19
2.5.1 Exponentially Distributed Lifetime . . . 19
2.5.2 Monte Carlo Simulation . . . 20
2.5.2.1 Sequential Monte Carlo Simulation (SMCS) . . . 20
2.5.3 Reliability indexes . . . 21

2.5.3.1 Sustained interruption indexes 22
2.5.3.2 Load and energy based indexes 23
2.6 Final considerations 23

Chapter 3 – Methodology 25

3.1 Initial considerations 25
3.2 Overview 25
3.3 Microgrid Architecture 27
3.3.1 Selection of Microgrid Operational Strategies 30
3.3.2 Islanding Operation 33
3.3.2.1 Time-varying islanding operation 34
3.3.2.2 Microgrid Formation Indices 36
3.4 Distributed Energy Resources Models 37
3.4.1 Modeling of PV system 37
3.4.1.1 PV Hourly Power 38
3.4.2 Modeling of battery energy storage (BES) 39
3.4.2.1 BESS Hourly Power 40
3.4.2.2 Power Restrictions of the BESS 40
3.4.3 Penetration levels 41
3.5 Technical Impacts 42
3.5.1 Monte Carlo simulation 44
3.6 Algorithm description 44
3.6.1 State selection procedure 48
3.6.2 State assessment procedure 52
3.6.2.1 Upstream Fault Protection Procedure 55
3.6.2.2 Downstream Fault Protection for Island Operation Procedure . 57
3.6.2.3 Topology Processor Procedure 57
3.6.3 Time-varying islanding procedure 59
3.6.3.1 BES System Charge and Discharge Operation 63
3.7 Final considerations 67

Chapter 4 – Materials and procedures 68

4.1 Initial considerations 68
4.2 Computational Environment 68
4.3 Validation of the developed code 69
4.3.1 Procedures for Code Validation 69
4.3.2 Data employed in validation 69

4.3.3 Presentation of validation results . . . 70
4.4 Presentation and assessment of the case study results . . . 71
4.4.1 Case Study Description . . . 71
4.4.2 Procedures for outcome generation . . . 71
4.4.3 Data employed to produce outcomes . . . 72
4.4.4 Graphical and numerical representations for displaying results . . . 74
4.5 Load Modeling . . . 74
4.6 Solar irradiation and temperature . . . 76
4.7 Reliability parameters . . . 77
4.8 Adopted Hypotheses . . . 77

Chapter 5 – Results and Discussion 79

5.1 Initial considerations . . . 79
5.2 Application to the Test System . . . 79
5.3 Case Study: brazilian distribution network . . . 80
5.4 Simulation Conditions . . . 81
5.5 Assessment of Technical Impacts . . . 82
5.5.1 Distribution Adequacy Indices . . . 82
5.5.1.1 System Average Interruption Frequency Index (SAIFI) . . . 82
5.5.1.2 System Average Interruption Duration Index (SAIDI) . . . 86
5.5.1.3 Customer Average Interruption Duration Index (CAIDI) . . . 87
5.5.1.4 Energy Not Supplied (ENS) . . . 90
5.5.2 Microgrid Formation Indices . . . 92

Chapter 6 – Conclusions 97

6.1 Recommendations for Future Work . . . 99
6.2 Published works . . . 100

References 101

Apêndice A – Data of the Brazilian distribution network 106

Apêndice B – Simulation Parameters 109

Apêndice C – Example of application of the State assessment procedure 110

Apêndice D – Simulation results tables 113

D.1 SAIFI 113
D.2 SAIDI 115
D.3 CAIDI 117
D.4 ENS 119

Apêndice E – Simulation Times 121

LIST OF FIGURES

1.1 Illustration of employed approaches. 4

3.1 Simplified diagram of the methodology used. 26

3.2 Schematic structure of microgrid. 28

3.3 Overview of microgrid topology. 29

3.4 Operational strategy for microgrids. 32

3.5 Illustration of the time-varying islanding operation. 35

3.6 Possible microgrid arrangements during time-varying islanding operation. 36

3.7 General reliability assessment procedure using SMCS. 47

3.8 Subprocess: State selection procedure. 51

3.9 Subprocess: State assessment procedure. 54

3.10 Subprocess: activation of the protection further upstream of the fault. 56

3.11 Subprocess: activation of the protection further downstream of the fault for island operation. 58

3.12 Subprocess: topology processor. 60

3.13 Subprocess: Time-Variable Islanding Operation Procedure. 61

3.14 Subprocess: charging the BES System. 65

3.15 Subprocess: discharging the BES System. 66

4.1 A traditional radial distribution network. 70

4.2 Brazilian distribution network configuration used in this study. 73

4.3 Daily load curves with average highlighted. 75

4.4 Daily irradiance nominal global incident for the City region, with average highlighted. . . . 76

5.1 Impact of BESS and PV penetration level on the SAIFI index. . . . 83

5.2 Distribution of state of charge (SoC) in percentage for three scenarios: PV-100% | BESS-50%, PV-100% | BESS-75%, and PV-100% | BESS-100%. . . . 85

5.3 Impact of BESS and PV penetration level on the SAIDI index. . . . 86

5.4 Impact of BESS and PV penetration level on the CAIDI index. . . . 88

5.5 Histogram with Kernel Density Estimation (KDE) for the variable duration in the failure state for the LP 68, accounting for scenarios with 100% photovoltaic penetration and varying levels of battery energy storage penetration. . . . 90

5.6 Impact of BESS and PV penetration level on the ENS index. . . . 91

5.7 Impact of BESS and PV penetration level on the Microgrid formation indices. . 94

5.8 Impact of BESS and PV penetration level on the Microgrid operation time and interrupted load. . . . 96

C.1 Illustrative example system utilized to demonstrate the application of the state assessment procedure. . . . 110

C.2 Application example: Procedure of activation of the protection further upstream of the fault. . . . 111

C.3 Application example: Procedure of activation of the protection further downstream of the fault for island operation. . . . 111

C.4 Application example: Procedure of the topology processor. . . . 112

LIST OF TABLES

3.1 Modeled uncertainty in the proposed assessment methodology. 43

4.1 Reliability parameters for the system of Figure 4.1. 70

4.2 Customers and load connected to the system of Figure 4.1. 70

4.3 Data from the analysed brazilian distribution network. 72

4.4 Reliability parameters. 77

5.1 Test System load point indices compared to (BILLINTON; ALLAN, 1996) results. 79

5.2 Comparison of the system indices in the Test System with (BILLINTON; ALLAN, 1996) results. 80

5.3 Information for the selected microgrids. 80

5.4 The total PV power and storage capacity of BES in each microgrid, considering the Penetration Levels Grouping, for all penetration levels. 81

5.5 Case studies performed. 81

A.1 Section lengths of the Brazilian distribution network. 107

A.2 Load data of the Brazilian distribution network. 108

B.1 Simulation Parameters. 109

D.1 Impact of BESS and PV penetration on SAIFI (oc./year) indice for the Microgrid 1 from the implementation of Microgrid 1. 113

D.2 Impact of BESS and PV penetration on SAIFI (oc./year) indice for the complete feeder from the implementation of Microgrid 1. 113

D.3 Impact of BESS and PV penetration on SAIFI (oc./year) indice for the Microgrid 2 from the implementation of Microgrid 2. 114

D.4 Impact of BESS and PV penetration on SAIFI (oc./year) indice for the complete feeder from the implementation of Microgrid 2. 114

D.5 Impact of BESS and PV penetration on SAIDI (h/year) indice for the Microgrid 1 from the implementation of Microgrid 1. 115

D.6 Impact of BESS and PV penetration on SAIDI (h/year) indice for the complete feeder from the implementation of Microgrid 1. 115

D.7 Impact of BESS and PV penetration on SAIDI (h/year) indice for the Microgrid 2 from the implementation of Microgrid 2. 115

D.8 Impact of BESS and PV penetration on SAIDI (h/year) indice for the complete feeder from the implementation of Microgrid 2. 116

D.9 Impact of BESS and PV penetration on CAIDI (h/oc.) indice for the Microgrid 1 from the implementation of Microgrid 1. 117

D.10 Impact of BESS and PV penetration on CAIDI (h/oc.) indice for the complete feeder from the implementation of Microgrid 1. 117

D.11 Impact of BESS and PV penetration on CAIDI (h/oc.) indice for the Microgrid 2 from the implementation of Microgrid 2. 117

D.12 Impact of BESS and PV penetration on CAIDI (h/oc.) indice for the complete feeder from the implementation of Microgrid 2. 118

D.13 Impact of BESS and PV penetration on ENS (MWh/year) indice for the Microgrid 1 from the implementation of Microgrid 1. 119

D.14 Impact of BESS and PV penetration on ENS (MWh/year) indice for the complete feeder from the implementation of Microgrid 1. 119

D.15 Impact of BESS and PV penetration on ENS (MWh/year) indice for the Microgrid 2 from the implementation of Microgrid 2. 119

D.16 Impact of BESS and PV penetration on ENS (MWh/year) indice for the complete feeder from the implementation of Microgrid 2. 120

E.1 Simulation time (in minutes) for each case study of Microgrid 1. 121

E.2 Simulation time (in minutes) for each case study of Microgrid 2. 122

LIST OF SYMBOLS

ASAI	Average Service Availability Index	[%]
CAIDI	Customer Average Interruption Duration Index	[h/oc.]
ENS	Energy Not Supplied	[MWh/yr]
MGF_{Comp}	Complete microgrid formation index	[%]
$MGF_{DERInsuf}$	No microgrid formation due to insufficient DER index	[%]
MGF_{fail}	No microgrid formation due to failure index	[%]
MGF_{Inc}	Incomplete microgrid formation index	[%]
r	Average load point outage duration index	[h]
SAIDI	System Average Interruption Duration Index	[h/yr]
SAIFI	System Average Interruption Frequency Index	[oc./yr]
U	Average annual load point outage or unavailability time index	[h/yr]
λ	Average load point failure rate index	[f/yr]

GLOSSARY

BESS	Battery energy storage systems
DERs	Distributed energy resources
MTTF	Mean time to failure
MTTR	Mean time to repair
PCC	Point of Common coupling
PV	Solar photovoltaic
SMCS	Sequential Monte Carlo Simulation

CHAPTER 1

INTRODUCTION

1.1 OVERVIEW

Increasing global awareness of rising greenhouse effect gases (GHE) emissions has led several countries to set ambitious objectives for incorporating renewable energy into their electricity grids and to reduce dependence on centralized power grids (AHMAD *et al.*, 2023; ELIZONDO; POUDINEH, 2023). This implies transformations in electricity distribution networks around the world, transitioning into a more distributed future, motivated by an increase of new distributed energy resources (DERs), including microgrids (ZINAMAN *et al.*, 2022; UDDIN *et al.*, 2023).

A microgrid is a group of interconnected loads and DERs that functions as a unified controllable and independent power system in relation to the grid. It can connect to and disconnect from the grid to operate in grid-connected or island mode (FUSHENG *et al.*, 2016). A microgrid powered by distributed renewable resources is called a renewable microgrid and is classified based on the renewable sources used. The solar microgrids are becoming more popular and deployed worldwide since they can be scaled up and used at any scale. Most systems include storage capacity to deal with the uncertain and intermittent production of solar photovoltaic (PV) generation (UDDIN *et al.*, 2023).

As an increasing number of policies facilitate self-consumption and the cost of DERs such as battery storage and distributed PV decreases quickly, microgrids are emerging as an economically viable alternative to the electricity grid to obtain cost-effective, resilient and cleaner energy (International Energy Agency, 2022). In 2023, global solar PV-distributed constituted nearly 40% of the total PV expansion (International Energy Agency (IEA), 2024). In Brazil, even though incentives are declining, distributed micro and mini solar photovoltaic generation reached 29,813 GWh and 26,366 MW of generation and installed power, respectively (Empresa de Pesquisa Energética (EPE), 2024). According to the International Energy Agency (IEA) Clean Energy Equipment Price Index, global average solar PV module and lithium-ion battery prices dropped by 30% and 14% in 2023 (International Energy Agency, 2024).

As severe natural disasters become more frequent due to climate change and increasing electrification, in conjunction with challenges of grid expansion and use of intermittent sources, such as high demands on transmission lines and risks of cascading blackouts, microgrids are recognized as flexible and scalable solution for: (i) enhance grid reliability and resilience, improving energy security for essential loads; and (ii) serve as a driver of decarbonization by serving as a central point for the aggregation of a larger number of DERs (ZINAMAN *et al.*, 2022; AHMAD *et al.*, 2023; UDDIN *et al.*, 2023). Although the current Brazilian legal and regulatory framework limits the viability of operating microgrids, they represent a significant technological innovation in the energy sector, providing alternatives to facilitate the energy transition (BAPTISTA, 2024).

The analyses conducted in the reliability of distribution systems until recent times were based on systems structured for a unidirectional power flow, where the energy, coming from a centralized generation, would initially be transmitted in high, and then in medium and low tensions to end consumers. Integrating renewable energy sources into the network presents some challenges for reliability analysis, especially because of the intermittent nature of renewable energy sources, which can intensify the system instability, particularly if alternative options like Energy Storage Systems (ESS) are improperly implemented (ISLAM *et al.*, 2024; AHMAD *et al.*, 2023).

Therefore, compared to traditional power systems, assessing the reliability of systems with microgrids is more complex, as it involves real-time operation and control modes of DERs to satisfy stability and additional requisites of the microgrid (REN *et al.*, 2020; AHMAD *et al.*, 2023). Despite the challenges arising from the integration of microgrids into distribution systems by allocating distributed generation and storage with islanded operation capacity, this represents a potential strategy for utilities to enhance grid flexibility under contingency conditions, thus improving reliability through an increased supply of electrical energy(TORRES *et al.*, 2024).

In this sense, it is understood that the developments related to the wide diffusion of DERs and the islanding process increase the complexity of the reliability analysis of distribution networks due to the addition of uncertainties about energy demand, which requires new methods of evaluating reliability from distribution systems.

This evaluation will provide information demonstrating the potential of microgrids to contribute to the stability of the electrical grid system and the quality of the continuity of the electrical energy supply. This facilitates the identification of potential challenges and limitations due to the complexity of the microgrid operation. In addition, it is important to consider the coordination of renewable sources, storage systems and load in this type of analysis to make rational use of the available resources.

This approach allows to identify the technical impacts and necessary adaptations in reliability studies derived from the insertion of DERs and microgrids. To contextualize the approaches employed in this study, Figure 1.1 summarizes the methodological options delineated in the theoretical framework, emphasizing the selection made in each category.

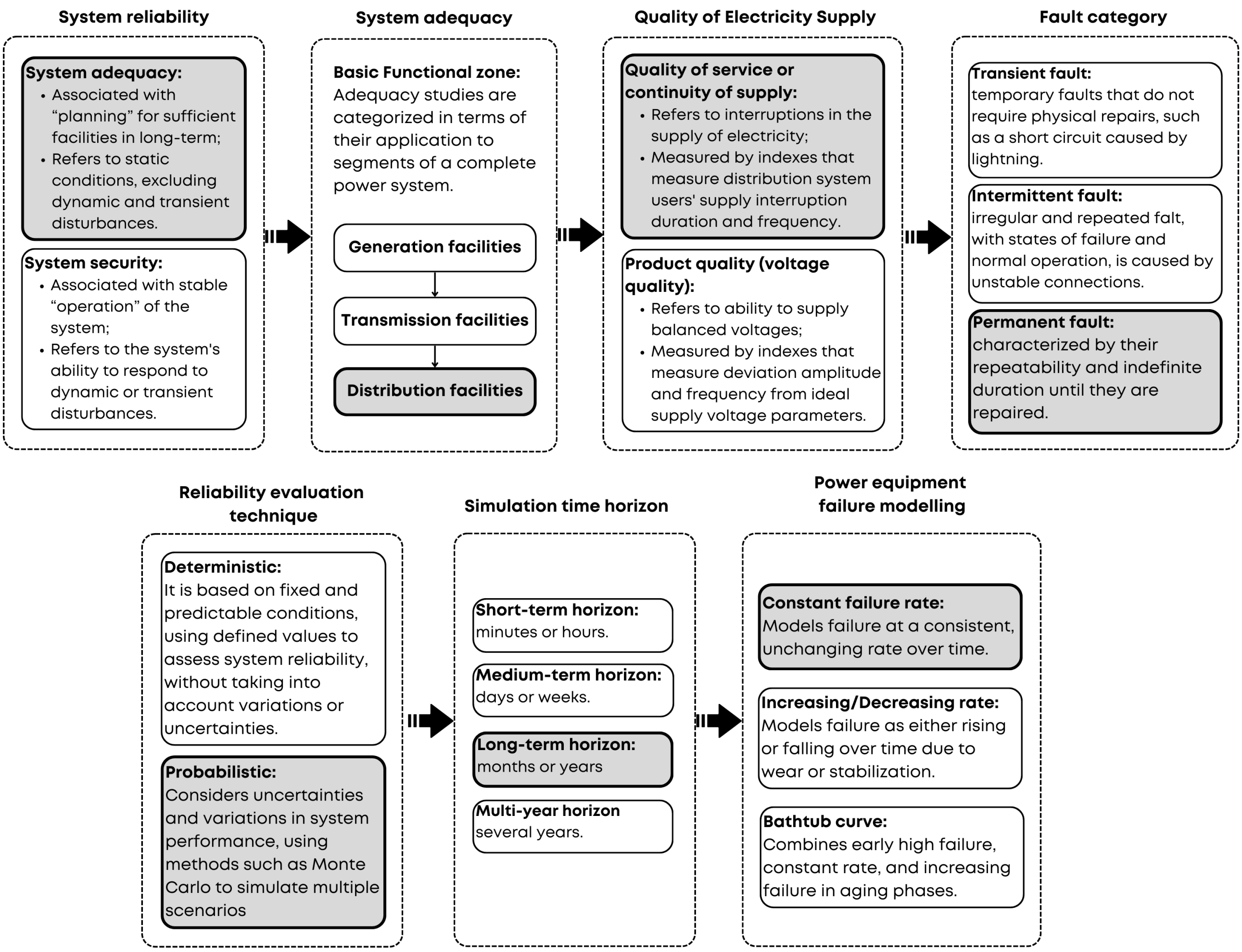

Figure 1.1: Illustration of employed approaches. Source: Own authorship.

Therefore, in the context of distribution system adequacy, this study focuses on service quality by analyzing permanent faults through a yearly probabilistic evaluation, considering equipment with constant failure rates.

1.2 STATE OF THE ART

Despite the scarcity of bibliographical references regarding the reliability assessment of distribution systems that contain microgrids, it is possible to find some works focused on the development of methodologies capable of incorporating the dynamism of some technologies covered by DER, such as Solar Photovoltaic Distributed Generation (PVDG), battery energy storage (BES) and electric vehicles (EVs). The main theoretical discussions are based on techniques for improving the reliability of distribution networks, such as ideal positioning of switches/circuit breakers, optimal allocation and sizing of DER, reconfiguration of distribution networks, and the relationship between reliability and economicity.

(ANAND *et al.*, 2022) proposes a methodology for reliability-oriented distribution system analysis considering PVDG, BES and EVs. The methodology comprises three main parts: (i) an EV charging station model based on DER; (ii) a reliability analysis model, introducing two new indices to assess the reliability and impact of renewable generation and energy storage on EV charging supply (Expected Electric Vehicles Grid Dependency - EEVGD - and Expected Unserved Electric Vehicle Load - EUEVL -); and (iii) an economic evaluation model. Finally, an optimization algorithm is employed to select the optimal resource sizes, considering the minimization of the cost associated with the charging station and the cost resulting from unreliability. The EV charging station model is robust, including submodels to estimate electric vehicle charging demand and photovoltaic energy production using long-term synthetic solar radiation data. Furthermore, the proposed model considers energy storage in batteries and defines the operational strategy of the electric vehicle charging station. However, it is worth emphasizing that the lack of reliability resulting from failures in components of the electrical system is not taken into account, with the justification that this could obscure the identification of the impacts of electric vehicles, renewable sources, and energy storage on reliability.

(ABDELSAMAD; LUBKEMAN, 2020) presents an economic and reliability analysis using sequential Monte Carlo simulation (SMCS). The proposed methodology is used for a power system consisting of a microgrid to serve a small commercial load. The fixed, operational and unreliability costs of each microgrid component are considered. For this, the MTTF and MTTR of the PVDG system, as well as the BES and diesel generator, are estimated to follow an exponential distribution. Furthermore, the article evaluates alternative scenarios for the penetration of renewable sources. The results indicate that targets for 100% renewable scenarios have exponentially high costs, without necessarily guaranteeing greater reliability for the system. However, it is worth noting that a detailed cost analysis is not provided and, as in (ANAND *et al.*, 2022), the article does not consider failures in other electrical system components.

In (SU *et al.*, 2019), a procedure to accurately assess the reliability of energy supply in distribution networks that have PVDG was developed considering: i) the aging period of conventional power equipment; ii) the failure and degradation of photovoltaic modules; and iii) the operation of time-variable islanding during main grid power outages. Furthermore, five new reliability indices have been added to reflect the characteristics of PV output power and increase sensitivity to reliability change during islanding operation: (i) Generation rate of DG (GRDG); (ii) Power interruption probability of DG (PIPDG); (iii) Power fluctuation of DG (PFDG); (iv) Average power supply time of island (APSTI); and (v) Average energy supplied from island (AESI). The evaluation procedure is applied in a case study using a real distribution network topology in China. This proves the improvement in reliability evaluation accuracy of the proposed procedure, in which the sensitivity of the new proposed reliability indices is much higher than conventional reliability indices. However, the reliability analysis carried out in this study does not have load priorities in the islanding operation and does not consider other DERs such as BES, EVs and charging structure, energy efficiency and demand-side management.

Based on the fact that usual indices such as loss of load expectation (LOLE) and expected energy not supplied (EENS) might not provide a thorough comprehension of microgrid reliability and resiliency, (GHOLAMI *et al.*, 2023) proposes three new reliability indices to offer additional details on performance of MG, among them are: (i) the Microgrid Resiliency Index (MRI), that gauges a MGs ability to recover from outages and disturbances; (ii) the Microgrid Renewable Energy Availability Index (MREAI), that signifies the percentage of total probable interruptions in the microgrid that can be attributed to failures in its Renewable Energy Sources (RESs); and (iii) the Microgrid Renewable Energy Energy Index (MREEI), that furnishes details about the ability of the microgrid to meet its energy demand during normal operation. The LOLE, EENS and the new proposed indices are calculated for different cases and applied to a microgrid with PVDG, wind turbine (WT), and BES components. The study considers the failure rate and repair time of the grid, PV, WT and BESS. The findings suggest that the proposed indices were able to capture the contribution of DER and the capability of the microgrid to bounce back from interruptions, highlighting the additional value of the new index for the reliability assessment. Moreover, the most favorable reliability and resiliency of the microgrid performance was accomplished when employing BES, which indicates that solely augmenting the output power of PV and WT sources might not prove to be an efficient approach for enhancing the resiliency and reliability of the MG.

In (XIAO *et al.*, 2022), a reliability assessment based on Monte Carlo simulation considering capacity factors is proposed to evaluate distribution networks composed of PVDG, BES and EVs. To achieve this, the authors consider the time to failure (TTF) and the time to repair (TTR) distributed exponentially. The results of the study indicate that the incorporation of renewable and distributed resources can improve the reliability of distribution systems, however the impact varies according to geographic location and the type of resources used. The presence of multiple DER and a time-varying islanding operation during main grid power outages is considered. Despite this, it is assumed that renewable and distributed resources are connected to the distribution system at the same point, although this may not be true in real-world scenarios.

(AGAJIE *et al.*, 2021) proposes an assessment of reliability, voltage profile improvement and voltage deviation reduction of voltage deviation in real electrical systems with DER units using Monte Carlo simulation (SMC). DER are allocated in varying locations and penetration levels. Additionally, the best position of DER is discussed based on comparing of reliability indices. The results demonstrate that all calculated indices are optimized when the DER are positioned at a significant distance from the main power point. Artificial intelligence techniques are suggested as future work to provide the ideal location of DER units and to improve system reliability.

Considering the context of diffusion of DER in distribution systems and the aforementioned works, it is possible to verify a tendency to use probabilistic methods to assess the reliability of distribution networks to i) allow a representation of systems that is increasingly closer to reality; ii) reduce, or even postpone, investments in distribution networks; and iii) analyze the impacts of the insertion of DER for distributors and consumers.

Although Monte Carlo simulation is not a novel concept and has been documented for over 50 years, its application in quantitative power system reliability assessment is favored over analytical model-based techniques, owing to advancements in high-speed digital computing and the acknowledgment that power systems and their components exhibit stochastic behavior.

In the relevant literature, no methodologies were identified that measure the impact on reliability indices of the transition to the variable island operation mode of microgrids. It is worth noting that most of the studies that were carried out evaluated the indices only from a systemic perspective, without taking into account the effect only on the loads that make up the microgrid. Furthermore, they do not employ an instructive approach to the methodology.

1.3 OBJECTIVES

Based on the increasing expansion of DER penetration, this work shows the importance of new methods for assessing the reliability of distribution systems. The objective of the study is to develop and apply a methodology for evaluating the reliability of distribution systems in the presence of PV generation and BES systems.

The specific objectives of this work are:

- Obtain a procedure for assessing the reliability of the distribution network with microgrids that allocate distributed generation and storage;
- Carry out a sensitivity analysis that takes into account the time-varying islanding operation, load priority and penetration levels of DER;
- Implement new microgrid formation indices to ensure appropriate sensitivity to changes in system reliability; and
- Apply the proposed modeling to a real system.

For the probabilistic analysis of the impact of these resources on customer-side reliability indices, the study adopts Sequential Monte Carlo Simulation (SMCS).

1.4 CONTRIBUTIONS

The main contributions are:

- Development of a stochastic method for reliability assessment considering the formation of MGs with many penetration levels;
- Proposal of four new reliability indices tailored specifically for microgrids; and

- The results achieved provide conclusions that facilitate: (i) decision-making in the planning areas of distributors; (ii) understanding impacts on the supply of electricity to consumers; and (iii) a guidance role in the pre-design stages and post-operation reliability impacts of microgrids.

1.5 DISSERTATION ORGANIZATION

The presentation of this thesis is organized as follows:

- The Theoretical Background is described in the chapter 2;
- The proposed method is described in Chapter 3;
- The materials to which the method is applied are described in Chapter 4;
- In Chapter 5, the results of applying the method are displayed and discussed; and
- Finally, conclusions and proposals for future work are presented in Chapter 6.

CHAPTER 2

THEORETICAL BACKGROUND

2.1 INITIAL CONSIDERATIONS

This chapter presents the necessary concepts for comprehending the study proposed in this work. Firstly the fundamental content concerning Distributed energy resources (DERs) is presented. Subsequently, the most pertinent concepts concerning microgrids are discussed. The discussion on the reliability of electrical systems is subsequently detailed, with a particular emphasis on distribution systems. Next, the concepts that are pertinent to reliability analysis are examined.

2.2 DISTRIBUTED ENERGY RESOURCES (DER)

A singular definition does not exist; however, DERs are typically understood as decentralized energy resources (both renewable and/or conventional resources) characterized by being small in scale, connected to the distribution grid, located close to customers and able to generate, store energy or manage its consumption, depending on the technology type. It comprises various technologies, including: solar photovoltaics (PV), battery energy storage systems (BESS), electric vehicles (EVs), demand response (DR), energy efficiency, wind generation, biomass-based generation, small-scale hydropower, reciprocating oil and diesel engines, combined heat and power (CHP), control systems of individual devices, and combinations of these resources aggregated within microgrids (NARANG *et al.*, 2022; IEA, 2022; ELIZONDO; POUDINEH, 2023).

That is, the concept of DERs includes an extensive range of technologies, independent of their location within the distribution grid (behind-the-meter or front-of-meter) and the type of fuel utilized (IEA, 2022). The definition for DERs from the The Energy Research Office - EPE in its Portuguese acronym - ((EPE), 2019), the The Energy Research Office (EPE in its

Portuguese acronym) of Brazil, includes DERs being located within the boundaries of a given distribution utility's area, focusing on the consumer side (behind-the-meter DER systems) but not excluding front-of-meter DERs.

Compared with front-of-meter DERs, behind-of-meter DERs present more obstacles for system operators in monitoring the energy system impacts of emerging resources. This difficulty comes from their generally small scale, little capacity to participate in energy markets without aggregation, and control by consumers who prioritize their own interests, which may not coincide with the needs of the grid. Despite standing at the base of the electricity supply chain, behind the meter DERs can provide advantages across multiple levels, extending from consumers to the transmission system (IEA, 2022).

The main objective of DERs is to fulfill all or part of customers' immediate electric and power needs. The system can utilize them to either reduce demand or provide supply to satisfy the distribution grid's energy, capacity, or ancillary service requirements. Some of its potential benefits are (ELIZONDO; POUDINEH, 2023):

- Minimize dependence on centralised generation;
- Decrease the load on the network;
- Diminish network reinforcement and losses;
- Reduce energy costs;
- Improve energy security;
- Enhanced energy access;
- Cost-effective electricity sources for remote areas and communities;
- Environmental benefits;
- Lessen the carbon footprint of countries; and
- Job creation.

DERs can generate new opportunities for power systems, as previously mentioned, but they may also present challenges if the grid is inadequately prepared. Therefore, some of the potencial disadvantages are (SAEED *et al.*, 2021; IEA, 2022):

- Lower voltage stability as a result of reduced energy distribution;
- Reduce operational demand (load shedding);
- Decrease in system inertia as renewable energy systems replace synchronised generators, resulting in angular instability and frequency instability;
- Increase frequencies disturbances;
- Bidirectional power flows; and
- More complex predicting consumer net loads.

Grid reinforcement service, such as fast frequency response (FRR), can address certain identified challenges; however, it may necessitate significant financial investments, potentially resulting in elevated energy costs for consumers. Certain DERs have the technical capability to deal with the challenges they generate or that arise from other DERs. For example, BESS can enhance system flexibility, while smart EV charging systems can redistribute charging loads to mitigate evening peak demand. However, many regulators and system operators do not have sufficient information on DERs and have no adequate distribution grid monitoring equipment to use these capabilities effectively. Thus, digital technologies, like network monitoring devices, behind-the-meter devices, advanced inverters and smart meters, can enhance visibility for distribution grids (IEA, 2022).

The accelerated expansion in DERs, particularly in distributed solar generation - a significant DER in developing economies - along with other resources such as BESSs - expected to grow rapidly in developed economies over the next decade - has been primarily caused by pricing incentives, technological advancements, and an increased need for affordable and reliable energy sources (ELIZONDO; POUDINEH, 2023). Therefore, this study examines these two technologies located behind the meter.

2.2.1 Solar Photovoltaics (PV) modelling

Multiple techniques have been proposed for prediction PV power. The methods for generating PV power predictions are rely on two main strategies (FOSE *et al.*, 2024):

- Physical method: which requires access to meteorological data, along with prior knowledge of the characteristics of photovoltaic materials and system information; and
- Data-driven method: which requires operational data to train or calibrate model coefficients, which are then used for making predictions.

This study employs the physical method. In mathematical terms:

$$\text{Power}_{\text{PV}}(t) = A_m \times G(t) \times F \times \eta \times \left[1 + \gamma \times (T_c(t) - T_{c,ref})\right], \tag{2.1}$$

In which: $\text{Power}_{\text{PV}}(t)$ is the power data of a PV system; A_m is the total area of modules, in $[m^2]$; $G(t)$ is the nominal global incident irradiance at the instant t, in $[kW/m^2]$; F is a factor that models the system's electrical losses, in [%]; η is the PV system efficiency, in [%]; γ is the temperature coefficient, in [%/°C]; and $T_{c,ref}$ is the module reference temperature, in [°C]. $T_c(t)$ is the operating temperature of the photovoltaic panels at instant t determined according to equation (2.2) (GILMAN *et al.*, 2018).

$$T_c(t) = T_a(t) + G(t) \times \left(e^{a+bv_w(t)} + \frac{\Delta T}{1000}\right), \tag{2.2}$$

T_a is the ambient temperature at the instant t, in [°C]; and $v_w(t)$ is the wind speed in a instant t, in [m/s]. The module temperature parameters, a, b and ΔT depend on the module structure (GILMAN *et al.*, 2018).

2.2.2 Battery Energy Storage Systems (BESS) modelling

Battery storage systems can offer various services to the grid, including storage energy during periods of excess renewable generation and discharging it during peak demand (IEA, 2022). The BESS modeling relies on the regulation of the battery's state of charge (SoC), represented as a percentage of total battery capacity. The battery system's $SoC(t)$ and the battery power rating ($P_{\text{BES}}(t)$) at a specific time are determined according to equations 2.3 and 2.4, respectively (GHOLAMI *et al.*, 2023):

$$SoC(t) = \frac{E_{BES}(t)}{C_{BES}^{max}} \times 100 \tag{2.3}$$

$$P_{\text{BES}}(t) = \frac{E_{BES}(t-1)}{\Delta t} + \left(P_{\text{BES}}^{c}(t) \times \eta_{\text{BES}}^{c} - \frac{P_{\text{BES}}^{d}(t)}{\eta_{\text{BES}}^{d}} \right) \tag{2.4}$$

in which: $E_{BES}(t)$ is the total energy stored in the BES at the instant t, in [kWh]; Δt is the dwell time in the state; $P_{\text{BES}}^{c}(t)$ is the total charge power of the BES at the instant t, in [kW]; $P_{\text{BES}}^{d}(t)$ is the total discharge power of the BES at the instant t, in [kW]; η_{BES}^{c} is the efficiencie of BESS charging, in [%]; and η_{BES}^{d} is the efficiency of BESS discharging, in [%].

2.3 MICROGRIDS

According to International Electrotechnical Commission (IEC) and US Department of Energy (DOE), microgrids are defined as (AHMAD *et al.*, 2023):

> *"a group of interconnected loads and distributed energy resources with defined electrical boundaries forming a local electric power system at distribution voltage levels, that acts as a single controllable entity and is able to operate in either grid-connected or island mode."*

Microgrids function as a central coordinator for a collection of DERs while acting as an aggregated control point for large quantities power system operators and facilitating collaboration of resources with adjacent microgrids (ZINAMAN *et al.*, 2022). Their importance consists in ensuring reliability and resiliency for the connected loads within their boundaries, and in certain instances, with the possibility of offer auxiliary services to the primary grid. Furthermore, Microgrid aims to ensure uninterrupted service to loads during natural disasters and faults in the primary grid, particularly in instances of grid outages (AHMAD *et al.*, 2023).

Microgrid topology and DER choosing (dispatchable or not) are incorporated within the framework of microgrid planning and design. Its depends on various factors, including the characteristics of the locally available power supply, the type of loads and power infrastructure (AHMAD *et al.*, 2023). Many microgrid topologies and combinations of DERs have been documented in the literature, with PV systems (non-dispatchable) and BESS (dispatchable), usually used to ensure stability within the microgrid, being the most utilized DERs (AHMAD *et al.*, 2023).

An important component of microgrids is the point of Common coupling (PCC), functioning as the physical connection point between the microgrid and the main grid. This functions as the interface for the exchange of electrical energy between the microgrid and the larger power system. The PCC integrates multiple devices and equipment - such as circuit breakers, protective relays, and synchronization equipment - to enable connection, power transfer, control and protection between the microgrid and the main grid (UDDIN *et al.*, 2023).

Since the intermittent output of renewable energy sources increases the complexity of the efficient operation of microgrids, the Energy management system (EMS) becomes an important component to guarantee the control and smart management of DERs and loads. The supervision of the instantaneous operation of the system is done by a suitable control strategy, the Information and communication technologies (ICTs), with the objetive to provide stable and constant power flow (UDDIN *et al.*, 2023).

2.3.1 Community Microgrids

A community microgrid is a concept that is included among the microgrid use cases. It supplies energy to at least two distinct properties located within the service area of a utility and serve to enhance local energy independence and resilience (ZINAMAN *et al.*, 2022). A community microgrid functions as a physical infrastructure that facilitates the operation of an energy community, permitting the sharing and management of local energy resources. The ownership and management of community microgrids varies considerably with possibilities including utility companies, local members, third-party investors, or a combination of them (EKLUND *et al.*, 2023)

2.4 RELIABILITY IN POWER SYSTEMS

The main function of a power system is to serve, in the most economical way possible, consumers, whether large or small, with electrical energy whose levels of reliability and quality are acceptable (BILLINTON; ALLAN, 1984). Reliability is understood to be the measure of any component, device or system that describes the degree of safety when performing its intended function (ALLAN, 1994). Reliability theory arises with the aim of developing principles that enable complex systems to function even if some of their components are defective. In the 1950s, during the Second World War, reliability theory gained momentum mainly due to the need to develop reliable equipment and systems in extreme situations (CAMARGO, 1981).

The reliability of power systems is typically categorized into "adequacy,"which pertains to long-term and operational planning activities, and "security,"which is associated with the operational phase (PEYGHAMI *et al.*, 2020). The term system adequacy is related to static system conditions. In other words, the presence of sufficient equipment throughout the system to meet the load. Therefore, it does not include dynamic and transient disturbances of the system. The term system security, on the other hand, is related to the responsiveness of a system to disturbances of any nature (LI *et al.*, 2013).

It is noteworthy that most of the probabilistic techniques currently available for assessing reliability in electrical power systems are concentrated in the domain of the system adequacy aspect. Therefore, this work is developed under the lens of evaluating the adequacy of distribution systems in radial configurations composed of multiple DER.

The generation, transmission and distribution segments are called functional zones of a power system and can be divided into three hierarchical levels. Hierarchical level one (HLI) concerns only the generation system and hierarchical level two (HLII) includes generation and transmission systems. Level HLIII covers the three functional zones of generation, transmission and distribution (LI *et al.*, 2013).

The first studies on the reliability of electrical systems were developed with an emphasis on the HLI and HLII levels, with little attention given to distribution systems. Although the indexes at HLI and HLII levels are extremely important, as their collapses have impacts on wide sections of an electrical system and widespread consequences, the contribution of failures is comparatively lower in the individual load point indexes (BILLINTON; WANG, 1995; LI *et al.*, 2013). From the customer's perspective, the main reason for interruptions lies in the effects of failures in distribution systems as they are more frequent and localized (BILLINTON; JONNAVITHULA, 1996; LI *et al.*, 2013).

Assessments of HLIII are usually the most complex due to the magnitude of the problem, for this reason, the functional distribution zone is usually assessed separately. This consideration is acceptable because the distribution system interfaces with the transmission system through a connection point (ALLAN, 1994). The adequacy analysis of a distribution system aims to evaluate the appropriate rates for consumer charging points (LI *et al.*, 2013).

It must be mentioned that distribution power grids are infrastructures for the transportation of energy at the medium and low voltage levels. Grid topology denotes the physical interconnection among electrical nodes and feeder segments. Typically, these power grids exhibit either a radial or a ring/ mesh topology. Radial topology is defined by the supply of the loads within a single feeder path; this leads to simplicity in connections and reduced costs; however, it may compromise supply reliability. The ring/mesh configuration supplies electrical energy to the loads through a minimum of two electrical paths; thus, reliability is enhanced with the mesh topology, even though the associated costs are elevated (CABALLERO-PEñA *et al.*, 2022). This study focuses on radial topology as it is the most prevalent design for secondary systems.

2.4.1 Impacts of Modern Power Systems

Traditionally, electricity generation has depended predominantly on large, centralized generators connected to transmission grids, facilitating a unidirectional flow of electricity to consumers. System operators faced significant risks from large generator and network failures, causing the development of advanced transmission systems. These systems incorporated digital technologies, including supervisory control and data acquisition (SCADA) systems, to facilitate real-time monitoring of large power plants and grids. On the other hand, the distribution grid's automation was both costly and complicated due to its size, and there was little incentive to comprehend small-scale consumer demand tendencies. This means that many of the distribution networks still use the same system and were built to work with energy systems and practices from the 20th century (IEA, 2022).

However, power systems are undergoing transformation. An increasing proportion of electricity is generated from variable, weather-dependent renewable energy sources, necessitating enhanced flexibility in power systems. The term flexibility refers to the capacity of a power system to effectively and economically handle the variability and uncertainty of demand and supply across various timescales, ranging from maintaining immediate stability to ensuring long-term supply security (IEA, 2022).

Although DERs represents an increase in uncertainty for the planning and operation of electrical systems, there is the potential to improve the reliability of distribution systems by increasing the supply of electrical energy. This becomes apparent in the islanded operation mode of microgrids, a situation in which energy supply is maintained during grid failures or interruptions (ROCHA, 2014).

An important point of attention is that the majority of behind-the-meter DERs are owned by consumers, who determine their installation locations and operational strategies for personal advantage. Although DERs and microgrids have the potential to enhance power quality, increase energy security for critical loads and optimize overall system efficiency, the conflict of interests between DERs owners and system operators, caused by inadequate consumer incentives, may limit the potential benefits of DERs to the grid (IEA, 2022; UDDIN *et al.*, 2023).

Other significant challenge refers to present grid infrastructures, which frequently lack the necessary resilience and advanced technology to support a considerable increase in DERs. Furthermore, the variability and intermittency of specific distributed energy resources, such as solar and wind energy, may present challenges to stability and reliability, particularly in areas with existing fragile grid infrastructures. The integration of DERs and microgrids, particularly at elevated penetration levels, requires resilient smart grid infrastructures that can effectively manage the bi-directional flow of electricity to maintain the stability regardless the variability inherent in some DERs (ELIZONDO; POUDINEH, 2023).

In this sense, it is understood that the potential advantages of DERs and microgrids integration depend on the existing grid infrastructure, the availability of adequate technology to integrate these resources, and the size and control strategy of the microgrid.

2.5 DISTRIBUTION SYSTEM ADEQUACY ASSESSMENT

2.5.1 Exponentially Distributed Lifetime

Predictive reliability analysis refers to the assessment of the reliability of a system in the face of changes in its configuration, operating conditions or protection strategies. In this type of analysis, reliability indexes are calculated based on failure data of system components (LI *et al.*, 2013).

For an exponential distribution, the failure distribution function $F(t)$, the failure density function $f(t)$, the reliability function $R(t)$ and the risk function $h(t)$ are calculated according to the equations (2.5) to (2.8), respectively:

$$F(t) = 1 - e^{-\lambda t}, \tag{2.5}$$

$$f(t) = \frac{dF(t)}{dt} = \lambda e^{-\lambda t}, \tag{2.6}$$

$$R(t) = 1 - F(t) = e^{-\lambda t}, \tag{2.7}$$

$$h(t) = \frac{f(t)}{R(t)} = \frac{f(t)}{1 - F(t)} = \frac{\lambda e^{-\lambda t}}{1 - (1 - e^{-\lambda t})} = \lambda, \tag{2.8}$$

in which: λ is the parameter that represents the failure rate at which the component transitions from an operating state to failure. With μ being the repair rate, which reflects the response speed for a system to return to operation, the calculations of the mean time to failure (MTTF) and the mean time to repair (MTTR) are made according to the equations (2.9) and (2.10), respectively.

$$MTTF = \int_0^\infty R(t)\,dt = \int_0^\infty e^{-\lambda t}\,dt = \left.\frac{e^{-\lambda t}}{-\lambda}\right|_0^\infty = \frac{1}{\lambda}, \tag{2.9}$$

$$MTTR = \frac{1}{\mu}, \tag{2.10}$$

Therefore, in the exponential distribution, the failure rate is inversely proportional to the average lifetime.

2.5.2 Monte Carlo Simulation

The mathematical expectation of a specific reliability index is a crucial parameter in assessing reliability, particularly in large-scale systems. Monte Carlo methods, a broad designation for stochastic simulations that utilize random numbers, are highly appropriate for this undertaking. The fundamental distinction between analytical and Monte Carlo approaches lies in the approach used to determine which system state possibilities should be assessed (LI *et al.*, 2013).

Its applicability is not limited to solving stochastic problems, but also covers deterministic problems (LI *et al.*, 2013). Monte Carlo Simulation goes through three analysis steps to model stochastic events: (i) state selection; (ii) state evaluation and (iii) index estimation (CALADO, 2015).

The reliability indexes are described by test functions $F(X)$ – equations (2.18) to (2.24) - and evaluated based on an estimate of the expected value $\widetilde{E}(F(X))$ calculated according to the equation (2.11)

$$\widetilde{E}(F(X)) = \frac{1}{n}\sum_{k=1}^{n} F(x_k), \tag{2.11}$$

in which: n is the number of simulated samples and k is the number of simulated periods. This study considers a simulation period of one year (8760 hours). The convergence of the simulation process is verified by the coefficient of variation β, calculated according to the equation (2.12)

$$\beta = \frac{\sqrt{\frac{\mathrm{Var}(E(F(X)))}{n}}}{\widetilde{E}(F(X))} = \frac{\sigma}{\bar{X}\sqrt{n}}. \tag{2.12}$$

in which: $\bar{X}$ is the average of the index under evaluation and σ is the standard deviation of the index under evaluation.

2.5.2.1 Sequential Monte Carlo Simulation (SMCS)

Monte Carlo Methods may employ two distinct representations to estimate reliability in accordance with the system's state or time sequence: (i) Nonsequential Monte Carlo: simulate the random behavior of the process by sampling a series of experiments in a non-chronological manner, with all states being independent; and (ii) Sequential Monte Carlo: generate an artificial history of the system by utilizing the operating-repair cycles of the system and the relationships between each element's state and the system's states. Sequential simulations can facilitate more accurate evaluations by allowing operational strategies to be considered, specially when the system contains numerous events that are interdependent (SOUSA *et al.*, 2019).

With the aim of considering the relationship of events over time, this study applies SMCS to assess the reliability of a distribution system considering the integration of PV. The sequential approach contributes to greater accuracy in estimates, despite being more computationally intensive.

Assuming that the failure rate λ and the repair rate μ are exponentially distributed, the calculation of MTTF and MTTR considering the generation of random numbers by the inverse transform method is given by the equations (2.13) and (2.14), respectively (LI *et al.*, 2013)

$$MTTF = -\frac{1}{\lambda} lnU, \tag{2.13}$$

$$MTTR = -\frac{1}{\mu} lnU, \tag{2.14}$$

in which: U is a sequence of random numbers uniformly distributed between [0,1].

2.5.3 Reliability indexes

The reliability indexes utilized in the methodology proposed in this work are presented as follows.

The fundamental load point indexes used to predict the reliability of distribution systems are: (i) the average load point failure rate (λ) [f/yr]; (ii) the average load point outage duration (r) [h]; and (iii) the average annual load point outage or unavailability time (U) [h/yr]. The average values of the three fundamental indexes caused by the operational history of each line section i in each year j are calculated according to the equations (2.15) to (2.17)(LI *et al.*, 2013)

$$\lambda_{ij} = \frac{N_j}{(\sum T_{up})_j}, \tag{2.15}$$

$$r_{ij} = \frac{(\sum T_{down})_j}{N_j}, \tag{2.16}$$

$$U_{ij} = \frac{(\sum T_{down})_j}{(\sum T_{up})_j + (\sum T_{down})_j} \approx \lambda_{ij} r_{ij} \tag{2.17}$$

In which: $\sum T_{up}$ and $\sum T_{down}$ represent the sum of the in-operation and out-of-operation times, respectively, of the equipment during year j; while N_j denotes the number of transitions between the 'in-operation' (*up*) and 'out-of-operation' (*down*) states also during year j.

Although the three fundamental load point indexes are meaningful from the perspective of individual loads, they are not suitable for obtaining an analysis of the performance of distribution systems in general. For this purpose, additional indexes for this purpose can be obtained from the three fundamental indexes and the number of consumers (N_i) at each load point. The definitions and formulas of the most commonly used reliability indexes from the consumer perspective are presented as follows (LI *et al.*, 2013).

2.5.3.1 Sustained interruption indexes

System Average Interruption Frequency Index (SAIFI)

The System Average Interruption Frequency Index (SAIFI), determined according to the equation (2.18), measures the frequency of prolonged interruptions over a period, usually one year, for an average network consumer.

$$SAIFI = \frac{\sum \lambda_{ij} N_i}{\sum N_i} \left[\frac{oc.}{yr}\right], \tag{2.18}$$

System Average Interruption Duration Index (SAIDI)

The System Average Interruption Duration Index (SAIDI), determined according to the equation (2.19), quantifies the average number of hours of interruption a consumer will experience over a period.

$$SAIDI = \frac{\sum U_{ij} N_i}{\sum N_i} \left[\frac{h}{yr}\right] \tag{2.19}$$

Customer Average Interruption Duration Index (CAIDI)

The Customer Average Interruption Duration Index (CAIDI), determined according to the equation (2.20), represents the average interruption duration per consumer impacted by the interruption annually.

$$CAIDI = \frac{\sum U_{ij} N_i}{\sum \lambda_{ij} N_i} \left[\frac{h}{yr}\right] \tag{2.20}$$

Average Service Availability Index (ASAI) and Average Service Unavailability Index (ASUI)

The Average Service Availability Index (ASAI) reflects the fraction of time that a consumer had energy service available, in percentage. On the other hand, the Average Service Unavailability Index (ASUI) measures the time in which energy service was not available to the consumer. The ASAI and ASUI indexes are calculated according to the equations (2.21) and (2.22), respectively.

$$ASAI = \frac{\sum N_i \times 8760 - \sum U_{ij} N_i}{\sum N_i \times 8760} \times 100\,[\%]\,, \tag{2.21}$$

$$ASUI = \frac{\sum U_{ij} N_i}{\sum N_i \times 8760} \times 100\,[\%] = 1 - ASAI \tag{2.22}$$

2.5.3.2 Load and energy based indexes

Energy Not Supplied (ENS) and Average Energy Not Supplied (AENS)

The ENS (Energy Not Supplied) index measures the total energy not supplied by the system. Meanwhile, the AENS (Average Energy Not Supplied) index measures the energy not supplied by the system to an average consumer. The ENS and AENS indexes are calculated according to the equations (2.23) and (2.24), respectively.

$$ENS = \sum L_i U_{ij} \left[\frac{MWh}{ano}\right], \tag{2.23}$$

$$AENS = \frac{ENS}{\sum N_i} \left[\frac{MWh}{cons.ano}\right] \tag{2.24}$$

in which: L_i is the average load connected to load point i.

2.6 FINAL CONSIDERATIONS

Following the introduction of fundamental concepts regarding Distributed Energy Resources (DERs), microgrids, and the reliability analysis of electrical systems to evaluate the impact of integrating these resources, it is now possible to proceed to examine the methodology proposed in the subsequent chapter, which attempts to accomplish the objectives outlined at beginning of this work.

CHAPTER 3

METHODOLOGY

3.1 INITIAL CONSIDERATIONS

This chapter presents the proposed methodology for assessing the reliability impacts of the distribution network with microgrids that allocate distributed generation and storage systems.

3.2 OVERVIEW

Introducing an innovative approach to decentralized and sustainable energy, the accelerated growth in DER, especially in distributed solar generation and BESS, has generated complex challenges, especially profound in the reliability of power systems (ELIZONDO; POUDINEH, 2023).

Based on the choices shown in Figure 1.1, Figure 3.1 displays, in a simplified way, the general idea of the proposed methodology used to identify the impacts on the reliability of distribution systems caused by the insertion of PV and BESS.

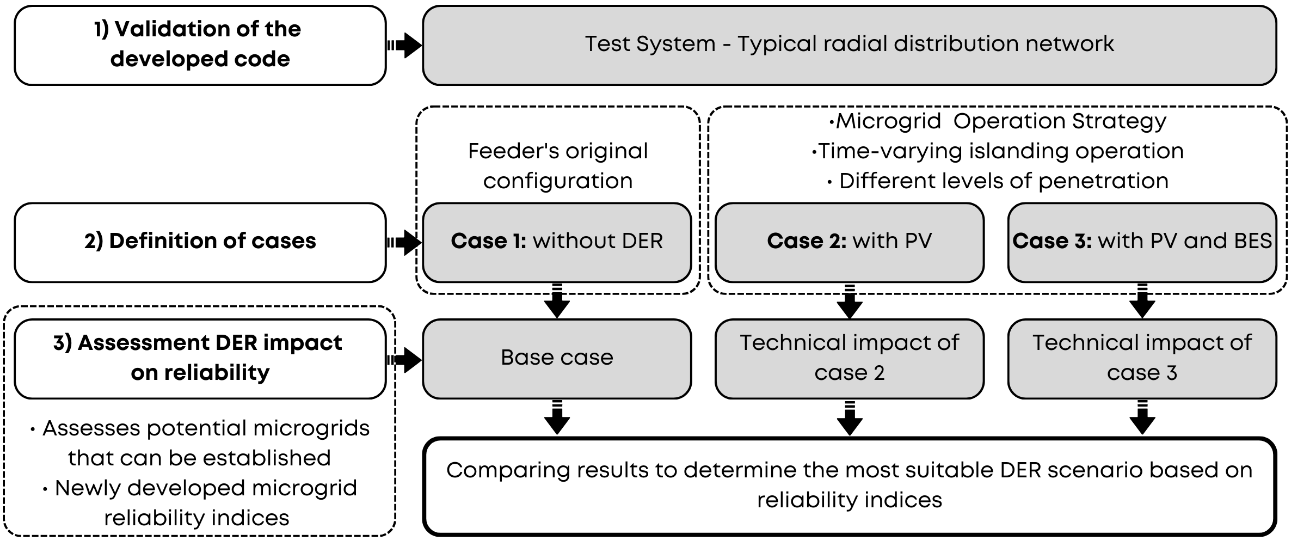

Figure 3.1: Simplified diagram of the methodology used. Source: Own authorship.

In the first stage, the methodology proposed is validated using a traditional radial distribution network. Subsequently, for the second stage, the cases to be evaluated are defined, exploring the following configurations between DER and the grid: 1) system without DER that will be employed as a reference for comparison with other scenarios; 2) PV only; and 3) PV together with BESS.

The control strategy implemented for the third configuration relies on comparing between the amount of power generated by the PV system and the amount consumed by the microgrid. The BESS are charged or discharged based on whether the PV generation exceeds or falls short of the microgrid's consumption. If there is excessive generation, energy is stored. The strategies for BESS discharge, outlined in Section 3.4.2, are classified into dual discharge for night consumption during peak hours and microgrid islanding.

In this study, the island mode is considered the time-varying islanding operation, described in Section 3.3.2, which is designed to dynamically configure the islanding operation's feeding areas in accordance with the load demand and the output of the DER at any given moment. In order to assess the effects of integrating PV with BESS, this study considers different levels of PV system penetration: 10%, 25%, 50%, 75%, and 100%. These values represent the proportion of the maximum PV capacity. The BESS assumes penetration values of 10%, 25%, 50%, 75%, and 100%, which represent fractions of the BESS maximum capacity.

In the third stage, the effects that the incorporation of DER can have on reliability indices related to the customer, load, and energy are analyzed for each proposed scenario. The methodology is designed to evaluate potential microgrids that can be implemented in the analyzed system, and adopts Sequential Monte Carlo Simulation (SMCS) for the probabilistic analysis. Four new microgrid formation indices are introduced to evaluate the changes in system reliability considering the time-varying islanding operation.

The methodology is applied to a Brazilian real distribution network topology, which doesn't have microgrids. However, in the context of this study, two fictional microgrid scenarios will be integrated into the simulations. The analysis will involve conducting an individual assessment of microgrids 1 and 2.

It should be emphasized that the approach of this study was designed to be implemented in radial distribution systems, the most common design for the secondary systems for serving residential, rural, and light-commercial areas (GONEN, 2015).

The following section presents the selected arrangement for the microgrids in this study.

3.3 MICROGRID ARCHITECTURE

The first stage of the methodology consists of selecting the microgrid structure.

The level of complexity from one microgrid to another can vary greatly depending on the set and variety of integrated DER (OLIVEIRA, 2017). The microgrids established in this study constitute systems that aggregate various generation, storage, and local loads. The classification adopted for the microgrids was based on a partial feeder microgrid, where the island zones can form sub-grids that can transit between islanded and connected modes of operation. The possibility of creating multiple simultaneous microgrids in the same system is considered.

As depicted in Figure 3.2, the microgrid and the main grid are integrated at a point of common coupling (PCC), which functions to switch between operation modes: either connected to the network or in an isolated mode.

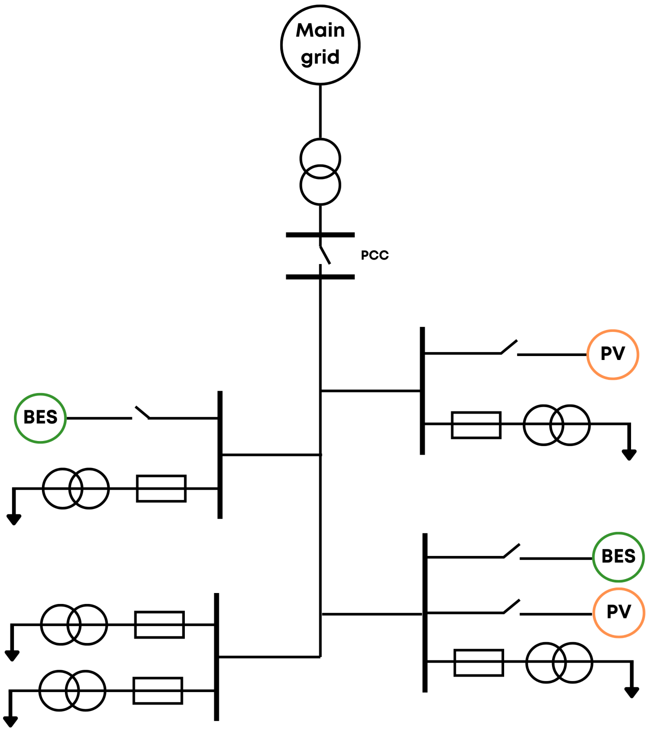

Figure 3.2: Schematic structure of microgrid. Source: Own authorship.

When disturbances occur in the grid, the microgrid can operate autonomously by disconnecting from the main grid and entering an isolated operation mode.This capability to disconnect from the main utility grid through upstream switches at the PCC is one of the defining characteristics of a microgrid. This disconnection, or islanding, can be implemented for economic and reliability reasons. In this mode, local DERs provide a reliable and continuous power supply to consumer loads (PARHIZI *et al.*, 2015).

Numerous microgrid topologies and DERs combinations have been documented in the literature, with PV systems and BESS being the most prevalent DERs. One reason is that their installation is comparatively simpler and more economical for the average consumer (AHMAD *et al.*, 2023). In microgrids, the utilization of BESS in conjunction with renewable energy sources serves as a method to alleviate the negative impacts of the mismatch between renewable energy output and microgrid load demand on its operation (FAN *et al.*, 2023). For this purpose, the DERs considered in this study, organized as a microgrid, includes PV and BESS, to improve security and flexibility in providing services. Figure 3.3 presents an overview of microgrid topology.

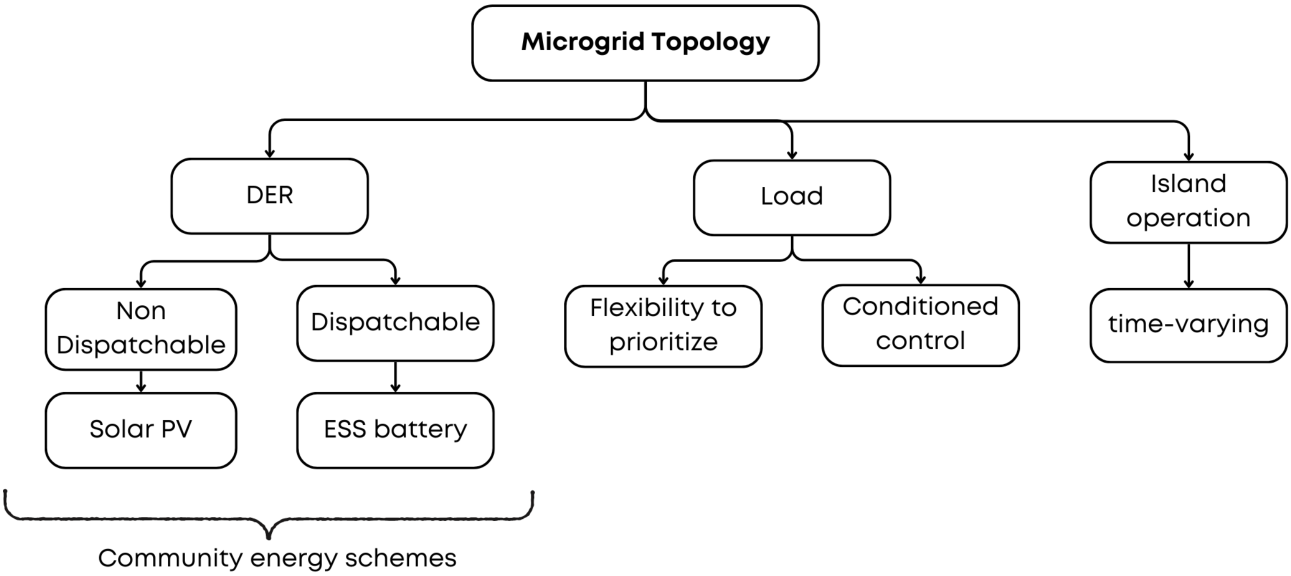

Figure 3.3: Overview of microgrid topology. Source: Own authorship.

The BESS and PV configurations within the microgrid area are considered to be partially aggregated units. These units can be situated at different locations within the microgrid area and are intended to cater to the entire microgrid. For this, the study considers the concept of community energy schemes, in which DER are collectively owned and the exported energy is shared among the members, which implies that the benefits resulting from heightened reliability in energy supply, resulting from the integration of DER, extend to all consumers located in microgrids. Currently, this concept is limited and restricted to the consumer unit that owns the DER. To accomplish this goal, it is assumed that there is a well-structured market design that incorporates the establishment of ancillary service markets. These markets would enable DER to operate as a unified entity, representing the consumers within the microgrid (ELIZONDO; POUDINEH, 2023).

Decisions to equilibrate the loads with the generation in microgrids operating in island mode might rely on the priority and reliability issues of the loads (LOPEZ-PRADO *et al.*, 2020). The primary attributes of the loads in the microgrid examined in this study are: (i) control of the load points, facilitating their disconnection or reconnection based on resource availability; and (ii) the capacity to prioritize load point service during supply periods. In islanding operation, the concept of variable supply areas is employed, which are dynamically modified at each moment based on the availability of DER. The details are given in Section

3.3.2.

It is presumed that each constituent microgrid balances supply and demand internally. Therefore, a load balance is carried out in the selected configuration as described by Eq. 3.1 at each stage of the simulation. Maintaining load balance ensures that, at each instant, the load demand on the microgrid is equivalent to the total power generated, covering both the PV output, BESS output, and imported power from the main grid (GHOLAMI *et al.*, 2023).

$$L_{MG}(t) = P_{\mathrm{PV}}(t) + P_{\mathrm{BES}}(t) + P_{Grid}(t) \tag{3.1}$$

In which: $L_{MG}(t)$ is the total load of the microgrid at instant t, in [kW]; $P_{\mathrm{PV}}(t)$ is the total power of PV at instant t, in [kW]; $P_{\mathrm{BES}}(t)$ is the total power of the BESS at instant t, in [kW]; and $P_{Grid}(t)$ is the imported power from the main grid at instant t, in [kW].

The parameters related to the microgrid's load, generation, and storage are considered variables that encompass the values associated with each point within the microgrid. The microgrid's load is determined by the value displayed in Eq. 3.2. The generation, represented as $P_{\mathrm{PV}}(t)$, and the storage, represented as $P_{\mathrm{BES}}(t)$, are explained in subsections 3.4.1 and 3.4.2, respectively.

$$L_{\mathrm{MG}}(t) = \sum_{i=1}^{n} L_{\mathrm{MG,\ i}} \times L(t) \tag{3.2}$$

In which $L_{\mathrm{MG,\ i}}$ is the annual peak load at each node of the microgrid at instant t, in [kW]; n is the number of nodes in the microgrid; and $L(t)$: represents the annual standardized hourly load curve, normalized to the range [0, 1].

3.3.1 Selection of Microgrid Operational Strategies

DERs can significantly enhance the distribution system's reliability if appropriately coordinated (MEERA; HEMAMALINI, 2022). When microgrids are connected to the grid, interruptions in the main grid may result in the operation of microgrids in island mode. This mode employs a control strategy centered on production and storage within the microgrids to equilibrate load with generation and prevent load shedding (LOPEZ-PRADO *et al.*, 2020).

Implementing complex restoration, particularly in distribution systems, is challenging due to the intrinsic inability to regulate outputs of DER and variations in connected loads, alongside the necessity to address the extensive range of outage-specific conditions (AMLEH *et al.*, 2018). In this study, to improve the reliability, the control strategy is planned to work in parallel with the main grid.

In situations of failure in the main system, the load at each point i of the microgrid represents the amount of the power generated by the microgrid can supply. It is assumed that the PV system will provide the load whenever possible. The BESS is designed to come into operation only in cases where the PV cannot independently meet the load requirements, as represented by Eq. 3.3.

$$P_{\mathrm{MG}}(t) = \begin{cases} P_{\mathrm{PV}}(t) & \text{if } L_{\mathrm{MG,\,i}}(t) + L_{\mathrm{MG}}(t-1) \leq P_{\mathrm{PV}}(t) \\ P_{\mathrm{PV}}(t) + P_{\mathrm{BES}}(t) & \text{if } L_{\mathrm{MG,\,i}}(t) + L_{\mathrm{MG}}(t-1) > P_{\mathrm{PV}}(t) \end{cases} \tag{3.3}$$

In which $P_{\mathrm{MG}}(t)$ is the total power of the microgrid at the instant t [kW]. This equation considers the possibility of the PV generation partially supplying the load, while the BESS provides the additional power required by $L_{\mathrm{MG,\,i}}(t)$.

Residential consumers' load curve exhibits a relatively stable consumption pattern during the day, with a modest rise in the late afternoon and a maximum demand peak at night. The peak time of a distributor refers to three hours defined by the highest energy consumption in a specific area, which aligns with the highest kWh tariffs. Within this particular framework, the strategic moment for discharging BESS during normal operation was selected as the peak period, with the objective of either completely or partially supplying demands.

The operational strategy for microgrids for the normal and islanding conditions is presented in Figure 3.4. The specific details of the limits of the battery are explored more thoroughly in Subsection 3.4.2.

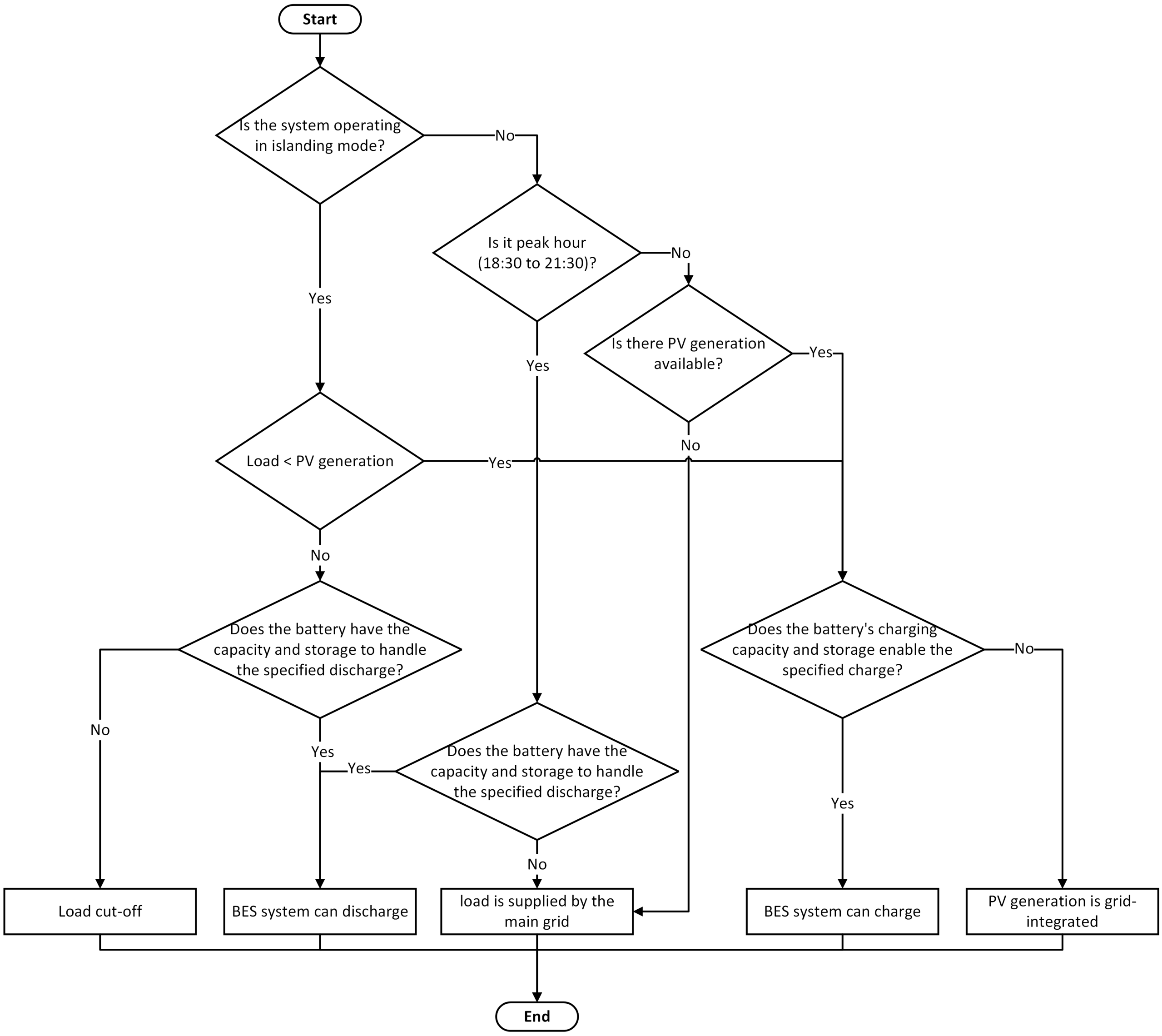

Figure 3.4: Operational strategy for microgrids. Source: Own authorship.

Figure 3.4 illustrates that the microgrids have the potential to achieve the following different operational outcomes:

- **Load cut-off**. Occurs during islanding operation when the subsequent DERs scenarios cannot meet the designated load: (i) PV system exclusively; (ii) PV system in conjunction with BESS; and (iii) BESS exclusively - during periods devoid of PV generation. The load cut-off is implemented in a selective manner, whereby priority orders are allocated to all loads to ensure the preservation of vital services in case of a system failure.

- **BESS can discharge**. Occurs in the following DER scenarios: (i) during islanding operation when the BESS has enough capacity and storage to handle the specified discharge of the total or partial microgrid load that the PV system is unable to supply; and (ii) during normal operation, when the BESS can manage the specified discharge of the total or partial, until the State of Charge (SoC) reaches 20%, microgrid load during peak hours (18:30 to 21:30), prior to depending on the main grid. The total discharge power of the BESS at the instant t ($P^d_{\text{BES}}(t)$ in [kW]), is calculated as outlined in Eq. 3.4;

$$P^d_{\text{BES}}(t) = \begin{cases} L_{\text{MG, i}}(t) - P_{\text{PV}}(t), & \text{islanding operation} \\ L_{\text{MG}}(t), & \text{normal operation} \end{cases} \tag{3.4}$$

- **Load supplied by the main grid**. Occurs only during normal operation in the following DER scenarios: (i) when the PV system has no available generation; and (ii) during peak hours when the BES system is unable to accommodate the specified discharge;

- **BESS can charge**. Occurs after determining the final size of the microgrid at each instant in the following DER scenarios: (i) during islanding operation when there is excess PV generation after meeting the load, that is, when the difference between the generation and the ultimate remaining total load capacity of the microgrid is positive; and (ii) during normal operation, when all PV generation is used to charge the BESS. The total charge power of the BESS at the instant t ($P^c_{\text{BES}}(t)$ in [kW]) is calculated as outlined in Eq. 3.5;

$$P^c_{\text{BES}}(t) = \begin{cases} P_{\text{PV}}(t) - L_{\text{MG}}(t), & \text{islanding operation} \\ P_{\text{PV}}(t), & \text{normal operation} \end{cases} \tag{3.5}$$

- **PV generation is grid-integrated**. Occurs only during normal operation when the BESS cannot store the available PV generation.

Overall, the selection of control strategies and the features of the BESS in the microgrid are determined by the amount of available PV generation.

3.3.2 Islanding Operation

Considering that the nodes of the main grid and those of the microgrid are sets, we can state, based on Eq. 3.6, that each microgrid is a subset of the main grid.

$$\text{Microgrids nodes} \subseteq \text{Grid nodes} \tag{3.6}$$

Each incident resulting in a failure in the main network can be symbolized by a set, including the network nodes associated with the failure. If there is a common occurrence of failure and microgrid nodes, as indicated by equation 3.7, the operational state becomes impractical, and all nodes inside the microgrid are deemed disrupted. Therefore, if any component in a microgrid fails, the entire microgrid will experience a load loss.

$$(\text{Failure nodes} \cap \text{Microgrids nodes}) \neq \emptyset \implies \text{No islanding operation will occur} \tag{3.7}$$

On the other hand, if the intersection between the failure and microgrid nodes is null, then an isolated operation mode is possible, as indicated in Eq. 3.8.

$$(\text{Failure nodes} \cap \text{Microgrids nodes}) = \emptyset \implies \text{islanding operation will occur} \tag{3.8}$$

In this situation, the nodes in each microgrid can still be interrupted, depending on the balance between load and generation within the microgrid. This study implements a time-varying islanding operation to maximize the number of nodes and fully utilize the PV output during this process.

3.3.2.1 Time-varying islanding operation

During the power outage of the main grid, the power supply areas of islanding operation are dynamically changed according to the time-vaying characteristics of loads and the DER output to improve the distribution network reliability. The approach adopted for the time-varying islanding operation was inspired by the structure proposed by (SU *et al.*, 2019). However, significant modifications have been made to meet the specific requirements of this study. Therefore, the time-varying islanding process adheres to the following principles in the islanding operation:

1. There are no component outages in the microgrid;

2. It is necessary for all the nodes to form a connected domain;

3. The analysis is conducted at each load point at every instant of time;

4. At every instant of time, the microgrid should continuously aim to provide power to as many load points as possible within the isolated network, while prioritizing the load at system points that the microgrid can supply during islanding;

5. Each load at each load point must be fully met, with no possibility of changing their energy usage based on the availability of DER; and

6. The microgrid is not formed when there are not enough DER to meet any load demand.

Figure 3.5 illustrates the procedure of the time-varying islanding operation.

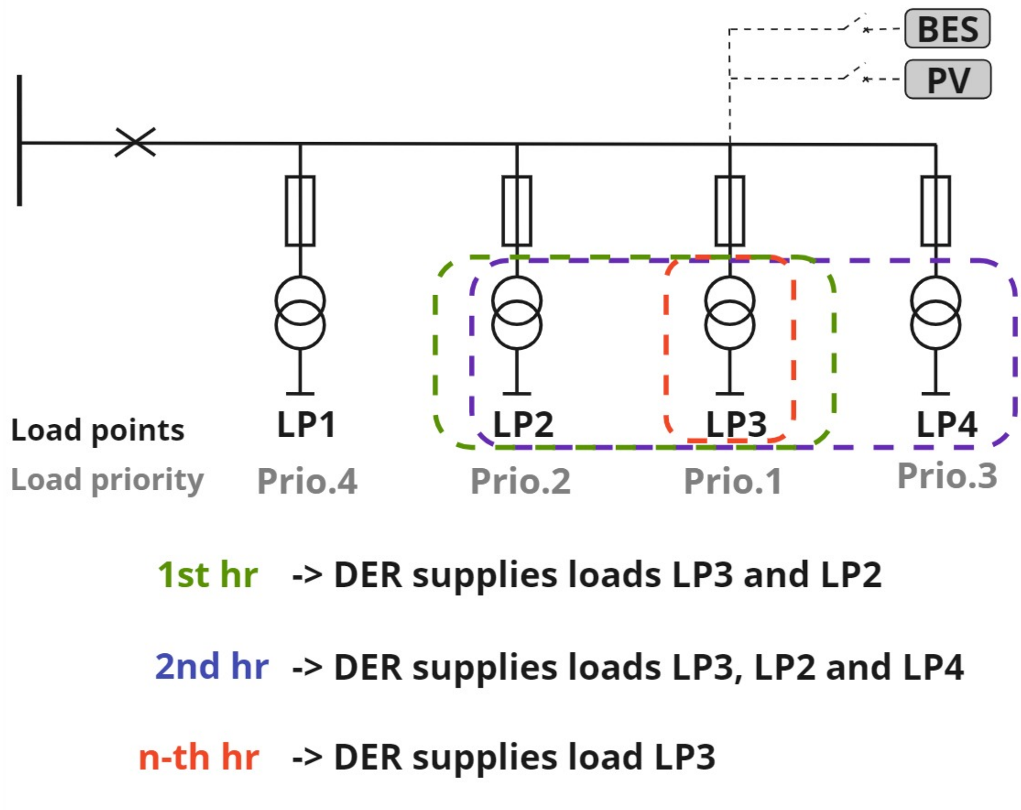

Figure 3.5: Illustration of the time-varying islanding operation. Source: Own authorship.

After examining all nodes of the microgrid, the final configuration of the microgrid for the analyzed moment is obtained, including only the load points whose power demand can be supplied by the total power available in the microgrid.

The proposed strategy for the time-varying island operation relies on the assumption that components of the information and communication technologies (ICTs) structure, including smart meters, will provide real-time data on energy consumption and generation for each load within the microgrid (EKLUND *et al.*, 2023). The microgrid configuration is assumed to incorporate effective protection equipment through the coordination and sequencing of protection device operation, with the fault detection, isolation from the main grid, and the automated re-coordination are all presumed to be executed using smart devices (SAEED *et al.*, 2021; UD-DIN *et al.*, 2023). For this, the conventional protection may prove inadequate or ineffective, requiring innovation.

3.3.2.2 Microgrid Formation Indices

To capture the change in microgrid reliability that occurs while islanding, four indices have been proposed, as depicted in Fig. 3.6:

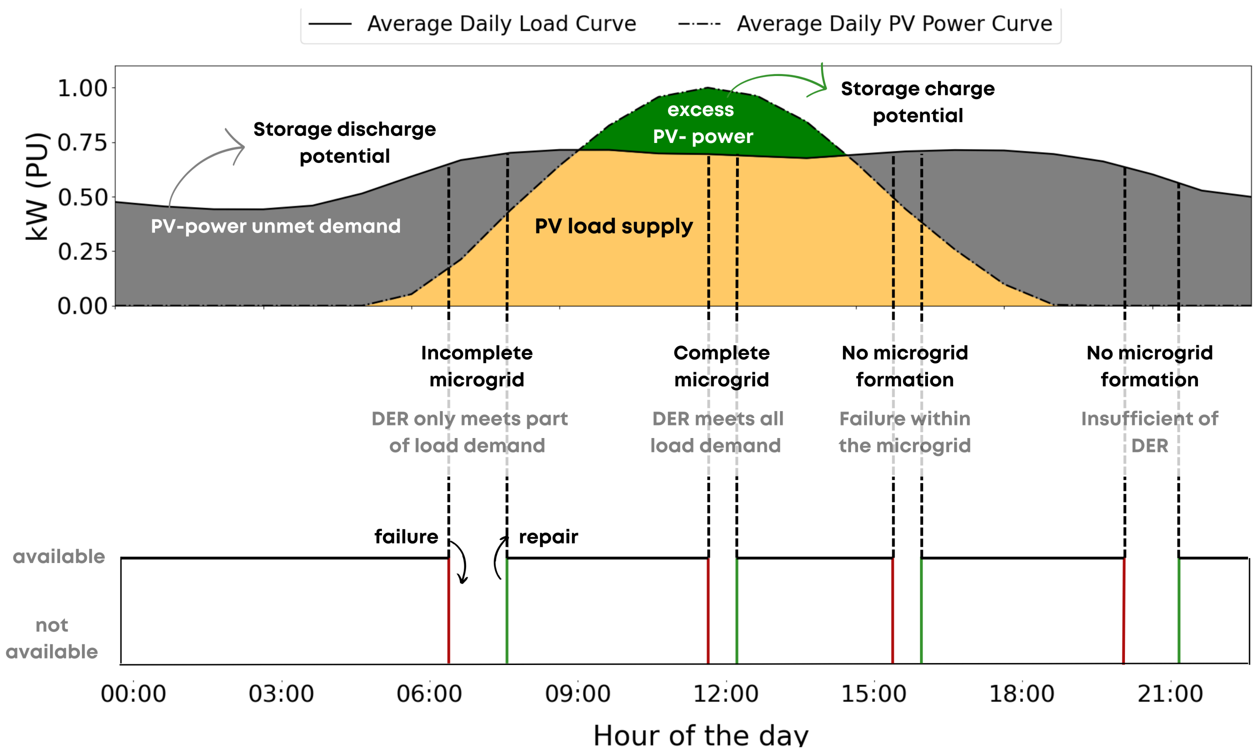

Figure 3.6: Possible microgrid arrangements during time-varying islanding operation. Source: Own authorship.

1. Incomplete microgrid formation (MGF_{Inc}): the percentage of establishment of a microgrid

that can meet only a portion of the load demand.

$$MGF_{Inc} = \frac{\text{Frequency of incomplete microgrid formation}}{\text{Total n}^{\text{o}}\text{ of failures}} \times 100\% \quad [\%] \tag{3.9}$$

2. Complete microgrid formation (MGF_{Comp}): the percentage of establishing a microgrid that can meet the entire 100% load requirement.

$$MGF_{Comp} = \frac{\text{Frequency of complete microgrid formation}}{\text{Total n}^{\text{o}}\text{ of failures}} \times 100\% \quad [\%] \tag{3.10}$$

3. No microgrid formation due to failure (MGF_{fail}): the percentage of non-microgrid formation caused by a failure within the microgrid.

$$MGF_{fail} = \frac{\text{Frequency of failures in the microgrid}}{\text{Total n}^{\text{o}}\text{ of failures}} \times 100\% \quad [\%] \tag{3.11}$$

4. No microgrid formation due to insufficient of DER ($MGF_{DERInsuf}$): the percentage of non-microgrid formation resulting from insufficient DER.

$$MGF_{DERInsuf} = \frac{\text{Frequency of DER shortages}}{\text{Total n}^{\text{o}}\text{ of failures}} \times 100\% \quad [\%] \tag{3.12}$$

3.4 DISTRIBUTED ENERGY RESOURCES MODELS

The proposed methodology enables the allocation of DER within the microgrid area in a concentrated and/or distributed manner serving the entire microgrid. To accomplish this, the installed capacities of PV and BESS are determined at the designated points within the microgrid where the systems are expected to be installed. Once the overall power capacity of the microgrid is determined, it can be utilized in the operational strategies of the microgrids outlined in Section 3.3.1.

3.4.1 Modeling of PV system

The photovoltaic potential of each designated node for installing PV systems in the microgrid is assessed based on the local consumption that is intended to be supplied, as outlined in

Equation (3.13) (STECANELLA *et al.*, 2020).

$$P_{\mathrm{PV,i}} = \frac{\mathrm{E,i} \times k}{\mathrm{PR} \times I_{rr}} \tag{3.13}$$

In which: $P_{\mathrm{PV,i}}$ is the installed power of the PV at each node assigned for the implementation of the PV system, in [kW]; E,i is the average daily consumption that the PV system installed at node i is expected to supply, in [kWh]; k is the solar constant on the Earth's surface, in [kWh/m^2]; PR is the performance ratio, in [%]; and I_{rr} is the monthly average daily solar irradiation, in [kWh/m^2/day].

To determine E,i, is taken into account the total annual peak load required by the microgrid (L_{i}), which is powered by the photovoltaic system installed at node i. This load can either be equal to node's load or larger. The load is allocated throughout the year based on the annual standardized hourly load curve ($L(t)$), and these values are combined to calculate the yearly average load.

$$\mathrm{E,i} = \frac{\sum_{t=1}^{t=8760} \left(\sum_{i=1}^{n} L_{\mathrm{i}} \times L(t)\right)}{365} \tag{3.14}$$

As shown in Equation (3.15), which considers the fact that it will operate as a unified entity, the total installed power of the PV (P_{PV}) in the microgrid is computed by summing the installed capacities of PV at individual points within the microgrid.

$$P_{\mathrm{PV}} = \sum_{i=1}^{N} P_{\mathrm{PV,i}} \tag{3.15}$$

In which N is the number of microgrid nodes assigned for the implementation of PV systems.

3.4.1.1 PV Hourly Power

The study examines the output model of the PV system at every instant of time ($P_{\mathrm{PV}}(t)$) for each year. The model is derived by multiplying P_{PV} by a standardized generation profile (SGP). The SGP is a variable that represents the typical annual hourly solar energy values for a specific region, considering factors such as radiation intensity, ambient temperature, efficiency, and electrical losses. The determination of SGP involves the process of normalizing the hourly

PVDG power to values ranging from 0 to 1 (per unit). The equation (3.16) represents this model.

$$P_{\text{PV}}(t) = P_{\text{PV}} \times SGP(t) \tag{3.16}$$

This adjustment procedure aims to depict the actual generation of the PV system more accurately. The $SGP(t)$ profiles are obtained by normalizing the values using the equation (3.17). This equation utilizes the annual power data of a PV system, denoted as $\text{Power}_{\text{PV}}(t)$, and is calculated using equation (2.1), which incorporates the weather data specific to the study region. It is important to note that, for the purpose of this study, it is conceivable to use arbitrary values for the total area of the modules, as these values will be normalized for future use.

$$SGP(t) = \frac{\text{Power}_{\text{PV}}(t) - \text{Power}_{\text{PV, Minimum}}}{\text{Power}_{\text{PV, Maximum}} - \text{Power}_{\text{PV, Minimum}}} \tag{3.17}$$

The operating temperature $T_c(t)$ at instant t of the photovoltaic panels, necessary to calculate $\text{Power}_{\text{PV}}(t)$, is determined by the equation (2.2).

To account for stochastic variability in the data, normalized regression functions are applied to each year of historical meteorological data available for the study region, and a random profile is selected during the reliability assessment for each simulated year.

3.4.2 Modeling of battery energy storage (BES)

Batteries are crucial in microgrids as they provide power when other sources are inadequate. The calculation of the battery capacity of each designated node for installing BESS in the microgrid is determined by Equation (3.18) (BACHA *et al.*, 2024):

$$C_{BES,i} = \frac{E,i}{DOD \times \eta_{\text{BES}}} \tag{3.18}$$

In which: $C_{BES,i}$ [kWh] is the battery capacity at each node assigned for the implementation of the BES system; DOD is the depth of discharge, in [%]; and η_{BES} represents the BESS inefficiency factor, in [%].

The total installed capacity of the BESS (C_{BES}) in the microgrid is calculated by incorporating the aggregate of the installed capacities of BESS at each individual point within the microgrid, as shown in Equation (3.19). This equation considers that the BESS is designed to serve the entire microgrid.

$$C_{BES}^{max} = \sum_{i=1}^{N} C_{BES,i} \tag{3.19}$$

In which: N is the number of microgrid nodes assigned for implementing of BESS.

3.4.2.1 BESS Hourly Power

The battery is charged or discharged at each iteration, depending on the difference between the PV generation and the load, respecting the charge and discharge capacity limits and the battery's minimum and maximum storage limits. The battery system's state of charge ($SoC(t)$) and the battery power rating at a specific time ($P_{\text{BES}}(t)$) are determined using equations 2.4 and 2.3, respectively.

3.4.2.2 Power Restrictions of the BESS

The aggregate power restrictions of the BESS within the microgrid are computed by summing the power restrictions at individual points within the microgrid, as outlined in Eqs. 3.20 to 3.22.

$$P_{BES}^{\text{min}} = \sum_{i=1}^{n} P_{\text{BES, i}}^{\text{min}} \tag{3.20}$$

$$P_{BES}^{\text{max}} = \sum_{i=1}^{n} P_{\text{BES, i}}^{\text{max}} \tag{3.21}$$

$$P_{\text{BES}}^{\text{max, d/c}} = \sum_{i=1}^{n} P_{\text{BES,i}}^{\text{max, d/c}} \tag{3.22}$$

In which:

$P_{\text{BES, i}}^{\text{min}}$ [kW]: is the minimum storage capacity at each node.

$P_{\text{BES, i}}^{\text{max}}$ [kW]: is the maximum storage capacity at each node.

$P_{\text{BES}}^{\text{max, d/c}}$ [kW]: is the maximum power at which the BESS can be discharged and charged at each node.

The total power restrictions of the BESS are defined in Eq. 3.23, aiming to ensure that the power flow remains within the predefined BESS capacity limits.

$$P_{\text{BES}}^{\text{min}} \leq P_{\text{BES}}(t) \leq P_{\text{BES}}^{\text{max}} \tag{3.23}$$

In which:

$P_{\text{BES}}^{\text{min}}$ [kW]: is the total minimum storage capacity.

$P_{\text{BES}}^{\text{max}}$ [kW]: is the total maximum storage capacity.

The total discharge and charge power of the BESS at every instant of time must adhere to the maximum discharge and charge power specified in Eq. 3.24.

$$P_{\text{BES}}^{d}(t) \leq P_{\text{BES}}^{\text{max, d/c}} \geq P_{\text{BES}}^{c}(t) \tag{3.24}$$

3.4.3 Penetration levels

The ratio of electric energy or power provided from any renewable energy sources is commonly known as the penetration. It is generally supplied in percentage (GONEN, 2015). The penetration level of DER in this study is determined by Eq. 3.25.

$$pen = \frac{\text{Power supplied by DER}}{\text{Total power demanded for loads (kW)}} \times 100 \tag{3.25}$$

The different scenarios of penetration levels are then incorporated using Equations 3.26 and 3.27.

$$P_{PV\ pen} = P_{\text{PV}} \times pen \tag{3.26}$$

$$C_{BES\ pen} = C_{BES} \times pen \tag{3.27}$$

In which:

$P_{PV\,pen}$ [kW] is the total PV power of the microgrid to obtain a penetration level.

P_{PV} represents the maximum power of the PV of the microgrid, which entails a penetration level of 100%.

$C_{BES\,pen}$ [kW] is the total BES power of the microgrid to obtain a penetration level.

C_{BES} represents the maximum power of the BESS of the microgrid, which entails a penetration level of 100%.

It is important to emphasize that the generation of PV energy is inherently intermittent, since it can surpass the previously committed penetration level during periods of intense sun activity. Nevertheless, when solar energy is scarce, the amount of energy generated can be considerably reduced or even nonexistent. Therefore, while the overall penetration rate may appear to be equal to or near a specific value over the research period, the situation can differ considerably when examined hourly (PALIWAL *et al.*, 2020).

3.5 TECHNICAL IMPACTS

After defining the operational strategies and characteristics of the microgrid, the technical impacts on reliability resulting from the integration of DERs into the distribution network are determined. Therefore, Subsection 3.5 describes, in detail, how these impacts are obtained.

A computational technique was developed to evaluate the impact of integrating PV and BESS on the reliability of distribution systems. This algorithm comprises three primary routines: one for executing the depiction of the system states - operational or failure -, another for verifying the efficacy of the protection devices, and a third for implementing the time-varying islanding operation procedure.

When simulating various residence times for the equipment, the methodology considers the randomness inherent in the definition of random failures caused by deterioration in both electrical and mechanical components. Solar irradiance, temperature, and wind speed exhibit unpredictable variations that are highly connected with time and the load curve. Based on this, the simulation data for each moment varies annually.

This technique incorporates the inherent randomness associated with these properties. This study examines the uncertainty outlined in Table 3.1.

Table 3.1: Modeled uncertainty in the proposed assessment methodology. Source: Own authorship.

Component	**Parameter**
PV system	SGP profiles
Distribution lines Transformers Circuit breakers Fuses	Mean Time to Failure (MTTF) Mean Time to Repair (MTTR)

The simulation scenarios of the system are determined by combining the load of consumers, the output power of the microgrid, and the random failure and repair statuses of the system components. For each year analyzed in this study, the scenarios are assessed hourly.

At every position of the DER and every level of PV penetration, the algorithm is initialized by assuming that the components of the system are in their optimal state, meaning they are operating normally. From this point onwards, a routine procedure is followed to arrange the duration of equipment in its present condition. When assessing the equipment in the shortest time, a routine examination of the system's state is carried out to identify the impacted consumers.

The proposed islanded mode routine is executed within the system's state evaluation procedure. It has a load management algorithm that identifies situations with insufficient power supply to meet the load demand. It then systematically removes loads from the system to ensure the islanding operation can be sustained and operational limitations can be met. After resolving the problem, the microgrid will be re-synchronized with the main grid.

The performance of protections is evaluated to activate the protection both upstream and downstream of the fault, enabling the identification of which nodes and their respective consumers are disconnected from the network after the activation of post-failure protections.

Afterward, the reliability indices for the given scenario are acquired, followed by the identification of the future transition to continue sampling the system states routine. This transition involves altering the status of the currently specified equipment - from success to failure in the event of failure, and from failure to success in the event of success. The proposed process is iterated for every scenario in the current year. Subsequently, the reliability indices are computed until statistically reliable results are obtained, considering numerous years.

The proposed algorithm is integrated into a probabilistic assessment environment based on the Sequential Monte Carlo method (SMC), defined in the following subsection, for the selection of time-residence scenarios in the failure/operation states of each equipment, of solar irradiation, temperature and wind speed, which makes it possible to calculate performance indices of the microgrid in islanding operation.

3.5.1 Monte Carlo simulation

The technical implications are measured based on the index specified in Section 2.5.3, which can be described by test functions $F(X)$ and evaluated based on an estimate of the expected value $\widetilde{E}(F(X))$ calculated according to the equation (2.11). The level of accuracy of Monte Carlo simulation can be expressed by the coefficient of variation β, which is calculated according to the equation (2.12).

Statistically correct outcomes are replies with coefficient of convergence (β) values that are less than or equal to a specified maximum value. Therefore, the coefficient of variation is calculated for each index, and it must be ensured that all of them fall within the predetermined maximum threshold for the variation coefficients.

The annual scenarios iteration is concluded after the maximum value among the variation coefficients reaches the predetermined threshold. To guarantee the statistical validity of the obtained values, a minimum of 10 distinct years are simulated, with each year consisting of 8760 assessed hours.

The subsequent part comprehensively explains the algorithm, emphasizing the input data and the resultant outcomes.

3.6 ALGORITHM DESCRIPTION

A computational algorithm was developed in the SCILAB software to understand the impacts of the widespread dissemination of DER on the reliability of a real distribution system.

The input information for the correct functioning of the algorithm is:

- Parameters of an electrical network;
- Hourly load curves per node;
- Load priority;
- Consumer number per load point;
- Sending and receiving nodes for each section ("from node"and "to node");
- Protective devices (circuit breakers, fuses);
- Transformers.

For the development of the photovoltaic system, it is essential to consider the variables related to the production and conversion of electrical energy to create standard generation curves by specifying the required data:

- Installed capacity of solar power generation per load point;
- Geographical location and corresponding meteorological information;
- Solar irradiance curves (hourly values for every day of the year);
- Hourly ambient temperature data for each day of the year;
- Hourly wind speed data for each day of the year, represented as curves;
- Electrical equipment efficiency.

Input data for the PV system will depend on annual data availability for each hour of the year.

Next, the features of the energy storage system are examined, focusing on the parameters:

- Installed capacity of energy storage systems per load point;
- The battery's minimum and maximum storage limits.
- The charge and discharge capacity limits;

- Efficiency.

The required reliability parameters are:

- Failure rate data of distribution lines, circuit breakers and transformers;
- Repair rate data of distribution lines, circuit breakers and transformers;

The algorithm created to model the analyzed electrical system sets each line of code to a particular component, such as transformers, circuit breakers, fuses, or distribution lines. In the code stages who does a line-by-line analysis, each line indicates the behavior and performance of the corresponding equipment.

The complete SMCS procedure adopted in this study, illustrated in Figure 3.7, is described as follows:

1. Insert the parameters of the power grid into the simulation;
2. Initialization of the BESS storage based on the total installed capacity across the microgrid nodes using Equation 3.19. After the first year, each simulated year starts with the storage level from the previous year;
3. Initialization of components: initialize the components that model the power distribution system in the success state. A convention has been established to indicate the operational state of the system components. The value '1' is adopted to represent that it is in operation. On the other hand, the value '0' refers to a state of inactivity;
4. Initialize the counter of simulated years (ny = 0);
5. Increment the value of 'ny' by 1 (ny = ny + 1);
6. Selecting a standardized generation profile (SGP) at random from the various normalized generation profiles that are available, as described in Section 3.4.1.1;
7. Perform the subprocess named "State selection", which involves determining the operational or faulty states of the system, verifying the effectiveness of the protection devices, and keeping track of the counters required for calculating the annual indices. Figure 3.8 provides a more accurate and detailed description of this subprocess;

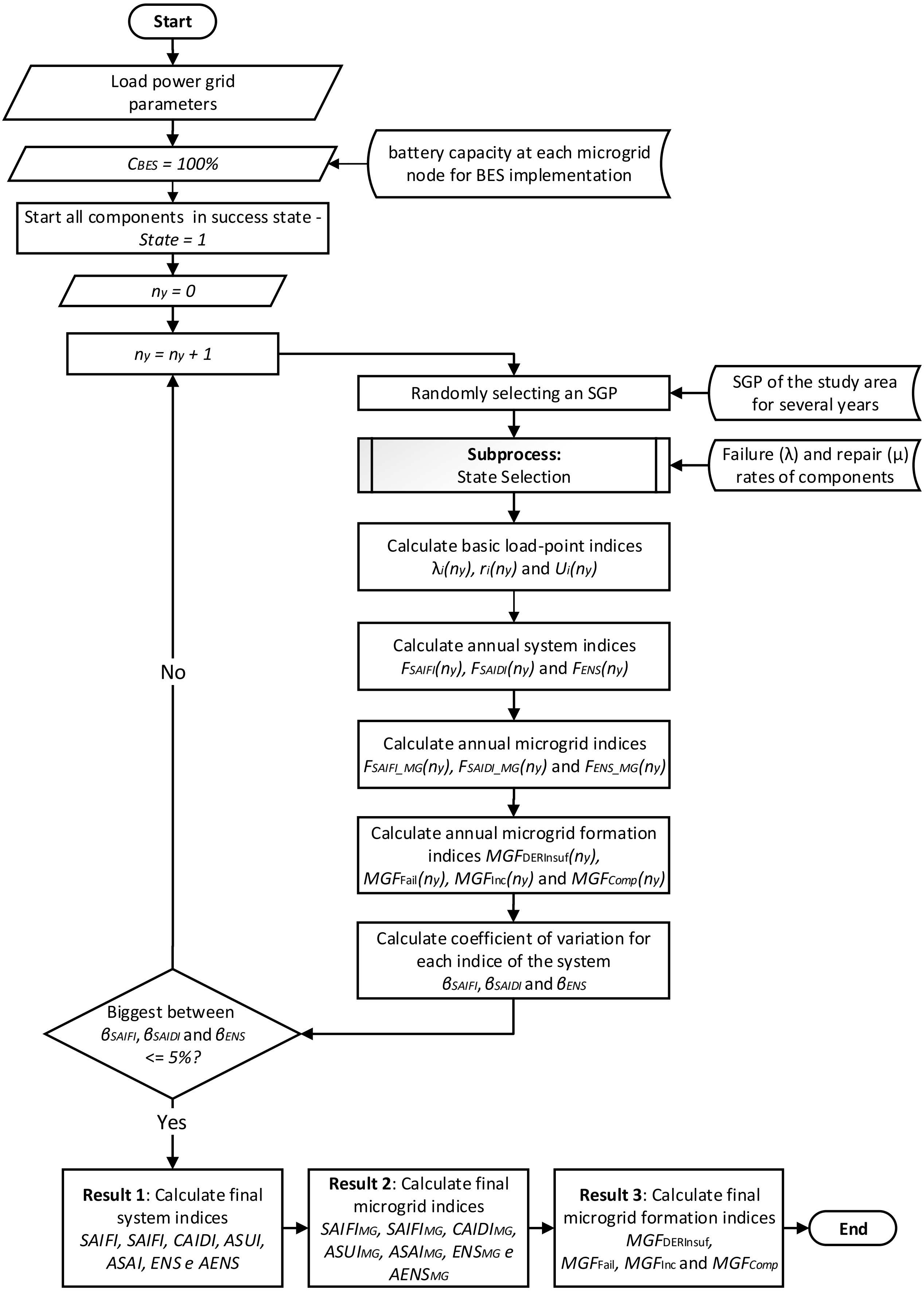

Figure 3.7: General reliability assessment procedure using SMCS. Source: Own authorship.

8. Obtain the basic load point indexes, accounting for both the system and the existing microgrid for the specified year, using equations (2.15) to (2.17);

9. Determine the analyzed year's reliability system and microgrid indexes using the previously calculated indexes and equations (2.18) to (2.24). Equations (3.11) to (3.10) are used to calculate microgrid formation indices for the analyzed year. A specified selection of microgrid nodes from the system's nodes is used to generate their indices. With this subsampling, microgrid-specific indices can be calculated;

10. Evaluate the coefficient of variation for all reliability system indices by employing equation (2.12). If convergence is reached, the procedure can proceed to step 11. Otherwise, the method returns to step 5;

11. The simulation is concluded by computing the ultimate reliability indices for both the system and microgrid, as well as the microgrid formation indices using Equation 2.11.

3.6.1 State selection procedure

The complete state selection procedure adopted in this study is depicted in Figure 3.8, and is described as follows:

1. Initialize required variables:

    - Total simulation time in hours $T_{sim} = 8760$;
    - The instant of the next transition $T_{trans} = 0$;
    - Simulation time $t_{clock} = 0$;
    - The total number of transitions between the up and down states for the system nodes $N_j = 0$;
    - Downtime occurrences through the entire sample for the system nodes $T_{down}) = 0$;
    - Uptime occurrences through the entire sample for the system nodes $T_{up} = 0$;
    - Disconnected nodes $DisNode = 0$. A convention has been established to indicate the connection state of the system nodes. The value '1' is adopted to represent that it is disconnected. On the other hand, the value '0' refers to a state of normal operation;

- Previous disconnected node status $prevDisNode = 0$;

2. Draw the Initial Residence Times (T) for each system line. To accomplish this, generate random values (U) and employ the failure (λ) and repair (μ) rates for each piece of equipment to determine the MTTF when the equipment is in a state of failure, or MTTR when the equipment is in an operational state, respectively, using the equations 2.13 and 2.14;

3. Store the computed T values in a vector (Tac);

4. The residence time (T) in vector Tac is the shortest. If it is an equipment transition, identify it;

5. Determine whether t_{clock} is larger than T_{sim}. If it is, set t_{clock} equal to T_{sim} to prevent t_{clock} from exceeding T_{sim};

6. Compute the dwell time in the state (ΔT) by subtracting T_{sim} from t_{clock};

7. Perform the subprocess named "State Assessment", which implies verification of the number of consumers impacted by the topology processor and verifying the formation of islands. Figure 3.9 provides a more accurate and detailed description of this subprocess;

8. Perform the accountants' update. Each node in the system is examined to determine if it is a disconnected node $DisNode = 1$. If it is not, the value of T_{up} is updated by adding ΔT, and the previously disconnected node status for the next iteration is updated to $prevDisNode = 0$. If the condition is true, increment the value of T_{down} by adding ΔT and update the previous disconnected node status for the next iteration $prevDisNode = 1$. Additionally, if it was previously in normal operation, increment the value of N_j by 1 ($N_j = N_j + 1$);

9. Update the instant of the next transition (T_{trans}) with the shortest residence time (T) in vector Tac;

10. Generate random values (U);

11. If the shortest residence time (T) in vector Tac during step 4 indicates a change in the load, increase the value of Tac by 1. If there is a transition of equipment, determine the

current state. If the equipment is in a failed state, transition it to a state of success and calculate MTTF using the equation 2.13. If the equipment is successful, transition it to a state of failure and calculate the MTTR using equation 2.14. Following the alteration in the condition of the equipment, increase the value of Tac by the T value;

12. Confirmation of the simulation period: the procedure is concluded upon completing of one year of simulation. If not, return to step 4.

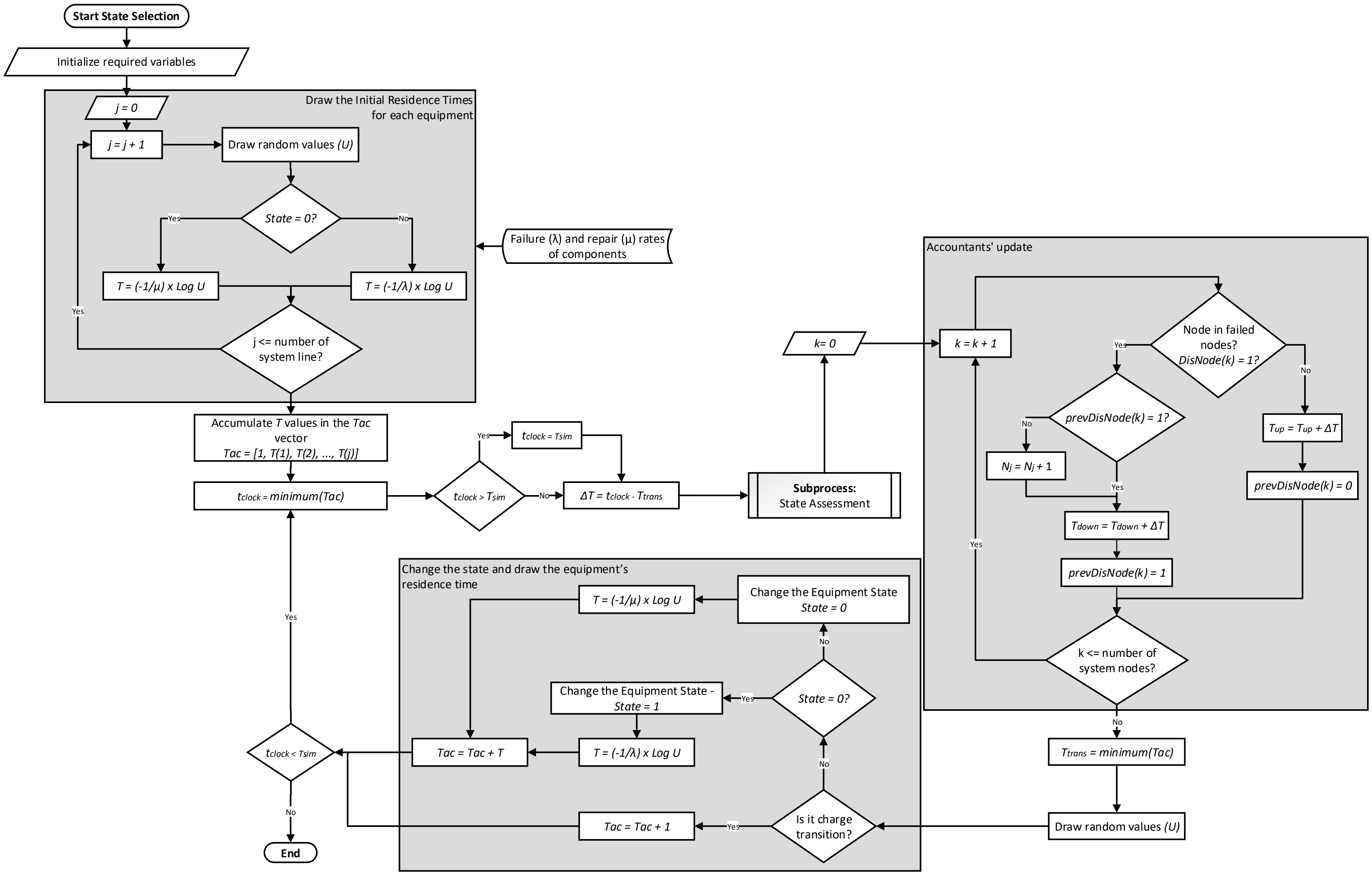

Figure 3.8: Subprocess: State selection procedure. Source: Own authorship.

3.6.2 State assessment procedure

The complete state assessment procedure adopted in this study, illustrated in Figure 3.9, is described as follows:

1. If a fault is detected, execute step 2. Otherwise, execute step 6;

2. Identify the line where the fault occurred (State = 0);

3. Implement the subprocess designated "Activation of the protection further upstream of the fault". This subprocess result updates the state of each line, indicating that the line with upstream protection of the fault has been activated (State = 0). Subsection 3.6.2.1 provides a clear and detailed representation of this subprocess;

4. Execute the subprocess titled "Activation of the protection further downstream of the fault for island operation". This subprocess's result updates each line's state, indicating that the line with downstream fault protection has been activated (State = 0) to allow islanded operation. Subsection 3.6.2.2 offers a precise and comprehensive depiction of this subprocess;

5. Execute the subprocess titled "Time-varying islanding operation"and execute step 10. This subprocess resizes microgrids according to the generation capacity available in each one of them. Subsection 3.6.3 offers a precise and comprehensive depiction of this subprocess;

6. If there is the possibility of forming microgrids, execute step 7. Otherwise, perform step 10;

7. If it is peak hour (18:30 to 21:30), execute step 9. Otherwise, carry out step 8;

8. Execute the subprocess titled "Charge BES system". Subsection 3.6.3.1 offers a precise and comprehensive depiction of this subprocess;

9. Execute the subprocess titled "Discharge BES system". Subsection 3.6.3.1 offers a precise and comprehensive depiction of this subprocess;

10. Execute the subprocess titled "topology processor". The result of this subprocessis the identification of the circuits connected to the same node, represented by the variable 'F'. Subsection 3.6.2.3 offers a precise and comprehensive depiction of this subprocess;

11. Perform the accounting for disconnected consumers examining each node in the system. If it is connected to the main supply (node 1) $F = 1$, execute step 16. Otherwise, perform step 12;

12. If the formation of microgrids is possible and this node is included in one of these microgrids, proceed to execute step 13. Otherwise, define the node as disconnected ($DisNode = 1$);

13. Examine each microgrid in the system. If the node is connected in this microgrid's in the initial configuration, execute step 14. Otherwise, carry out step 12;

    - This step will be repeated until all microgrids have been evaluated.

14. If the node remains connected in this microgrid after resizing during the time-varying islanding procedure and is not classified among the failed nodes, proceed to execute step 15. Otherwise, define the node as disconnected ($DisNode = 1$);

15. If all microgrids have been analyzed, execute step 16. Otherwise, the procedure returns to step 13;

16. If all nodes have been analyzed, the procedure is concluded by computing the disconnected nodes. Otherwise, the method returns to step 11.

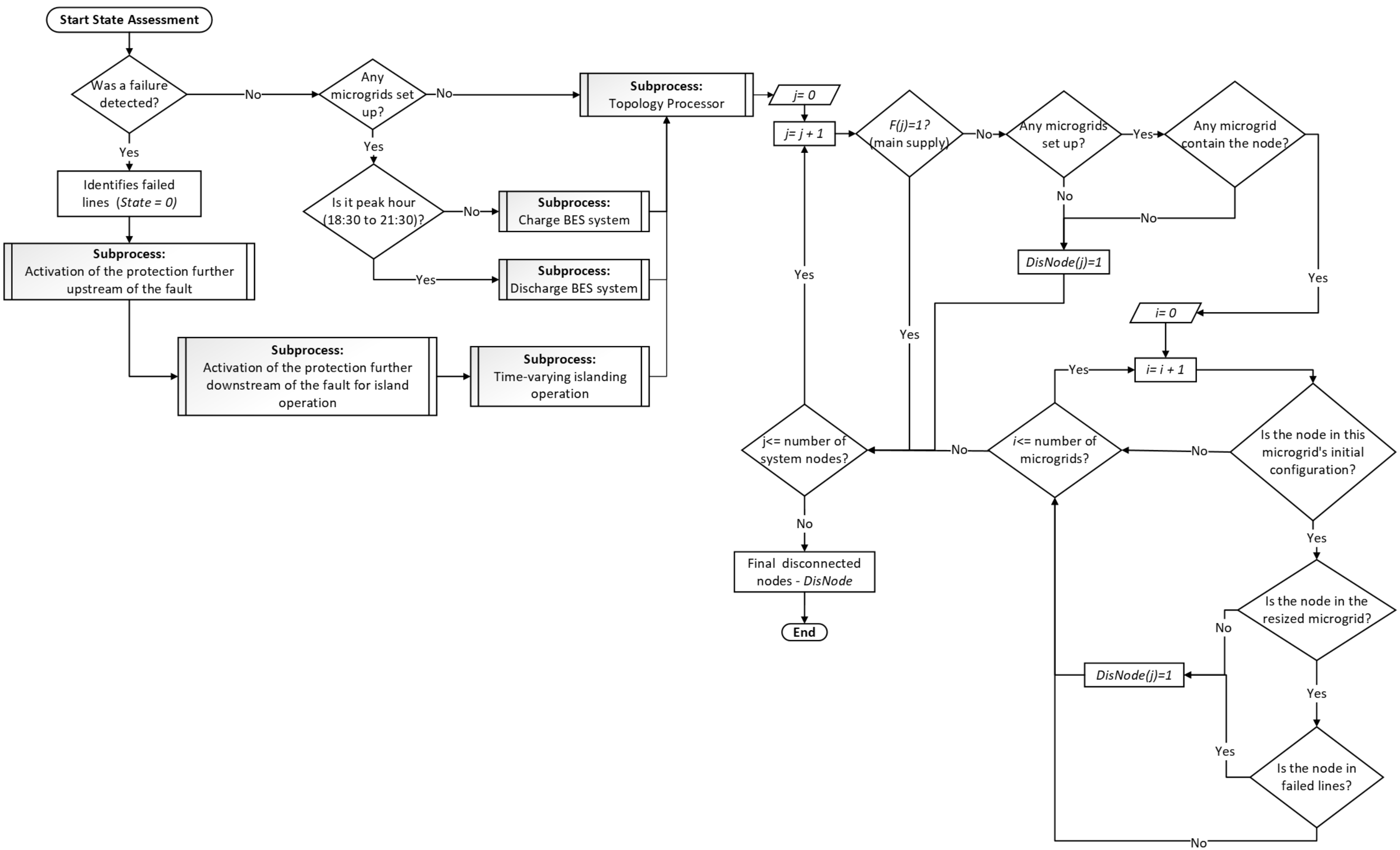

Figure 3.9: Subprocess: State assessment procedure. Source: Own authorship.

In Appendix C it is available an example to demonstrate the application of the following subprocesses in the state assessment procedure: (i) Activation of the protection further upstream of the fault, described in Subsection 3.6.2.1; (ii) Activation of the protection further downstream of the fault for island operation, described in Subsection 3.6.2.2; and (iii) topology processor procedure, described in Subsection 3.6.2.3.

3.6.2.1 Upstream Fault Protection Procedure

The subprocess designated as "Activation of the protection further upstream of the fault", illustrated in Figure 3.10, is described as follows:

1. Store initial state of lines ($State_0 = State$);
2. Initialize a list of zero elements, represented by $K = []$
3. Examine each line in the system. If the line is in the state of inactivity, i.e., $State(line) = 0$, execute step 4. Otherwise, perform step 7;
   - This step will be executed for every line in the system.
4. If the line has fault protection, execute step 7. Otherwise, execute step 5;
5. Identify the "from node"and "to node"and their respective outgoing lines;
6. Change the state of the identified outgoing lines to the state of inactivity (State = 0);
7. If all lines have been analyzed, execute step 8. Otherwise, the procedure returns to step 3;
8. Change the State of all the nodes in the list 'K' ($State(K) = 1$);
9. If $State_0$ is equal to $State$, meaning the initial state of lines corresponds to the actual state condition, the procedure concludes by activating the protection upstream of the fault. Otherwise, return to step 1.

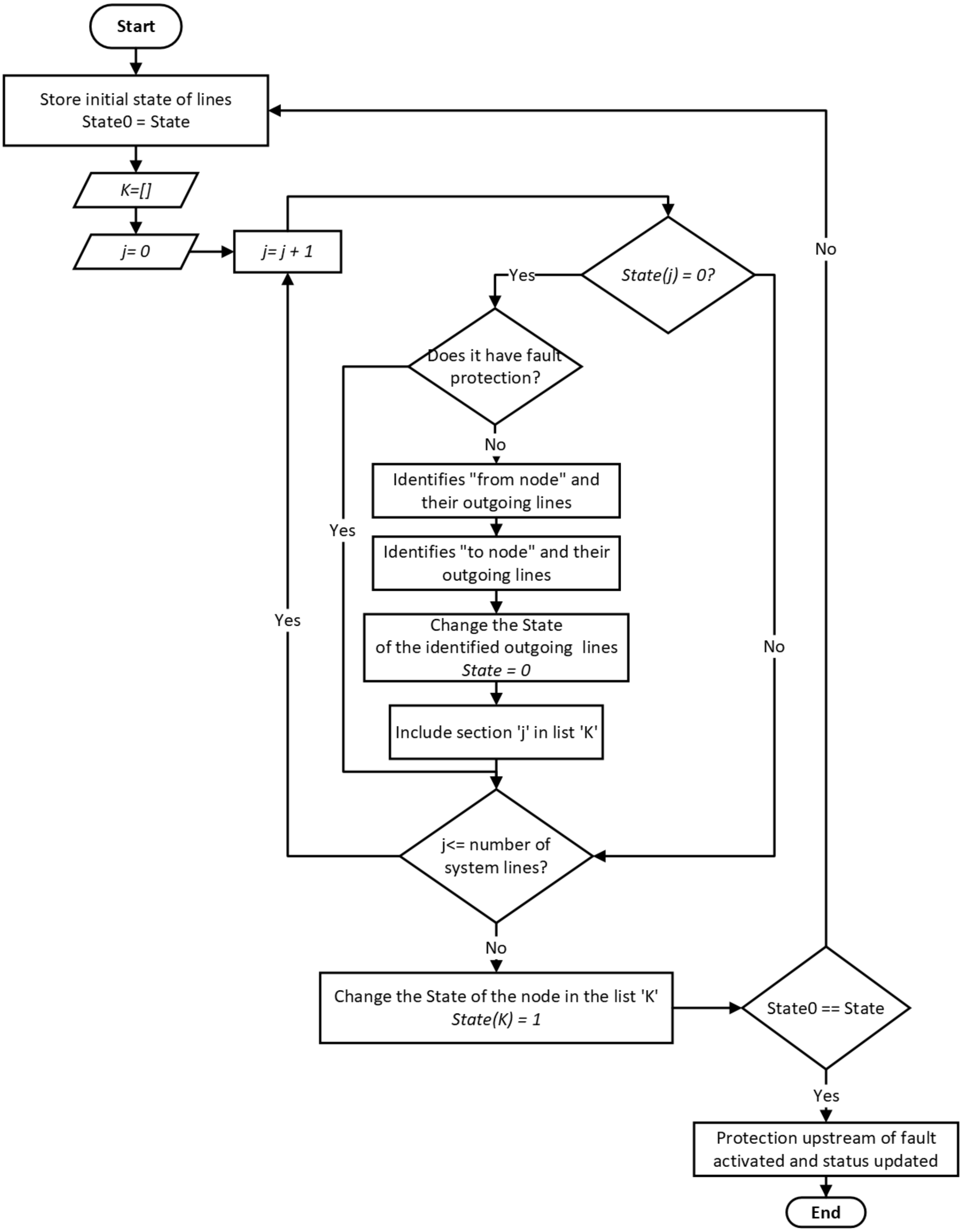

Figure 3.10: Subprocess: activation of the protection further upstream of the fault. Source: Own authorship.

3.6.2.2 Downstream Fault Protection for Island Operation Procedure

The subprocess designated as "Activation of the protection further downstream of the fault for island operation"is a recursive function in the algorithm, meaning it calls itself within its definition. The self-referential process continues until all incoming lines involved up to the last node in the system are identified. At this stage, the function stops invoking itself, allowing the advance to subsequent steps. Figure 3.11 illustrate this subprocess, and it is described as follows:

1. Following the identification of the disconnected line in the Subprocess outlined in Subsection 3.6.2.1, identify the "to node";
2. For the "to node", if any incoming lines are identified, execute step 3. Otherwise, execute step 6;
   - This step will be executed for every "to node"identified.
3. For the identified incoming line, if it has a circuit breaker, protection can be enabled by changing the state ($State = 0$). Otherwise, execute step 4;
   - This step will be executed for every incoming line identified.
4. Identify the "to node". If any incoming lines are identified for this "to node", return to step 3. Otherwise, execute step 5;
5. If all incoming lines have been analyzed, execute step 6. Otherwise, the procedure returns to step 3;
6. If all "to node"have been analyzed, the procedure concludes by activating the protection downstream of the fault. Otherwise, the procedure returns to step 2;

3.6.2.3 Topology Processor Procedure

The subprocess designated as "topology processor"is illustrated by Figure 3.12. The process aims to identify potential grid islands via a connectivity analysis. Islands containing DERs are

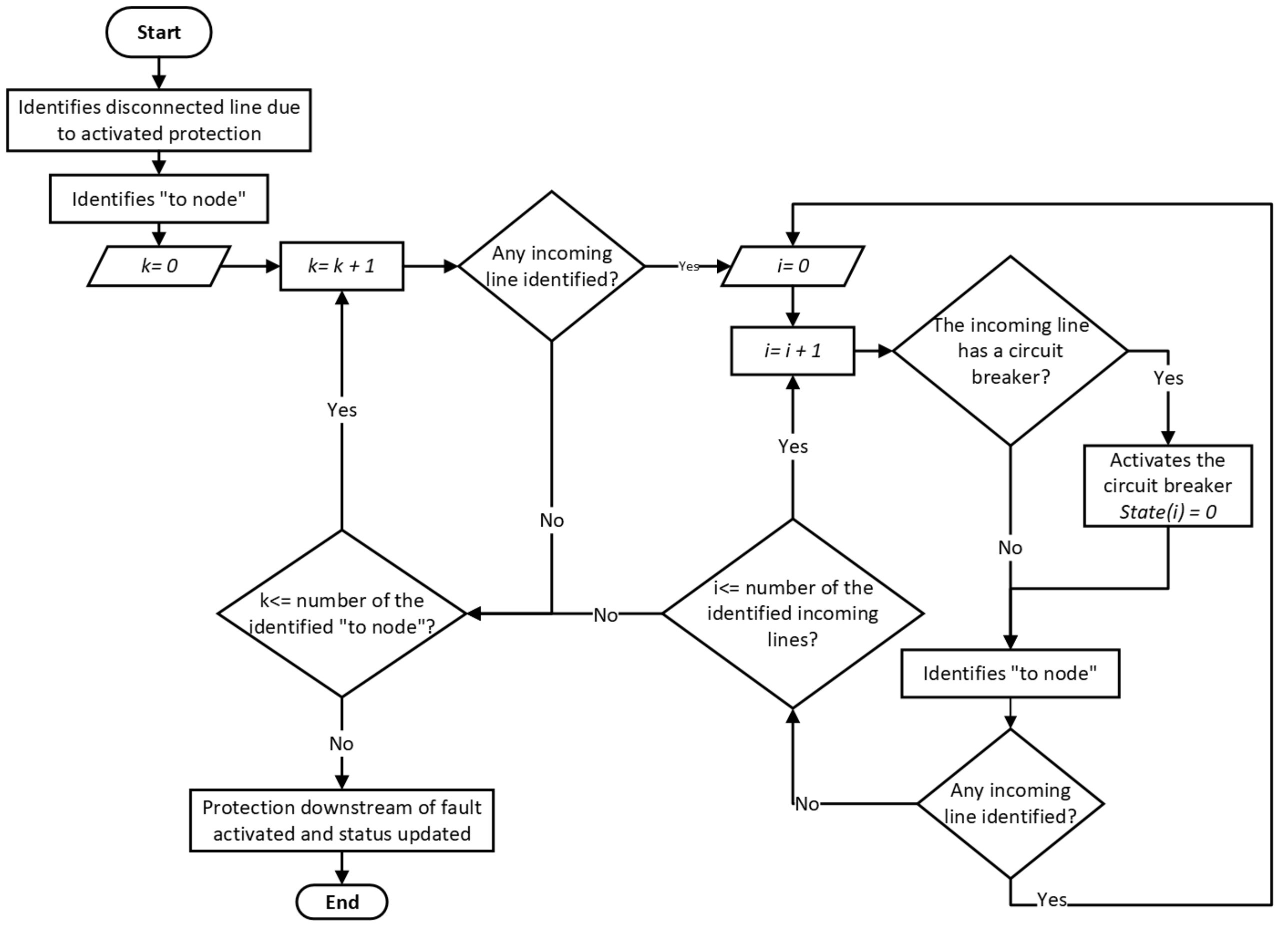

Figure 3.11: Subprocess: activation of the protection further downstream of the fault for island operation. Source: Own authorship.

characterized by the integration of distribution lines. Each islanded circuit is characterized by its transformation into a singular electrical node after the tripping of all circuit breakers. A circuit is defined as any line that is electrically connected to a circuit breaker, which is always positioned between two circuits only (COSTA, 2019). The subprocess is described below.

1. Designate a variable, represented here with the vector F, to identify which circuits are connected to the same node;
2. Initialize $F_0 = F$;
3. If the line is in operational state ($State = 1$), execute step 4. Otherwise, perform step 6;
   - This step will be executed for every line of the system.
4. Identify the Identify the "from node"and "to node";
5. Update the *F(from node)* and *F(to node)* equating the biggest of these to the smaller to connect or not its terminal circuits;
6. If all lines have been analyzed, execute step 7. Otherwise, the procedure returns to step 3;
7. If F_0 is equal to F, the procedure concludes with identifying the circuits connected to the same node. Otherwise, the procedure returns to step 2;

3.6.3 Time-varying islanding procedure

The complete Time-varying islanding operation procedure adopted in this study, illustrated in Figure 3.13, is described as follows for each possible Microgrid (j):

1. Initialize $j = 0$;
2. If the fault event happened within the microgrid, execute step 4. Otherwise, account no microgrid formation due to failure, not being possible to perform the charge/discharge of the BESS, and the procedure concludes;

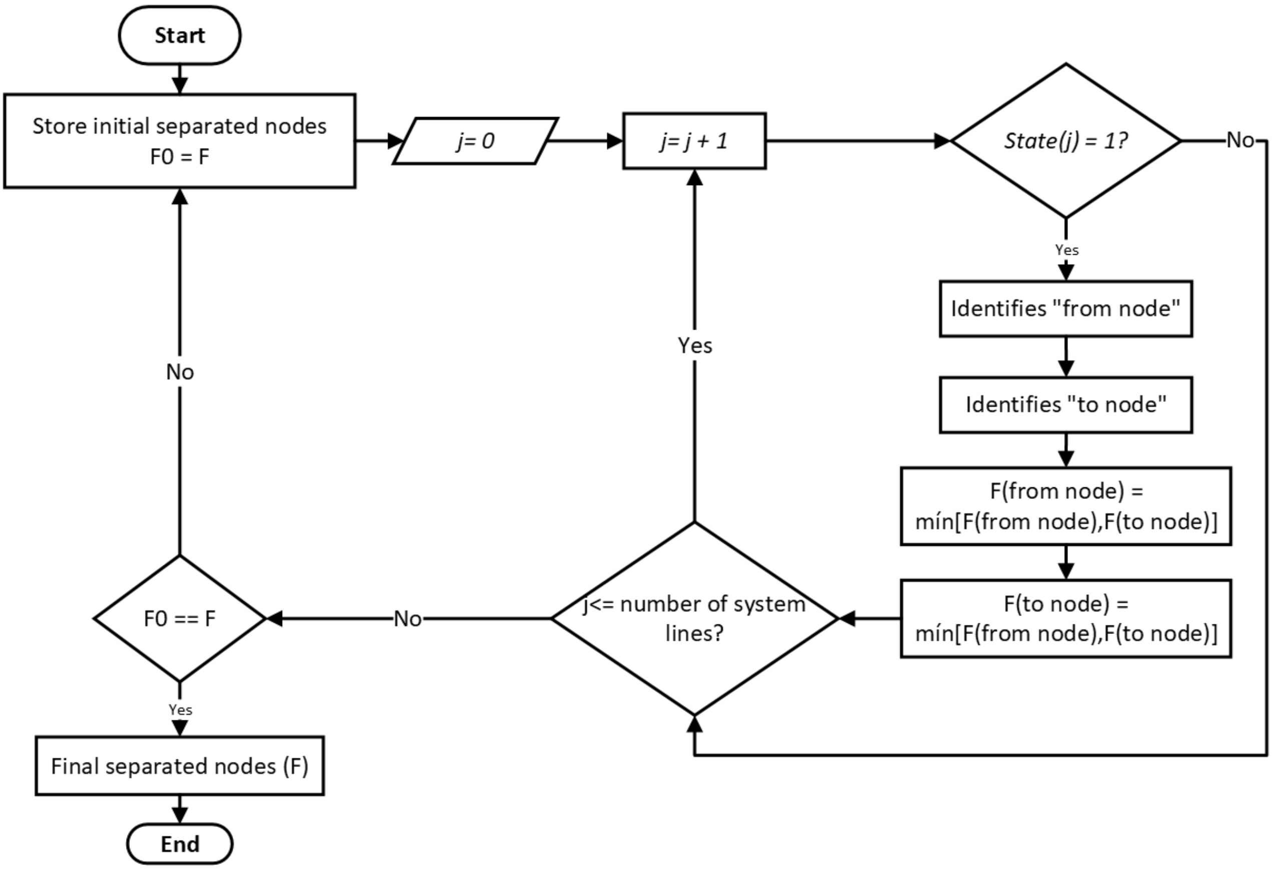

Figure 3.12: Subprocess: topology processor. Source: Own authorship.

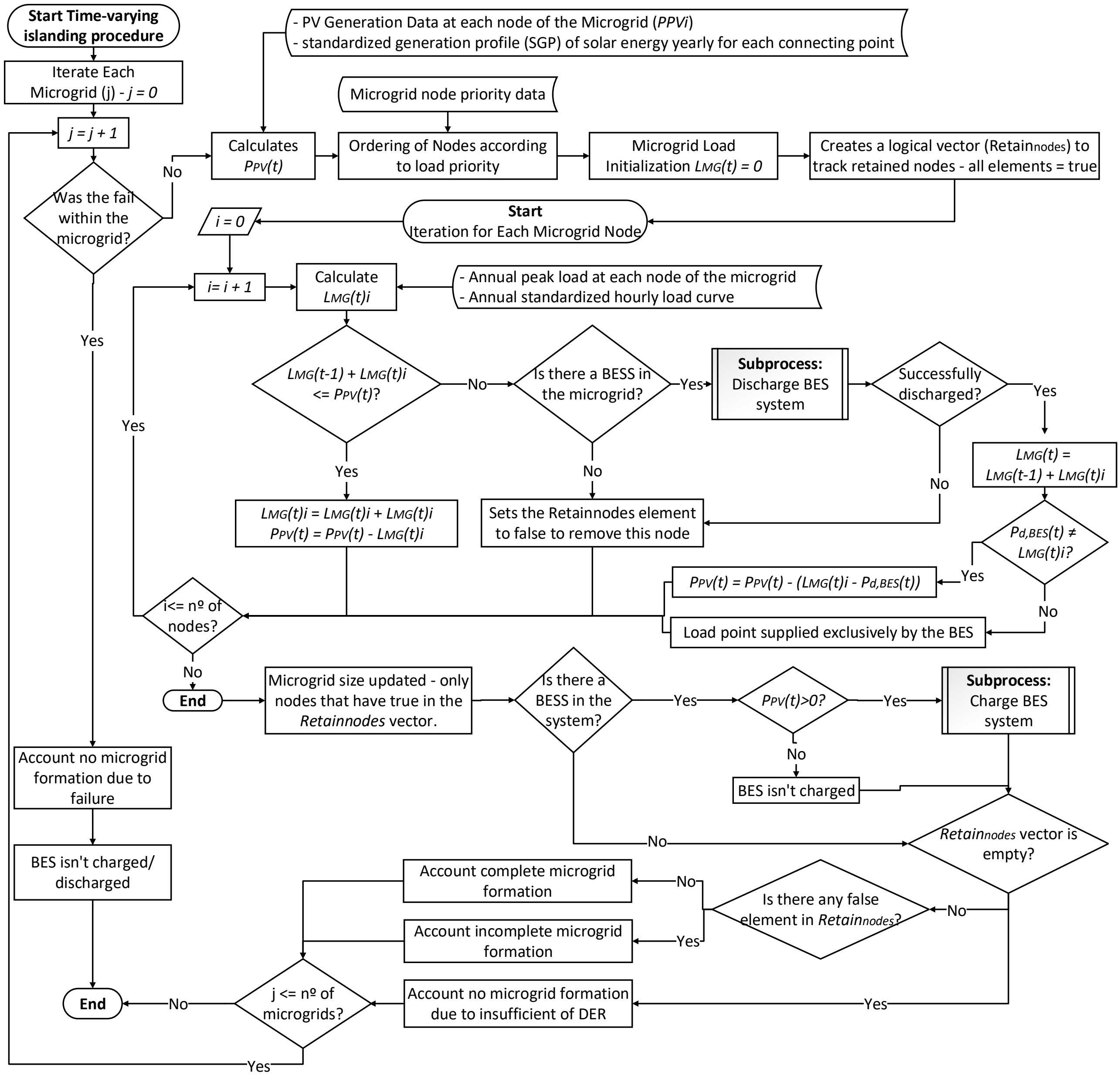

Figure 3.13: Subprocess: Time-Variable Islanding Operation Procedure. Source: Own authorship.

3. Increment the value of 'j' by 1 ($j = j + 1$)

4. Calculates the total PV generation at instant t of the microgrid $P_{\mathrm{PV}}(t)$, according to the Eq. (3.16);

5. Order the Nodes according to load priority;

6. Initialize the microgrid Load $L_{\mathrm{MG}}(t) = 0$;

7. Creates a logical vector ($Retain_{nodes}$) to track which nodes will be retained. Set all elements = true;

8. Iteration for Each Microgrid Node (i). Initialize i = 0;

   (a) Increment the value of 'i' by $1(i = i + 1)$ and calculate the current node load $L_{\mathrm{MG,\,i}}$ multiplying it to the instant annual standardized hourly load curve ($L(t)$);

   (b) Add $L_{\mathrm{MG,\,i}}$ to $L_{\mathrm{MG}}(t)$ and verify if $P_{\mathrm{PV}}(t)$ can supply the additional load. According to Eq. 3.3, if the condition is true, execute step 8c. Otherwise, execute step 8d;

   (c) The node can be maintained in the microgrid. Update $L_{\mathrm{MG}}(t)$ and $P_{\mathrm{PV}}(t)$, respectively, adding and discounting the $L_{\mathrm{MG,\,i}}$;

   (d) Verify if there is a BESS in the microgrid, if the condition is true, execute step 8e. However, if the condition is false, execute step 8i;

   (e) Execute the subprocess titled "Discharge BES system". Subsection 3.6.3.1 offers a precise and comprehensive depiction of this subprocess;

   (f) If it was possible to discharge the BESS to supply $L_{\mathrm{MG,\,i}}$, execute step 8g. Otherwise, execute step 8i;

   (g) Update $L_{\mathrm{MG}}(t)$ by adding $L_{\mathrm{MG,\,i}}$ and verify if the total discharge power of the BESS at the instant t ($P^{d}_{\mathrm{BES}}(t)$) is different from $L_{\mathrm{MG,\,i}}$, indicating that BESS was capable of supplying all or just part of $L_{\mathrm{MG,\,i}}$. if the condition is true, execute step 8h. Otherwise, execute step 8j;

   (h) Determine the load contributed by the BESS by verifying the remaining load that $P_{\mathrm{PV}}(t)$ could not supply. Proceed to step 8j;

(i) Sets the corresponding element in $Retain_{nodes}$ to false, indicating that this node should be removed from the resized microgrid;

(j) After completing the operation on the current node, if no more nodes are to be processed, execute step 9, otherwise, return to step 8a;

9. Update the microgrid size only to keep nodes that have true in the $Retain_{nodes}$ vector;

10. If there is a BESS in the microgrid, execute step 11. Otherwise, meaning that the charge of the BESS is not performed, proceed to step 12;

11. If there is any available generation to charge the BESS, execute the "Charge BES system"subprocess. Subsection 3.6.3.1 offers a precise and comprehensive depiction of this subprocess;

12. If the $Retain_{nodes}$ vector has no elements, it account for no microgrid formation due to insufficient DER. Otherwise, execute step 13;

13. If there are any false elements in $Retain_{nodes}$ vector, account for incomplete microgrid formation. Otherwise, account complete microgrid formation;

14. After completing the operation on the current microgrid, if there are more microgrids to be processed, return to step 3. Otherwise, concludes the process.

3.6.3.1 BES System Charge and Discharge Operation

This Subsection gives the algorithm routine for the procedures defined in Section 3.3.1 for the charge and discharge operational strategies.

The subprocess designated as "Charging the BES System", illustrated in Figure 3.14, is described as follows:

1. If there is PV generation $P_{\mathrm{PV}}(t) > 0$ available, execute step 3. Otherwise, execute step 2;

2. The charge of the BESS is not performed and the procedure concludes;

3. In the event of a detected fault, the total charge power of the BESS at time t ($P^c_{\text{BES}}(t)$) is computed as specified in Eq. 3.5 for islanding operation. Otherwise, $P^c_{\text{BES}}(t)$ is computed in accordance with the normal operation of the same equation;

4. Check the limits established for charging the BESS in Subsection 3.4.2.2. If $P^c_{\text{BES}}(t)$ satisfies with the maximum charge power ($P^{\text{max,c}}_{\text{BES}}$) defined in Eq. 3.24, compute the total energy stored in the BES at time t ($E_{BES}(t)$) based on Eq. (2.4), utilizing $P^c_{\text{BES}}(t)$. Otherwise, utilize $P^{\text{max,c}}_{\text{BES}}$ in place of $P^c_{\text{BES}}(t)$;

5. Ensure that $E_{BES}(t)$ remains within the predefined BESS capacity limits defined in Eq. (3.23). Finalizes the procedure.

The subprocess designated as "Discharging the BES System", illustrated in Figure 3.15, is described as follows:

1. In the event of a detected fault, execute step 2. Otherwise, execute the step 4;

2. If $P_{\text{PV}}(t)$ added to $E_{BES}(t)$ can supply the additional load $L_{\text{MG, i}}$, execute the step 3. Otherwise, execute the step 7;

3. Calculate the total discharge power of the BES at the instant t ($P^d_{\text{BES}}(t)$) as specified in Eq. 3.4 for islanding operation. Proceed to step 6;

4. If it is peak hour (18:30 to 21:30), execute the step 5. Otherwise, execute the step 7;

5. $P^d_{\text{BES}}(t)$ is computed as specified in Eq. 3.4 for normal operation. Proceed to step 6;

6. Check the limits established for discharging the BESS in Subsection 3.4.2.2. If $P^d_{\text{BES}}(t)$ satisfies the maximum discharge power ($P^{\text{max,d}}_{\text{BES}}$) defined in Eq. 3.24, compute the total energy stored in the BESS at time t ($E_{BES}(t)$) based on Eq. (2.4), utilizing $P^d_{\text{BES}}(t)$. Otherwise, execute the step 7;

7. The discharge of the BESS is not performed and the procedure concludes;

8. Ensure that $E_{BES}(t)$ remains within the predefined BESS capacity limits defined in Eq. (3.23). Finalizes the procedure.

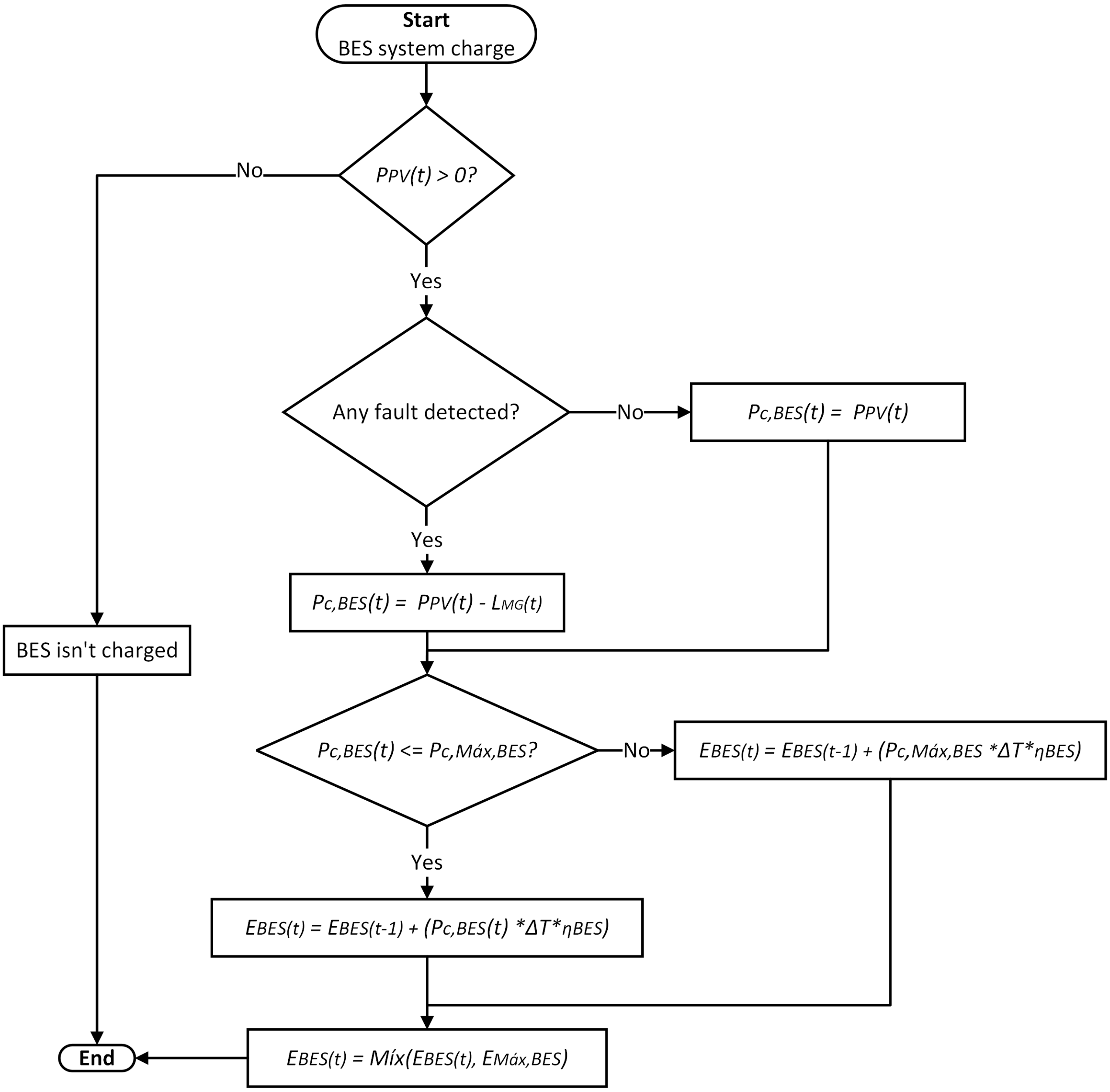

Figure 3.14: Subprocess: charging the BES System. Source: Own authorship.

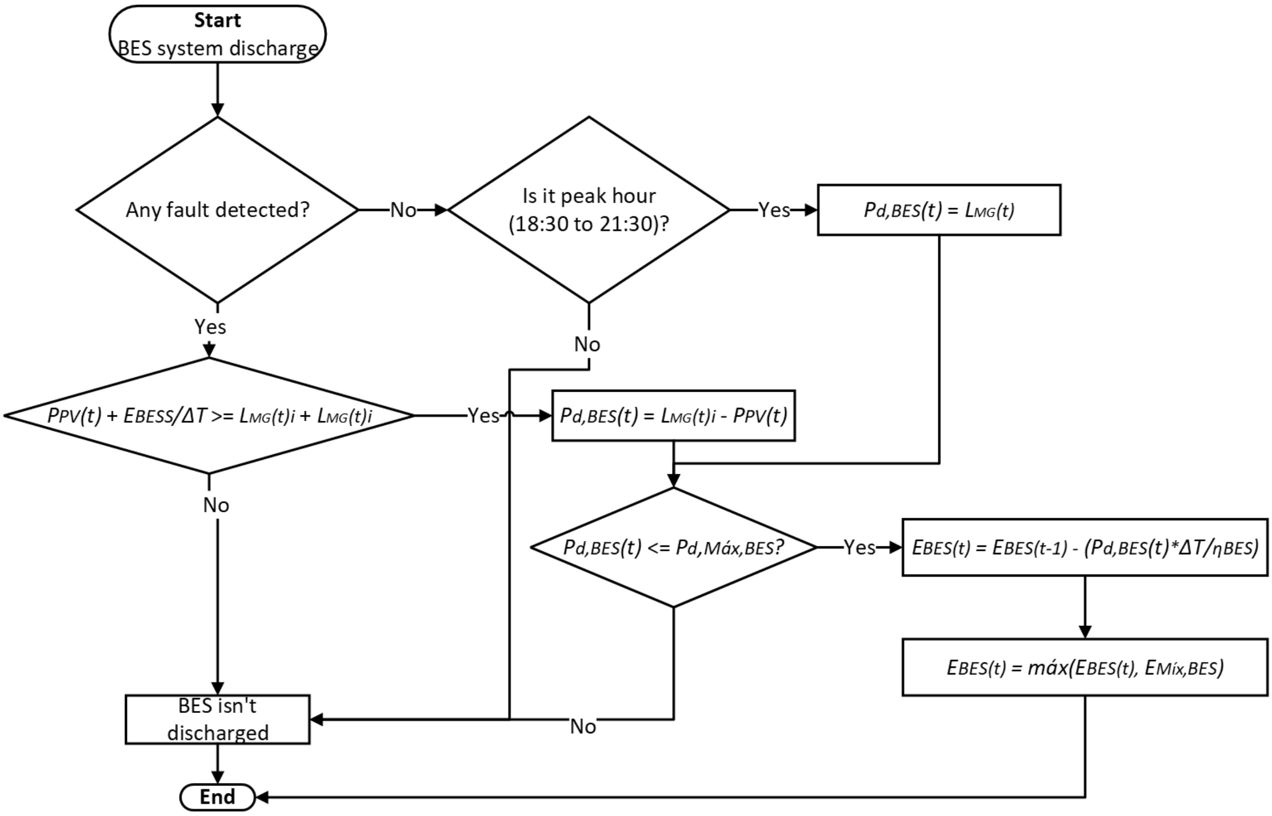

Figure 3.15: Subprocess: discharging the BES System. Source: Own authorship.

3.7 FINAL CONSIDERATIONS

This chapter presented the necessary information needed to effectively implement the proposed methodology. Firstly, elucidating the configuration of the proposed microgrids. Afterwards, a comprehensive explanation of the implemented DERs modeling is provided. Ultimately, a comprehensive explanation of the executed algorithms was provided. The subsequent chapter provides a description of the materials that will be subjected to the proposed methodology.

CHAPTER 4

MATERIALS AND PROCEDURES

4.1 INITIAL CONSIDERATIONS

This chapter provides an overview of the resources that will be used to implement the approach suggested in the methodology. It provides a detailed description of the computational tools used and the results presented in the next, which is structured into the validation of the developed code and the subsequent presentation and analysis of the case study results. The specific characteristics of the assessed load curve, climatic data, and reliability parameters employed in the simulations are presented. Lastly, the assumptions made in the case study are outlined.

4.2 COMPUTATIONAL ENVIRONMENT

This work requires identifying computational tools for the suggested method to handle a large amount of data, both as input and output. Additionally, it is important to acknowledge that the above method demands the completion of numerous simulations, including all possible scenarios. Moreover, the intricate nature of the represented select system entails a substantial computing endeavor. The Scilab software, developed by Scilab Enterprises, was used to implement the computational algorithm and meet these specifications. Additionally, Scilab, well-known for its adaptability and resemblance to MATLAB software, is freely available and open source. This approach entails conducting multiple simulations using randomly chosen parameters to examine risk and evaluate probabilities in different scenarios. Scilab's computational capabilities and adaptability make it very suitable for this task.

The data obtained from the simulations conducted in Scilab were processed and analyzed using Microsoft Excel and Python graphical tools. They enabled detailed visual analysis and made it easier to interpret the simulated results.

4.3 VALIDATION OF THE DEVELOPED CODE

This section outlines the procedures, data utilized, and anticipated format of the results validation of the developed code.

4.3.1 Procedures for Code Validation

The code validation and the methodology established to evaluate the reliability of distribution systems with DERs are conducted utilizing a problem with a known analytical solution. Despite the code containing updated variables, including PV generation, energy storage, and time-varying islanding operation, the validation test system does not integrate these variables. Nonetheless, the code must produce outcomes that are commensurate with the analytical solution, guaranteeing that, despite the updates, it remains aligned with theoretical consistency. The discrepancy between the results produced by the code and the analytical results is evaluated in percentage error.

This validation step ensures the accuracy of the base case utilized in the second phase of results, as they will serve as a benchmark for comparison with the outcomes of the modified system incorporating DERs.

4.3.2 Data employed in validation

A traditional radial distribution network, displayed in 4.1, is analyzed to validate the proposed methodology to evaluate comparable findings. Table 4.1 contains the lengths and reliability parameters of the feeder sections and distributors, while Table 4.2 presents the load data. Within the framework of this simulation, supplementary protections are implemented at the tee-point of every lateral distributor. Furthermore, it is assumed that the substation supply bus is completely reliable.

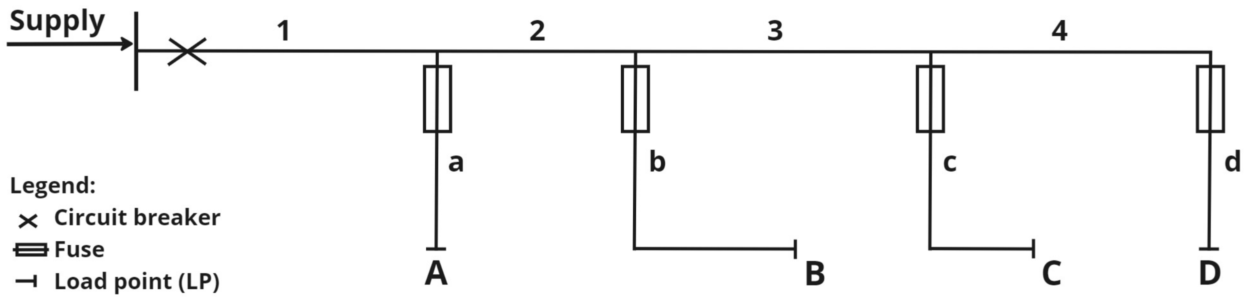

Figure 4.1: A traditional radial distribution network. Source: Own authorship.

Table 4.1: Reliability parameters for the system of Figure 4.1. Source: (BILLINTON; JONNAVITHULA, 1996).

Component	Length (km)	λ (f/yr)	r (h)
Section			
1	2	0.2	4
2	1	0.1	4
3	3	0.3	4
4	2	0.2	4
Distributor			
a	1	0.2	2
b	3	0.6	2
c	2	0.4	2
d	1	0.2	2

Table 4.2: Customers and load connected to the system of Figure 4.1. Source: (BILLINTON; JONNAVITHULA, 1996).

Load point	Number of consumers	Average load connected (MW)
A	1000	5
B	800	4
C	700	3
D	500	2

4.3.3 Presentation of validation results

The indexes employed to assess the test system are the basic indices for each load point: (i) λ; (ii) r; and (iii) U, as delineated in Equations (2.15) to (2.17), respectively. Furthermore, the systemic indices SAIFI, SAIDI, CAIDI, and ENS, delineated by Equations (2.18), (2.19), (2.20), and (2.23), respectively, are assessed. Since the ASUI, ASAI, and AENS indices can be easily deduced from the aforementioned indices, it was decided not to calculate them. Their exclusion seeks to prevent the presentation of results from being burdened with redundant data.

The analysis is conducted by examining the error percentage between the results generated by the code and the analytical results, which are displayed in two tables: one for the basic indices per load point and another for the systemic indices.

4.4 PRESENTATION AND ASSESSMENT OF THE CASE STUDY RESULTS

This section delineates the description, procedures, data employed, and expected format of the results for the case study examined in the research.

4.4.1 Case Study Description

This case study assesses a distribution system integrating distributed energy resources, including photovoltaic and battery energy storage systems. The impact of each scenario on the system reliability indices can be analyzed by starting with a base case and implementing various scenarios with different penetration levels of these resources. The systemic indices employed in this analysis are SAIFI, SAIDI, CAIDI, and ENS, defined by Equations (2.18), (2.19), (2.20), and (2.23), respectively. They are used for assessing the microgrid formation's performance during the time-varying islanding operation: (i) MGF_{Inc}; (ii) MGF_{Comp}; (iii) MGF_{fail}; and (iv) $MGF_{DERInsuf}$, specified by equations 3.9 to 3.12, respectively.

Initially, the indexes will be computed based on the feeder's original configuration. Subsequently, two microgrids will be established, with comprehensive descriptions given in subsection 4.4.3.

4.4.2 Procedures for outcome generation

Simulations are conducted separately for each microgrid to assess its impact on system reliability. Each scenario produces outcomes for both the complete feeder and the individual microgrid. By concentrating on the analysis of systemic indices that account only for the loads within the microgrid, the sensitivity of the impact is heightened, facilitating a clear depiction of the effects on both the microgrid and the feeder collectively.

4.4.3 Data employed to produce outcomes

The case study utilized a portion of an urban air distribution network operated by a utility company in Brazil's southern region. Table 4.3 presents the amount of simulated equipment, the annual peak load and the quantity of load points categorized by load type. With 7126 consumer units, the load system predominantly consists of residential loads, accounting for 87% of the total annual peak load. The information regarding the load data and length of the feeder sections is provided in Appendix A. Figure 4.2 displays the Brazilian distribution network model configuration. The substation supply bus is assumed to be fully reliable in the present arrangement.

Table 4.3: Data from the analysed brazilian distribution network. Source: Own authorship.

Parameter	**Data**	
Voltage level (kV)	13,8	
Number of lines	210	
Number of Fuses	93	
Number of Distribution transformers	93	
Number of Circuit breakers	2	
Basic annual peak load (MW)	8,211	
Number of load points	Residential	58
	Commercial	31
	Public	4

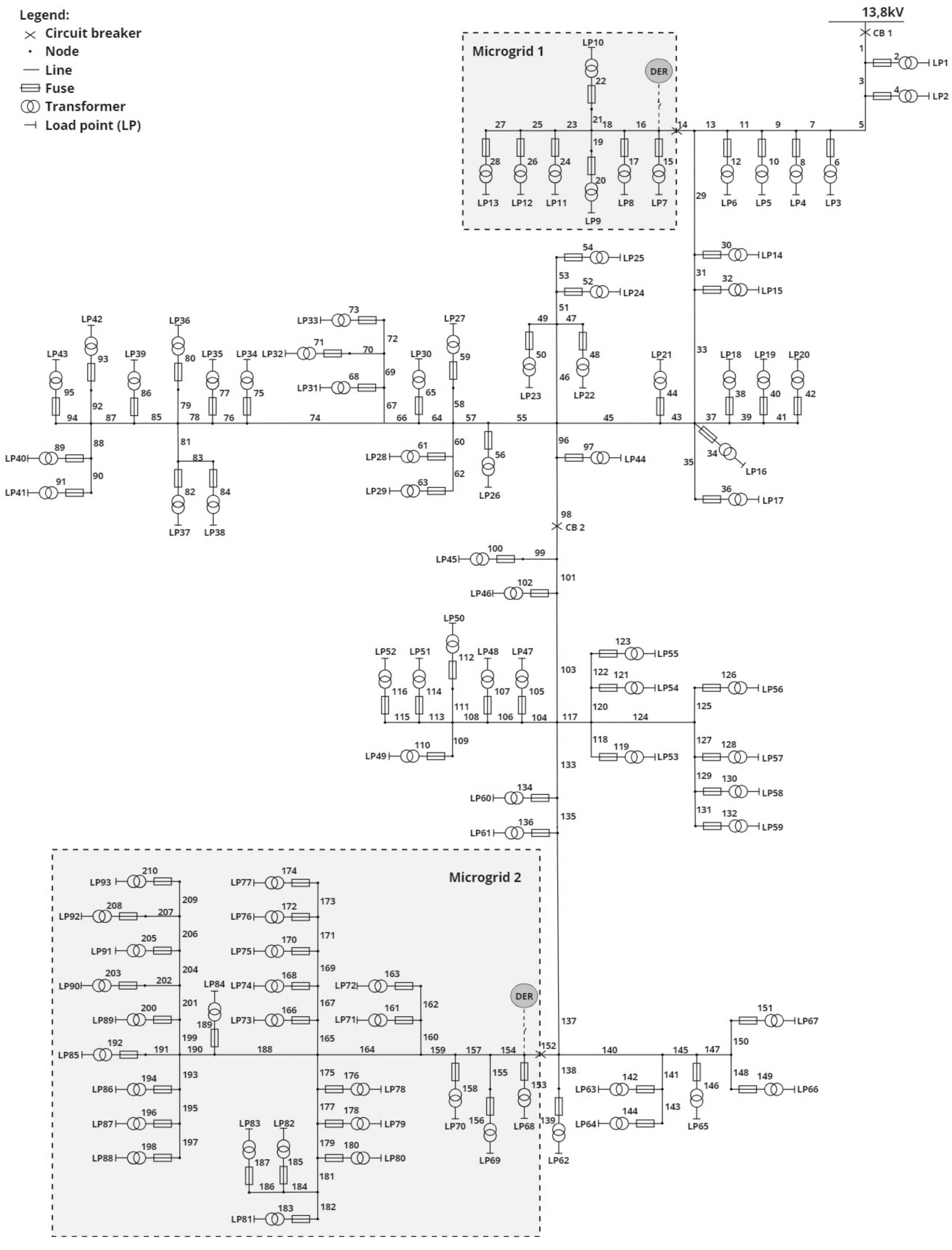

Figure 4.2: Brazilian distribution network configuration used in this study. Source: Own authorship.

In the actual distribution system, the circuit breaker labeled "CB 2", in section 98, functions as a recloser. Nevertheless, in the context of this study, the decision was made to substitute it with a circuit breaker based on specific justifications. The primary objective of the recloser is to detect electrical system malfunctions, such as short circuits or overloads, and restore power supply to the affected section of the system. If the fault is transitory and can be remedied without operator involvement, the system may be able to resume normal operation. Therefore, portraying the recloser entails the occurrence of what is known as temporary failures. To adhere to the proposed methodology, the recloser equipment in the system model was substituted with a circuit breaker, as this study exclusively examines permanent failures.

4.4.4 Graphical and numerical representations for displaying results

Different scenarios are simulated for each microgrid with many combinations of PV and BES systems. Each scenario produces index outcomes for both the microgrid and the complete feeder. The results will be illustrated in graphs, with the associated numerical values provided in tables in the appendix. Given that microgrids sizes are smaller than the complete feeder, the results will be presented per unit in the graphs, thereby enabling comparison between the two systems. Furthermore, the graphs will include an axis displaying the actual values, providing the reader a clear reference for the magnitude of the results.

4.5 LOAD MODELING

The standardized load profile utilized in this study to calculate the load of the microgrid at each specific moment, as represented by the equation (3.2) in Section 3.3.1 of the methodology, exhibits variability based on factors such as the time of day, day of the week, and week of the year. The year is represented in this load model according to the three seasons: winter, spring/autumn and summer. The development of a variable load per hour model is carried out by creating the following curves (WANG; BILLINTON, 1999; LI *et al.*, 2013):

1. Hourly load curve for weekdays and weekends expressed as a percentage of daily peak load.

2. The weekly peak load curve expressed as a percentage of the annual peak load.

3. Daily peak load curve expressed as a percentage of weekly peak load. It is assumed that the same weekly charging cycle is applicable to all seasons.

In this way, the annual standardized hourly load curve L(t), illustrated in Figure 4.3, can be developed using the equation (4.1)

$$L(t) = P_w \times P_d \times P_h(t), \tag{4.1}$$

In which:

P_w is the percentage of the weekly load in terms of the annual peak.

P_d is the percentage of daily peak load in terms of the peak weekly.

$P_h(t)$ is the percentage of the hourly load in terms of the daily load. To reach a total of 8760 hours, the average annual value is used.

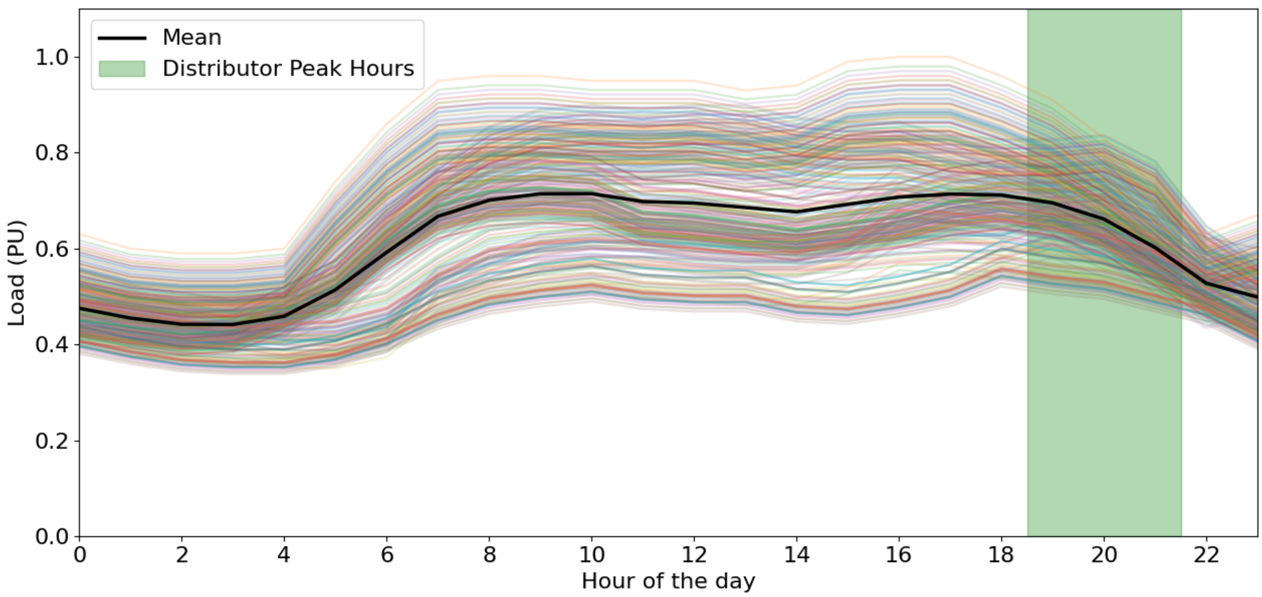

Figure 4.3: Daily load curves with average highlighted. Source: Own authorship.

In the real system used in this study, peak time was defined by the distributor for the period between 18h30 and 21h30, as illustrated in Figure 4.3. Although the load curve analysis revealed that the most frequent peak interval was in the morning period, namely from 8h to

10h, it was determined that the peak time should be maintained from 18h30 to 21h30. This decision was made since there is insufficient actual data available on the load curve of the system in question. It should be emphasized that the load curve is a versatile parameter in simulations and can be modified to suit various consumption profiles. Thus, incorporating data that is more closely aligned with the actuality of the studied system tends to enhance the precision of the obtained results.

4.6 SOLAR IRRADIATION AND TEMPERATURE

The database used is from NSRDB (National Solar Radiation Database), which uses *Physical Solar Model* from NREL (from English *National Renewable Energy Laboratory*) to provide hourly meteorological data or every 30 min. "The data period used is from 2019 to 2022 for a city in Brazil, with the specific location withheld to preserve the image of the distribution company, during which the monthly average daily solar irradiation I_{rr} is equal to 3,34 kWh/m^2/day.

Figure 4.4 illustrates the representation of the standardized daily photovoltaic generation profiles drawn at each simulation period, according to the description provided in 3.4.1. Each plotted curve corresponds to a single day within the analyzed period.

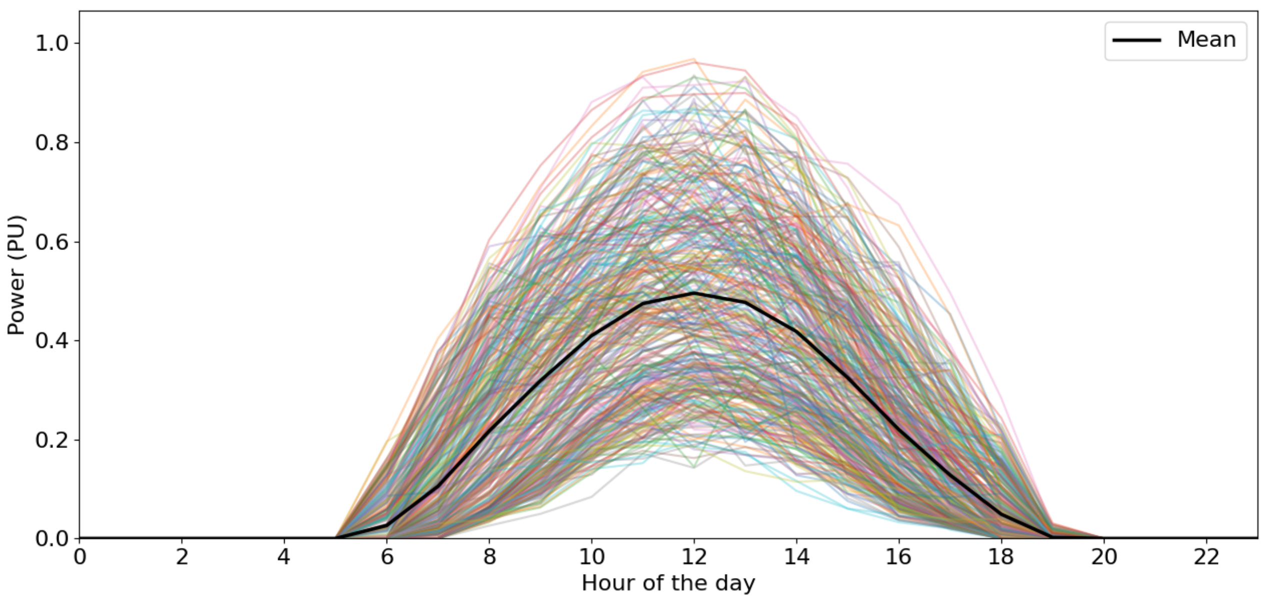

Figure 4.4: Daily irradiance nominal global incident for the City region, with average highlighted. Source: Own authorship.

4.7 RELIABILITY PARAMETERS

It is normally found in practice that lines and cables have a failure rate that is approximately proportional to their length (BILLINTON; ALLAN, 1996). The reliability parameters are shown in Table 4.4.

Table 4.4: Reliability parameters. Source: (ALLAN *et al.*, 1991).

Equipment	**Failure Rate (oc./km/year)**	**Repair Rate (h/year)**
Line (33 kV)	0.065	8
Line (11 and 13.8 kV)	0.065	5
Transformer (13,8 kV/0,38 kV)	0.015	10
Circuit breaker (33 kV)	0.002	4
Circuit breaker (11 and 13.8 kV)	0.006	4

4.8 ADOPTED HYPOTHESES

Below are the hypotheses adopted in this study.

a. This study evaluates the reliability of the power system in terms of adequacy, specifically to assess if the system contains adequate facilities to meet consumer load demand. Therefore, the simulations do not include dynamic and transient disturbances, as the focus is on the static conditions of the system, to support long-term operational planning studies. Following this approach, the study focuses on the quality of service of the electricity supply by analyzing continuity indexes. Aspects related to the quality of the product, i.e., the electricity itself, are not analyzed.

b. The research examines the concept of community energy schemes, wherein DER are collectively owned, and the generated energy is distributed among members;

c. The present study focuses solely on permanent faults, which are characterized by their repeatability and indefinite duration until they are repaired;

d. By presuming that electrical distribution networks have the ability to reconfigure themselves according to the operational requirements of time-varying islanding operation, it is assumed that the protection system is capable of dealing with the challenges of bi-directional power flow and intermittent characteristics resulting from the penetration of renewable sources;

e. In this research, the systems are depicted in a linear arrangement, and it is presumed that any fault, whether it is a single-phase fault or not, will cause all three phases to trip;

f. The failure and repair rates are assumed to be exponential;

g. Even though the loads follow a time-based load curve, they are classified as fixed. Each load at each load point must be fully met, with no possibility of changing their energy usage based on the availability or cost of energy;

h. The sizing of the BES and PV systems takes into account the data provided in the Appendix B;

i. Physical space is considered to be unlimited for the installation of BES and PV systems within the microgrid;

j. The proposed methodology enables the allocation of DER within the microgrid area in a concentrated and/or distributed manner. The likelihood of a substation failure coinciding with a failure within the microgrid is deemed to be minimal. In addition, considering the possibility of failures in the microgrid nodes, as demonstrated in sub-section 3.3.1, where the islanding operation is not possible in this particular context, the decision was made to simulate the DER as concentrated.

CHAPTER 5

RESULTS AND DISCUSSION

5.1 INITIAL CONSIDERATIONS

The methodology outlined in Chapter 3 was implemented on the materials outlined in Chapter 4, utilizing a maximum coefficient of variation (β) of 5% as a criterion for stopping simulations with varying scenarios. The chapter outlines the process of validating the code by applying it to the test system. Additionally, it offers an analysis of the technical implications that arise from integrating microgrids comprising BESS with PV systems in a Brazilian real distribution network topology. To achieve this objective, two distinct locations were chosen to implement microgrids, considering their size and proximity to the substation.

5.2 APPLICATION TO THE TEST SYSTEM

The computational simulation was used to compute the mean values of the load point and system indices, which were then compared to the analytical results described in reference (BILLINTON; ALLAN, 1996). To obtain a closer approximation of the actual value, a β coefficient of 1% was employed. Table 5.1 presents the load point indices, while Table 5.2 presents the mean values of the system indices for both approaches.

Table 5.1: Test System load point indices compared to (BILLINTON; ALLAN, 1996) results. Source: Own authorship.

Ld. point	**λ (f/yr)**			**r (h)**			**U (h/yr)**		
	(A)	**(S)**	**Rel. error (%)**	**(A)**	**(S)**	**Rel. error (%)**	**(A)**	**(S)**	**Rel. error (%)**
A	0.996	1.00	0.38	3.64	3.57	1.88	3.60	3.54	1.66
B	1.40	1.39	1.04	3.07	3.11	-1.39	4.40	4.30	2.28
C	1.20	1.19	0.83	3.15	3.28	-4.10	4.00	3.92	1.95
D	1.00	0.997	0.28	3.61	3.58	0.94	3.60	3.54	1.67

The abbreviation (A) stands for analytical data, while (S) stands for simulated data.

The results derived from the simulation, as shown in Tables 5.1 and 5.2, demonstrate a

Table 5.2: Comparison of the system indices in the Test System with (BILLINTON; ALLAN, 1996) results. Source: Own authorship

Indices	**Analytical**	**Simulated**	**Relative error (%)**
SAIFI (oc./yr)	1.15	1.15	0.40
SAIDI (h/yr)	3.91	3.83	2.00
CAIDI (h/oc.)	3.39	3.35	1.32
ASAI (%)	99.96	99.96	0.00
ENS (MWh/yr)	54.80	53.75	1.92

significant level of similarity to the analytical techniques. The load point C exhibits the highest difference in indices, with a maximum value of -4.10% for the load point average outage duration (r). The system indices have a maximum error of 2.00% for SAIDI. Thus, it can be inferred that the outcomes from the proposed methodology, which employs Monte Carlo simulation are consistent with those obtained from theoretical analysis.

5.3 CASE STUDY: BRAZILIAN DISTRIBUTION NETWORK

Two microgrids of different sizes and distances from the substation are considered for the impact analysis of DERs on service quality. The simulation incorporates microgrids with diverse characteristics and spatial placements to assess the influence of these variables on the network's reliability. It provides a more comprehensive and authentic perspective of the operational conditions in real-life situations. The microgrids are depicted in Figure 4.2, while Table 5.3 provides supplementary details.

Table 5.3: Information for the selected microgrids. Source: Own authorship.

Information	**Microgrid 1**	**Microgrid 2**
Distance from substation (km)	1,8712	2,5802
Number of consumers	363	1995
Annual peak load (MW)	0,2468	1,7911
Average annual load (MW)	0,1357	1,0012
Average daily consumption (MWh)	3,2573	24,0295

The total PV power and total capacity of the BESS installed for each microgrid are detailed in Table 5.4, organized by penetration level.

Table 5.4: The total PV power and storage capacity of BES in each microgrid, considering the Penetration Levels Grouping, for all penetration levels. Source: Own authorship

pen	**Microgrid 1**		**Microgrid 2**	
	P_{PV} [MW]	**E_{BES} [MWh]**	**P_{PV} [MW]**	**E_{BES} [MWh]**
10%	0.1362	0.4789	0.9887	3.4759
25%	0.3405	1.1972	2.4716	8.6897
50%	0.6810	2.3944	4.9433	17.3795
75%	1.0216	3.5916	7.4149	26.0692
100%	1.3621	4.7888	9.8865	34.7590

5.4 SIMULATION CONDITIONS

To highlight the importance of incorporating DERs, a sensitivity analysis is conducted for each microgrid in twenty distinct scenarios of DERs deployment, as illustrated in Table E.2. The size of the BESS is adjusted at fixed levels of solar PV penetration, ranging from 0% to 100%, in increments of 25%. It is considered that when aggregated PV systems are installed, aggregated BESS are also deployed. The penetration of BESS never exceeds that of PV systems. All of these case studies are regarded to be impractical.

Table 5.5: Case studies performed. Source: Own authorship

Case Studies		**BESS-pen**					
		0%	**10%**	**25%**	**50%**	**75%**	**100%**
PV-pen	**0%**	Base case	Impractical case	Impractical case	Impractical case	Impractical case	Impractical case
	10%	PV 10% BESS 0%	PV-10% BESS-10%	Impractical case	Impractical case	Impractical case	Impractical case
	25%	PV 25% BESS 0%	PV 25% BESS 10%	PV 25% BESS 25%	Impractical case	Impractical case	Impractical case
	50%	PV 50% BESS 0%	PV 50% BESS 10%	PV 50% BESS 25%	PV 50% BESS 50%	Impractical case	Impractical case
	75%	PV 75% BESS 0%	PV 75% BESS 10%	PV 75% BESS 25%	PV 75% BESS 50%	PV 75% BESS 75%	Impractical case
	100%	PV 100% BESS 0%	PV 100% BESS 10%	PV 100% BESS 25%	PV 100% BESS 50%	PV 100% BESS 75%	PV 100% BESS 100%

The information regarding the input parameters utilized is provided in Appendix B. The subsequent sections give the case studies that were analyzed. Appendix E presents the simulation times for each combination of PV (PV-pen) and BESS (BESS-pen) penetration across each microgrid.

5.5 ASSESSMENT OF TECHNICAL IMPACTS

This section provides the results of the adequacy assessment on distribution systems when microgrids consisting of PV and BESS are implemented.

The results of the effects on the distribution adequacy indices are presented in subsection 5.5.1, while subsection 5.5.2 especially evaluates the indexes of the microgrids. The outcome data are presented in graphical form, facilitating individual analysis of the impacts of implementing PV systems separately and in combination with BESS. Data presented in tabular form can be found in Appendix D.

5.5.1 Distribution Adequacy Indices

The following graphs depict the system adequacy index for the microgrid and the complete feeder outcomes. An axis with values per unit (PU) values was implemented to compare the microgrid and the system, which have different scales. A second axis with the associated real values is also presented, provided only as a reference.

5.5.1.1 System Average Interruption Frequency Index (SAIFI)

Figure 5.1 illustrates the variability in the SAIFI index resulting from the rise in penetration of both PV and PV combined with BESS.

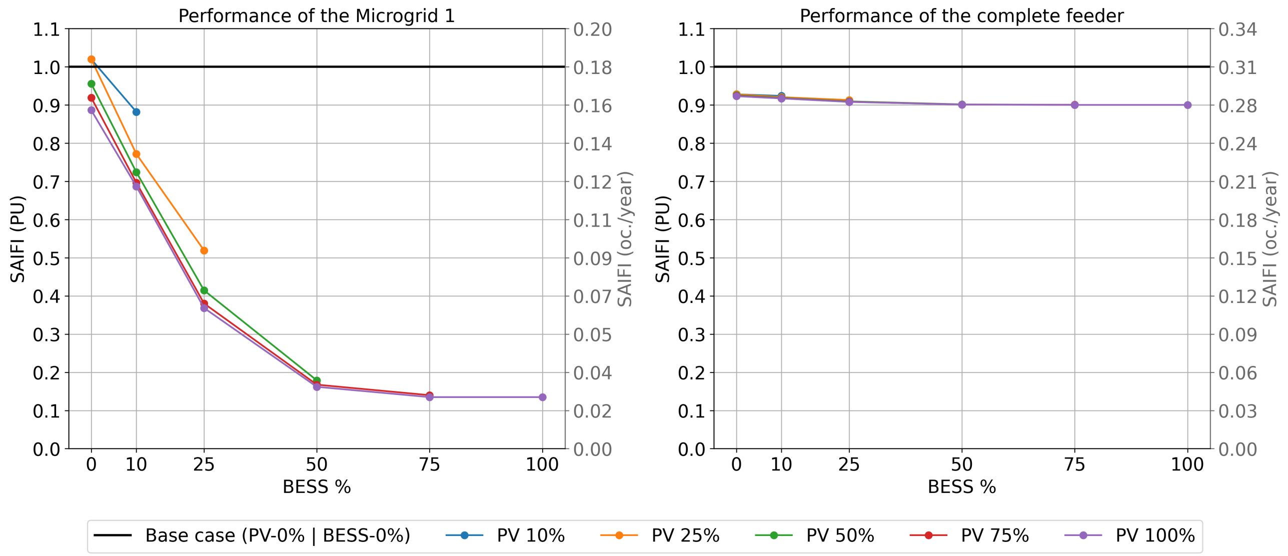

a. The impacts of implementing microgrid 1.

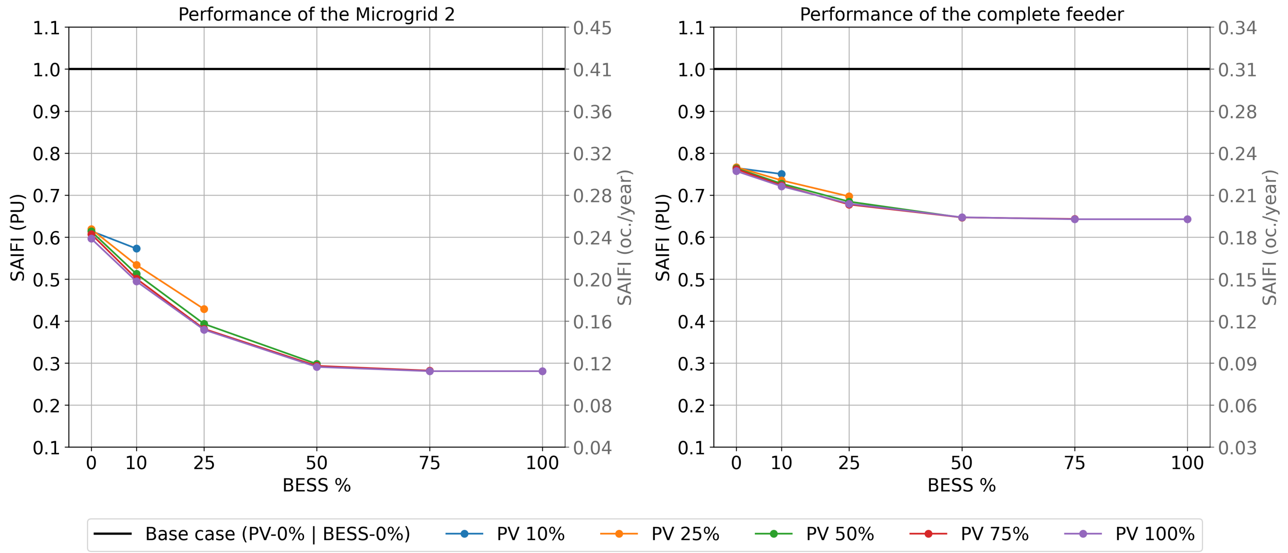

b. The impacts of implementing microgrid 2.

Figure 5.1: Impact of BESS and PV penetration level on the SAIFI index. Source: Own authorship.

From Figure 5.1, it is possible to observe an enhancement in the frequency of interruptions for an average consumer compared to the base case, except for the PV-10% | BES-0% and PV-25% | BES-0% scenarios of microgrid 1. The value exhibited a positive variation of +1.98% in both cases relative to the base case. Repeating the simulations for these two scenarios with a β coefficient of 3% generated results of 0.1977 for the base case, 0.1957 for PV-10% | BES-0%, and 0.1921 for PV-25% | BES-0%. This indicates a slight improvement in these scenarios compared to the base case; however, the magnitude was insufficient for a beta of 5% to detect it.

The influence of the coefficient of variation is relevant solely to microgrid 1, as the index SAIFI experiences minimal impact when only the inclusion of the PV system is considered. The impact on microgrid 2 is considerably more pronounced, exhibiting a minimum difference of -38.08%. This illustrates that the microgrid's size directly affects the index, particularly when only a PV system is incorporated.

An analysis of the increase in PV system penetration reveals a diminished impact on the index SAIFI. The maximum variation between the scenarios that solely modify PV system penetration is -13.3% in microgrid 1 and -2.28% in microgrid 2. The results suggest that, despite ample PV output availability during specific periods, system reliability may not be markedly enhanced without sufficient storage.

In situations with a fixed PV system and fluctuating BES penetration, the maximum value variations were -13.75%, -50.05%, -77.64%, -77.90%, and -75.17% for PV settings of 10%, 25%, 50%, 75%, and 100%, respectively, in microgrid 1. For microgrid 2, adhering to the same sequence, the maximum variations were -4.17%, -19.04%, -31.58%, -32.51%, and -31.55%.

The overall impact on the feeder is less significant than those observed within the microgrids. The maximum variation between scenarios adjusting only PV penetration for the feeder was -7.22% when incorporating microgrid 1 and -23.52% when incorporating microgrid 2. In cases where the PV system remains fixed and BES penetration fluctuates, the maximum variations when incorporating microgrid 1 were -0.41%, -1.48%, -2.39%, -2.38%, and -2.30% for PV levels of 10%, 25%, 50%, 75%, and 100%, respectively. When incorporating microgrid 2, following the same PV sequence, the maximum variations were -1.47%, -6.99%, -11.71%, -11.87%, and -11.44%. This indicates that smaller microgrids tend to have a lesser impact on the feeder overall.

The significant decrease in the SAIFI index, depicted in Figure 5.1 following the implementation of the BESS, correlates with the variable islanding operation over time, which optimizes the irregular availability of the PV source throughout the day. Following a 50% penetration of the BESS, it is observed that the index stabilizes due to the stability of the SoC, which diminishes the likelihood of abrupt declines.

Figure 5.2 illustrates the boxplot depicting the variation in SoC resulting from heightened BESS integration, with PV maintained at 100%, for microgrid 1.

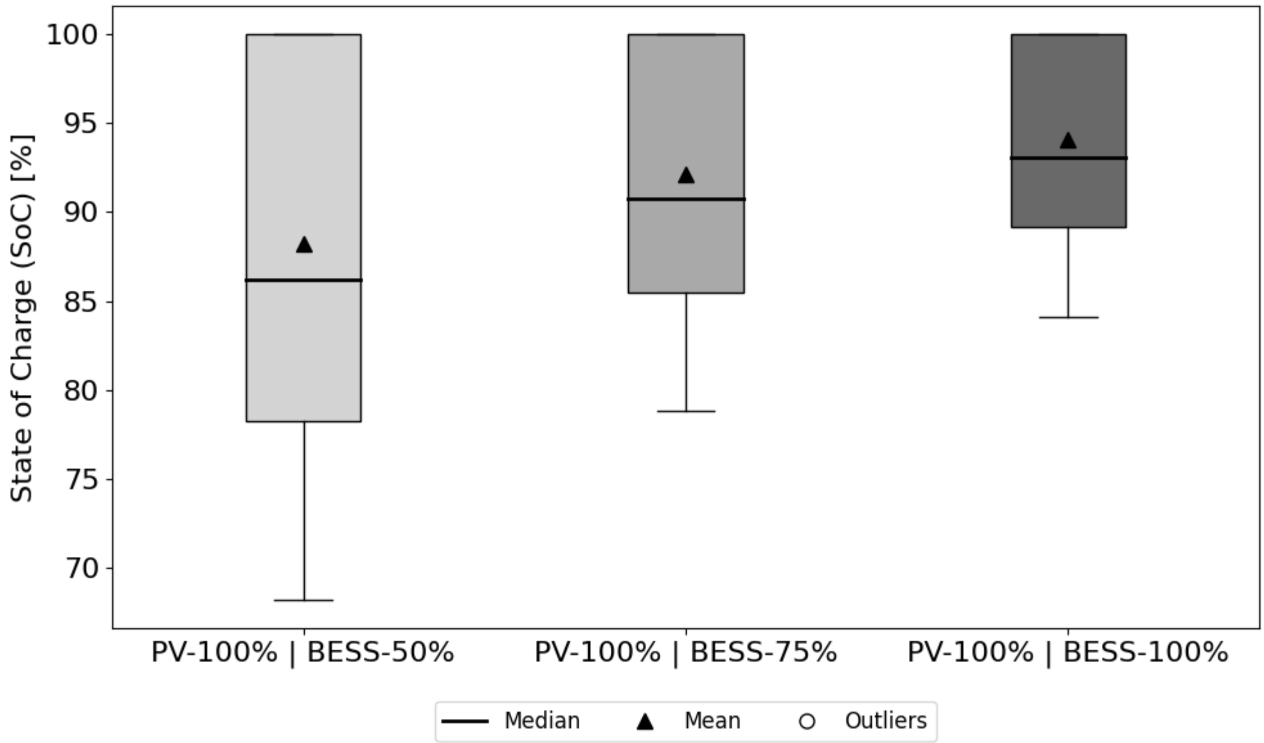

Figure 5.2: Distribution of state of charge (SoC) in percentage for three scenarios: PV-100% | BESS-50%, PV-100% | BESS-75%, and PV-100% | BESS-100%. Source: Own authorship.

In the 50% penetration scenario, the median is approximately 85%, meaning half of the SoC values are below and half are above this threshold. The interquartile range, spanning from the 1st to the 3rd quartile, fluctuates between 80% and 100%, indicating a broad distribution of values. Despite the absence of outliers, the SoC can attain minimum levels of approximately 70%, indicating increased variability in this context, characterized by more significant declines in the SoC.

In the 75% and 100% penetration scenarios, the median hovers around 90%, suggesting that enhanced storage capacity does not significantly change the fundamental SoC level. The interquartile range in the 75th percentile scenario is marginally smaller than in the 50th, suggesting reduced variability. The variation is marginally reduced in the 100% scenario indicating a more stable SoC.

5.5.1.2 System Average Interruption Duration Index (SAIDI)

Figure 5.3 exhibits the variability in the SAIDI index due to the increase in penetration of both PV and PV combined with BESS.

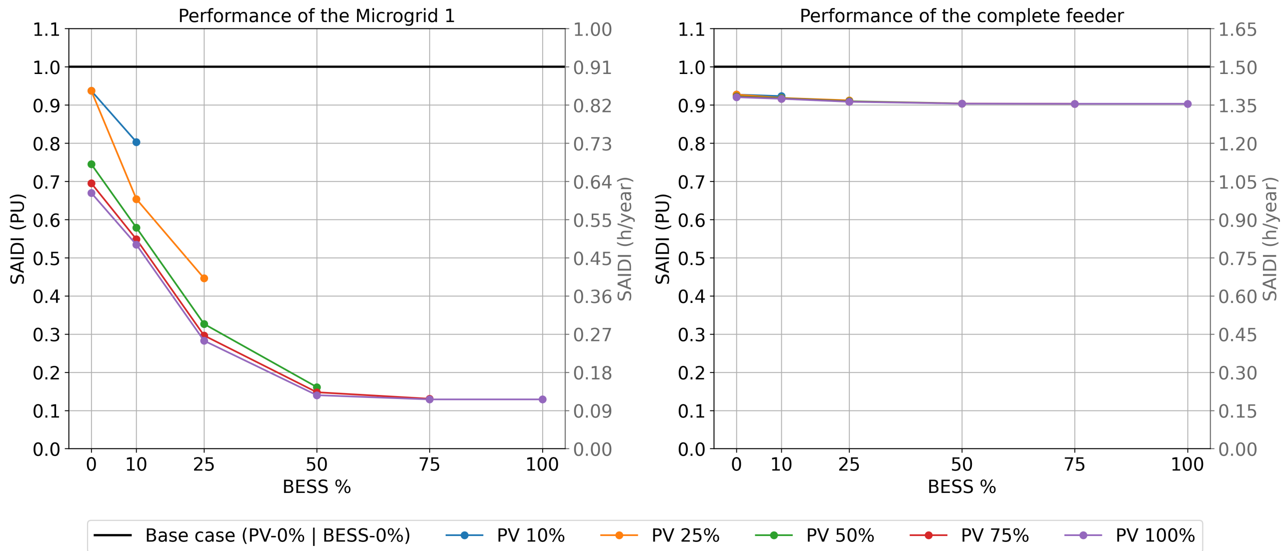

a. The impacts of implementing microgrid 1.

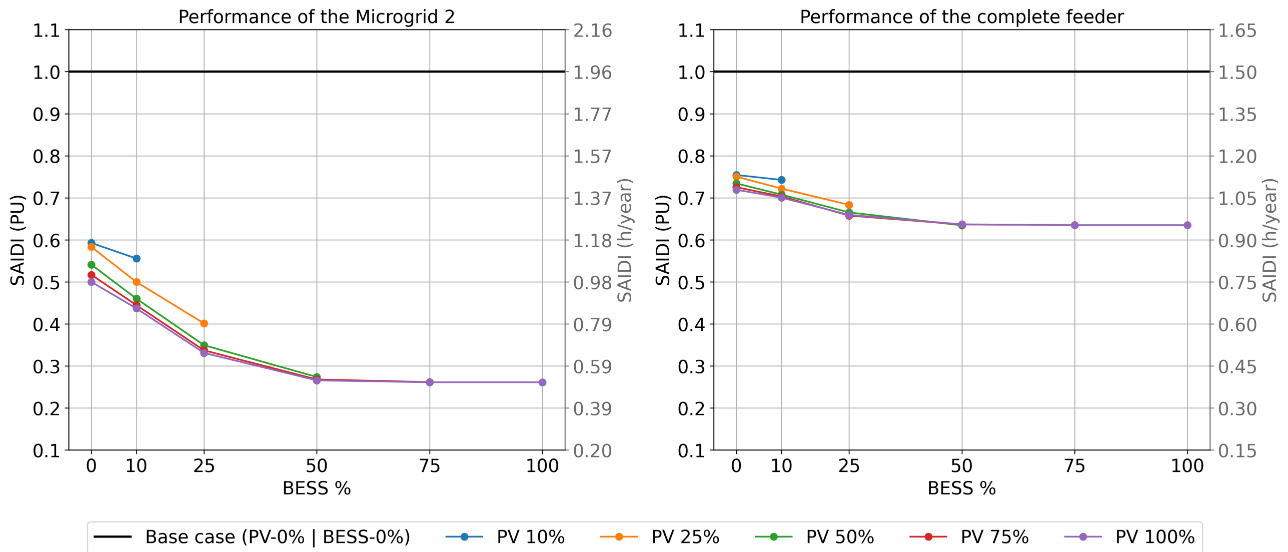

b. The impacts of implementing microgrid 2.

Figure 5.3: Impact of BESS and PV penetration level on the SAIDI index. Source: Own authorship.

Figure 5.3 corroborates the previously mentioned trend, indicating that the SAIDI index exhibits enhancement across all analyzed scenarios relative to the baseline case for both microgrids and the complete feeder. This behavior, similar to the SAIFI index, is substantiated by the concept that SAIDI is a linear combination of annual interruption durations, which are dependent upon component repair times and the number of consumers per load point.

It is evident that when only the PV penetration is altered, the points on the graph appear to overlap or remain nearby, indicating minimal or negligible variations. This suggests that the solitary rise in PV penetration does not produce substantial enhancements in the total number of hours of interruption that an average customer experiences.

Conversely, when the BESS penetration is altered, the graph tends a curve, particularly up to the 50% penetration level, where more pronounced declines manifest with varying slopes between the points. Beyond the 50% range, the index stabilizes, exhibiting an almost linear behavior, attributable to the stabilization of the SoC depicted in Figure 5.2.

The comparatively minor effect on the complete feeder index, in contrast to the more pronounced effect on microgrid 1 — smaller than microgrid 2 — indicates that the impact decreases as the system becomes larger, applicable to both the microgrid and the complete feeder.

5.5.1.3 Customer Average Interruption Duration Index (CAIDI)

The graph in Figure 5.4 displays the variation in the CAIDI index as the penetration of both PV and PV combined with BESS increases.

The CAIDI index represents the mean duration for service restoration and is mathematically correlated with the SAIFI and SAIDI indexes. While SAIFI and SAIDI exhibit analogous behaviors, the CAIDI index demonstrated distinct performance attributable to its non-linear correlation with failure and repair durations, according to Eq. (2.20).

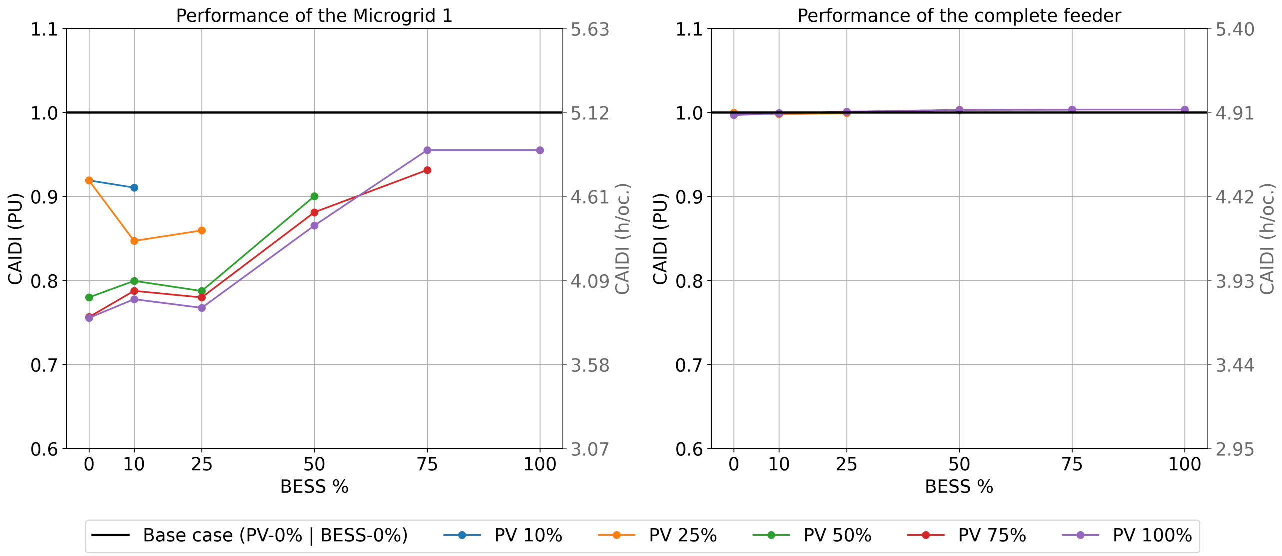

a. The impacts of implementing microgrid 1.

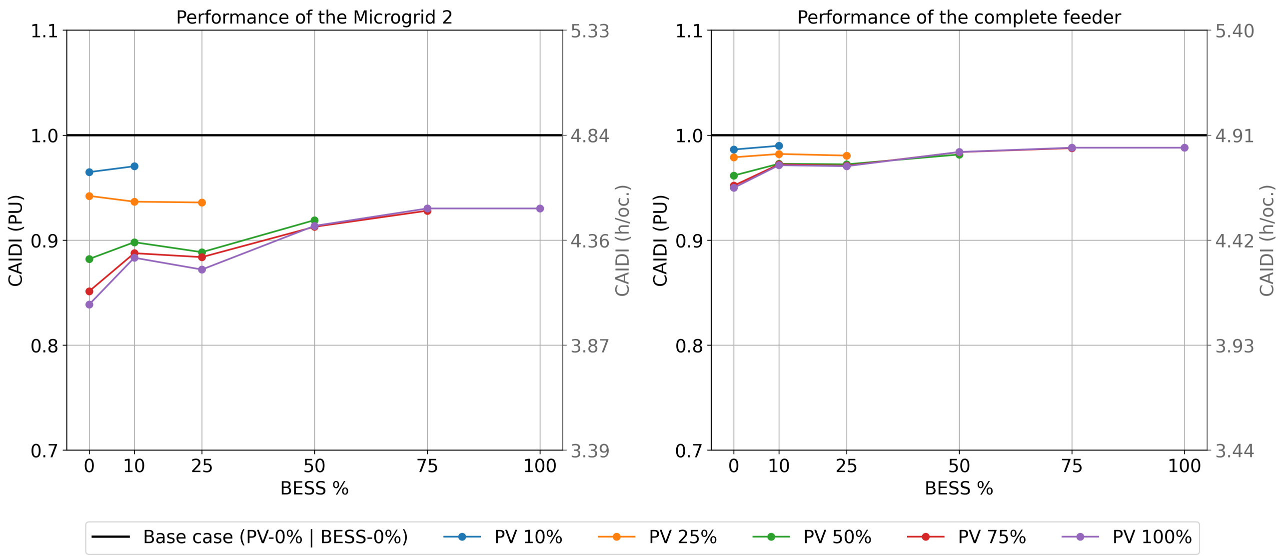

b. The impacts of implementing microgrid 2.

Figure 5.4: Impact of BESS and PV penetration level on the CAIDI index. Source: Own authorship.

Overall, in microgrids, the mean duration of customer outages does exhibit substantial enhancements relative to the baseline scenario. Nonetheless, a trend of enhanced stability in the index is noted as BESS penetration increases, with no significant progress beyond 50%.

The general impact of implementing microgrid 1 on the complete feeder is negligible, as the average outcomes of the scenarios closely resemble the baseline value. Microgrid 2, larger than microgrid 1, exhibits a more pronounced impact.

Analysis of the impact on microgrids reveals that all of the proposed scenarios lead to results surpassing the baseline case, which suggests an improvement in the system's capacity to respond to failures. Results were more irregular, exhibiting significant variations, up to 25% BES penetration. Subsequently, there was continuous growth that stabilized upon achieving 75% penetration.

To understand this non-linear behavior of the CAIDI index, the impact of the DERs analyzed in this study on the duration of the failure state in the microgrids was examined. The load point 68 within microgrid 2 was chosen to monitor this variable. This location was selected based on its closeness to the DER installations, a factor that affected the prioritization in the variable islanding operation. It is worth noting that the developed algorithm provides flexibility in load prioritization, allowing adjustments based on the relative significance of the load points within the analyzed system.

Figure 5.5 depicts the distribution of durations in the failure state through a histogram, overlaid with the Kernel Density Estimate (KDE) curve, that provides a smooth representation of the distribution. The varied colors indicate the different scenarios, each exhibiting 100% PV penetration and differing levels of BES penetration.

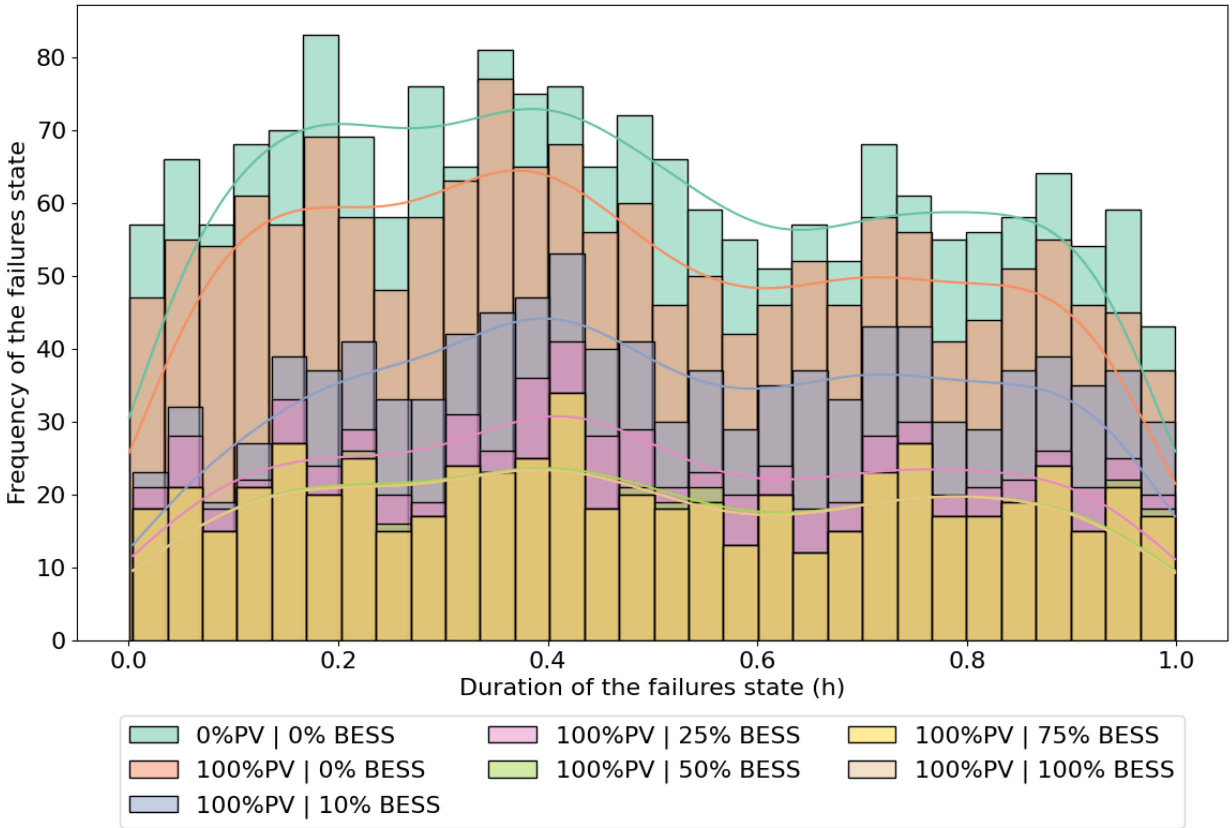

Figure 5.5: Histogram with Kernel Density Estimation (KDE) for the variable duration in the failure state for the LP 68, accounting for scenarios with 100% photovoltaic penetration and varying levels of battery energy storage penetration. Source: Own authorship.

Figure 5.5 reveals that incorporating of BESS has resulted in a decrease in the number of faults impacting LP 68, especially those with a duration of less than 0.4. In this range, there is a greater dispersion between the scenario without battery and the scenarios with battery, characterized by notable variations in the heights of the stacked bars and the smoothing lines.

Nonetheless, despite the decrease in the total number of faults, as evidenced by the SAIFI index, the residual faults generally exhibit prolonged durations. The CAIDI index rises due to the battery's inability to sustain the supply over a prolonged period.

5.5.1.4 Energy Not Supplied (ENS)

In Figure 5.6, the variation in the ENS index is shown as the penetration of both PV and PV combined with BESS increases.

As previously discussed, the SAIFI and SAIDI indices exhibited analogous behavior, which is also evident in the ENS index, that pertains directly to them and which refers to the quantity of energy that was expected to be supplied but wasn't, owing to disruptions in the distribution system.

Based on the findings, all scenarios demonstrate beneficial effects relative to the baseline, valid for both microgrids and the complete feeder. Nonetheless, this effect is relatively reduced in the complete feeder and becomes increasingly negligible as the microgrid's size diminishes.

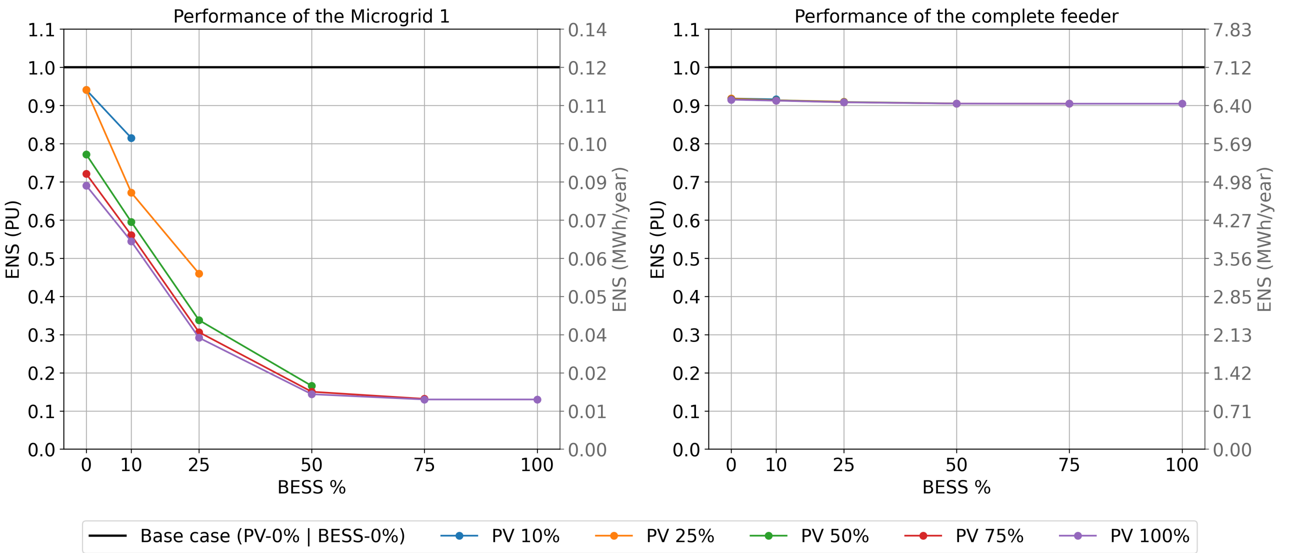

a. The impacts of implementing microgrid 1.

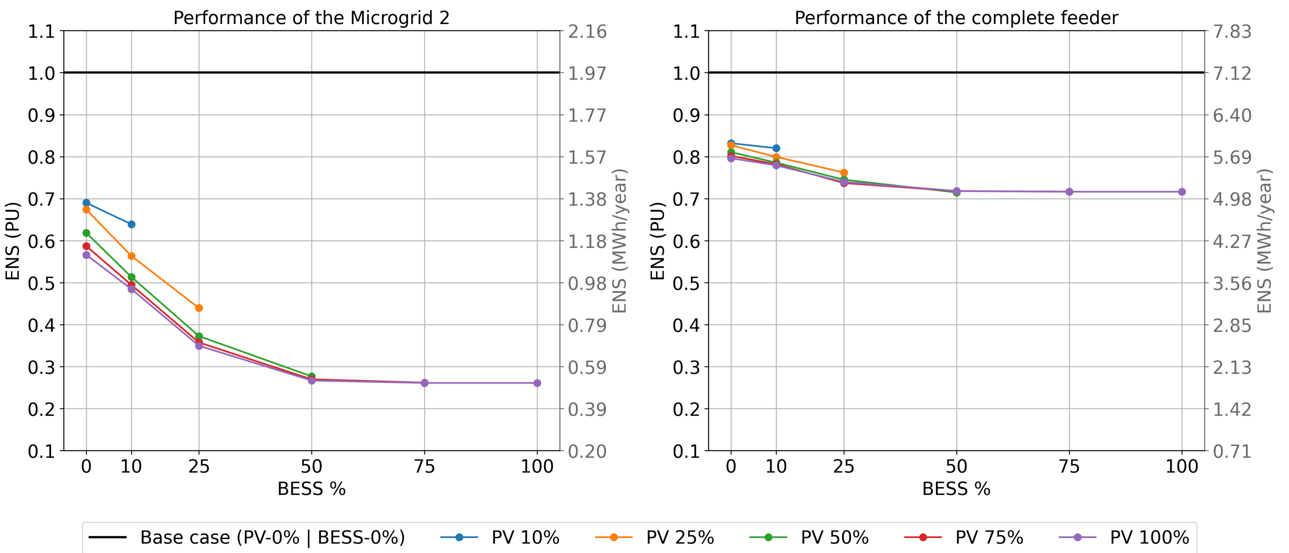

b. The impacts of implementing microgrid 2.

Figure 5.6: Impact of BESS and PV penetration level on the ENS index. Source: Own authorship.

The analysis reveals that, across the three indices, the dimensions of the microgrid significantly influence decrease rates as the integration of BESS increases, as well as the initial values up to 50% penetration of BESS. Consequently, it can be deduced that a larger microgrid results in a more gradual enhancement in performance indices, corresponding to a more stable behavior with the increased integration of DERs.

5.5.2 Microgrid Formation Indices

The application of equations 3.9 to 3.12 enabled the calculation of the values of the indices that assess the microgrid arrangements during time-varying islanding operations. Figure 5.7 displays the variation of the indexes for the PV and BESS, categorized by penetration level scenario.

Figure 5.7 illustrates that, in scenarios characterized by low penetrations of PV and BESS, the inability to establish microgrids due to inadequate resources constitutes a significant portion of potential occurrences during islanding operations. This indicates an increased incidence of system failures, as demonstrated by the findings of the SAIFI index in subsection 5.5.1.1.

With the rise of BES penetration, particularly exceeding 50%, there is a notable and incremental increase in the establishment of fully operational microgrids, which can fulfill 100% of the load demands. The findings indicate that enhanced energy storage levels augment microgrid performance, thereby reducing the number of consumers impacted during outages. This fact underscores the significance of energy storage in alleviating issues associated with photovoltaic generation and ensuring energy supply reliability.

Nonetheless, as indicated by prior results, in scenarios where BESS penetration exceeds 50%, the advantages regarding the full establishment of microgrids and reliability become insignificant, implying that further benefits stagnate beyond this threshold.

The incidence of microgrid non-formation due to internal failures remains consistent across various scenarios. This stems from the time-varying islanding operation employed in this study, which prevents enabling islanding if the fault that initiated the failure originated within the microgrid itself. Moreover, the Monte Carlo simulations employed the same random seed across all scenarios, thereby maintaining uniform stochastic conditions and permitting only the variables of interest, such as BESS and PV penetrations, to be systematically modified. The likelihood of failure at load points remains uniform across scenarios, with variations solely in the power supply conditions. This enables a direct and equitable comparison, ensuring that result variations stem from controlled model changes, while also validating the method for reproducibility and consistency of outcomes.

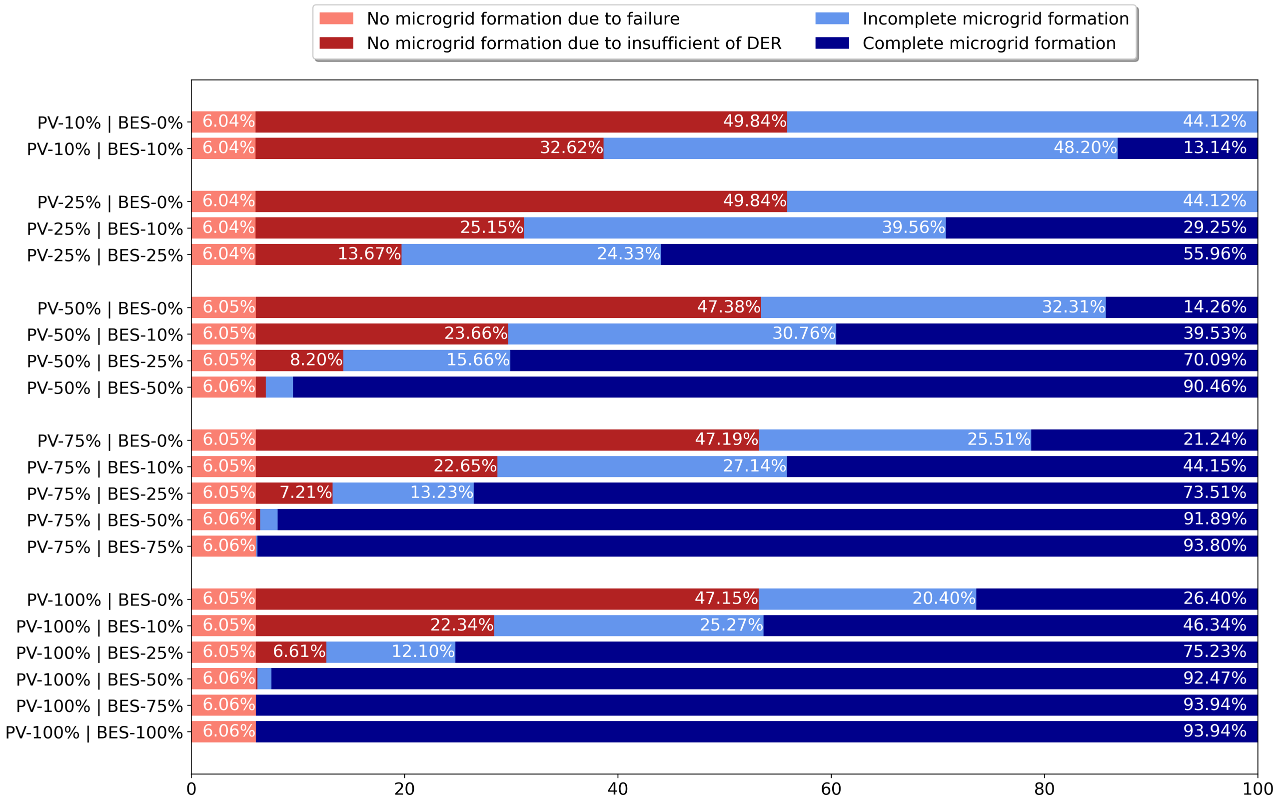

a. The impacts of implementing microgrid 1.

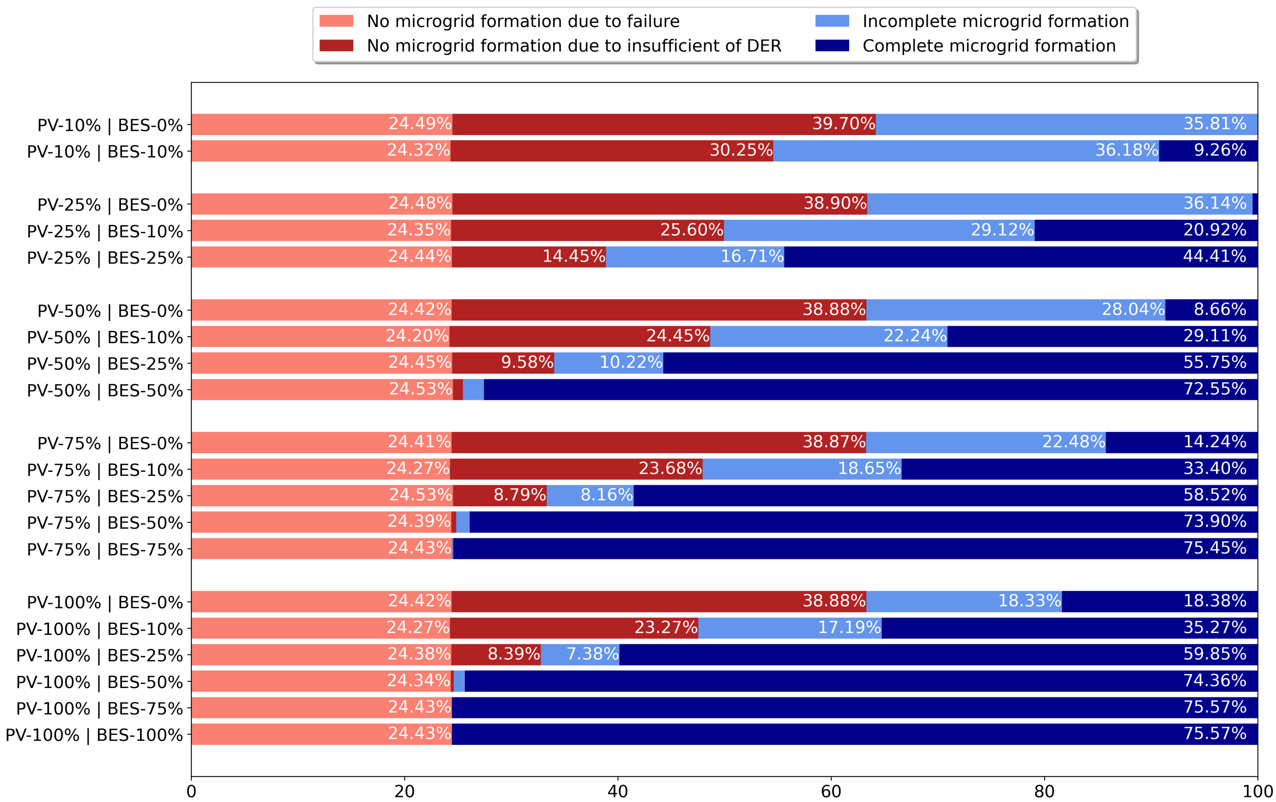

b. The impacts of implementing microgrid 2.

Figure 5.7: Impact of BESS and PV penetration level on the Microgrid formation indices. Source: Own authorship.

A graph depicting the percentage change in interrupted load and operating time of micro-grids, on island mode operating scenarios is shown in Figure 5.8.

Figure 5.8 illustrates a directly proportional relationship between the interrupted load and the operational duration of the microgrid, regardless of whether it is fully or partially formed. As BESS penetration escalates, both indices consistently enhance until attaining 50% BES. Subsequently, the advantages become minimal, indicating a saturation of BES benefits at elevated levels, with negligible additional variation.

The observed intersection is not merely a crossover point, but a significant milestone of mutual enhancement between the two indices. This underscores the notion that both parties gain proportionately from the rise in BESS penetration, although with diminished benefits beyond 50%. The results highlight the significance of flexibility in islanded operation, employing time-varying islanding to enhance the utilization of loads and available DER during failure scenarios.

This analysis underscores the essential function of storage systems in ensuring the reliability of distribution networks, particularly in microgrids characterized by a significant integration of intermittent DERs. Consequently, the operational strategy of BESS requires meticulous analysis, and the strategic expansion of DERs is essential to achieve stable and cost-efficient reliability improvements.

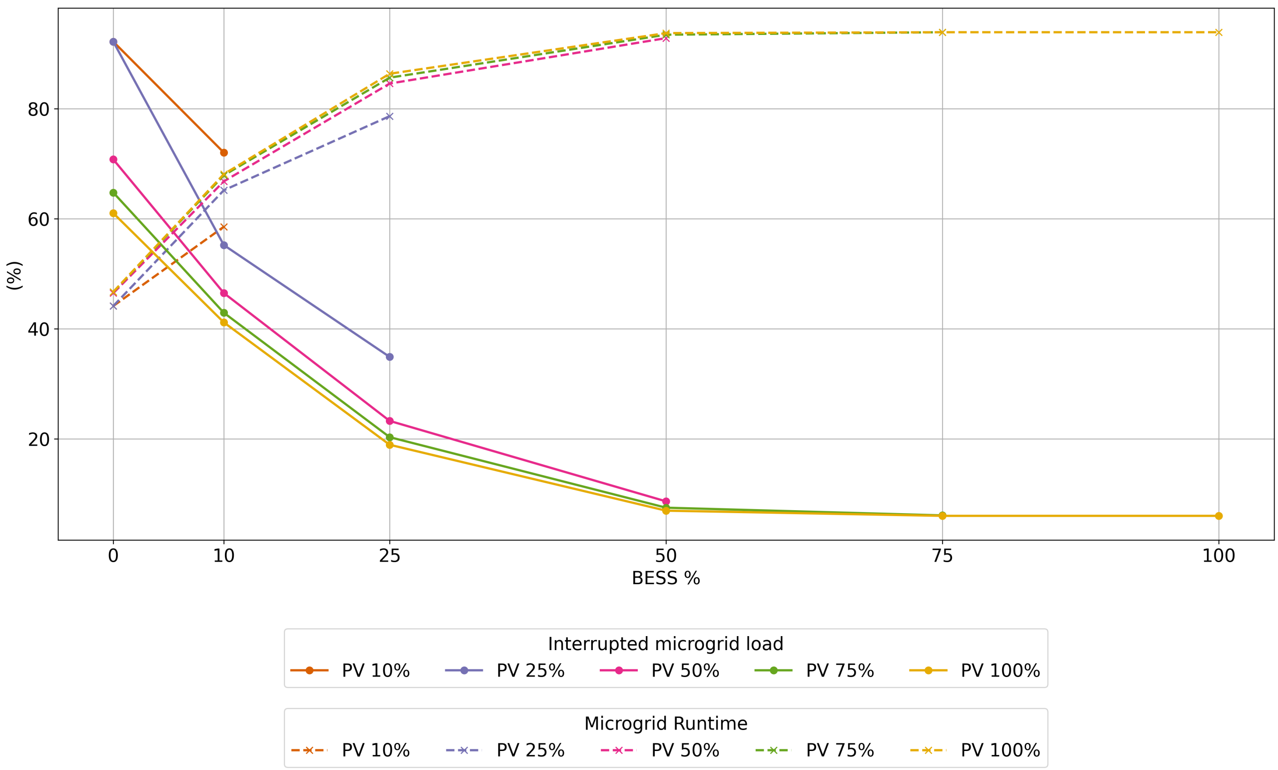

a. The impacts of implementing microgrid 1.

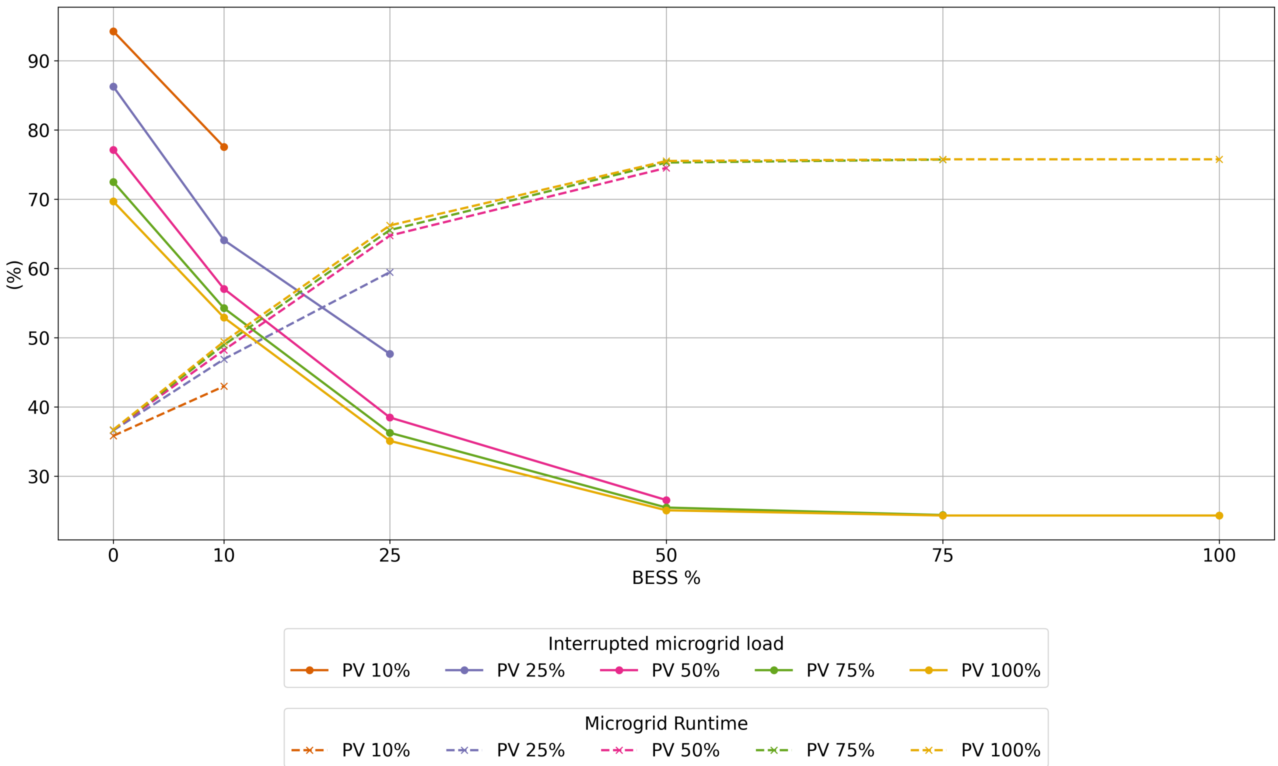

b. The impacts of implementing microgrid 2.

Figure 5.8: Impact of BESS and PV penetration level on the Microgrid operation time and interrupted load. Source: Own authorship.

CHAPTER 6

CONCLUSIONS

This study proposed a methodology for assessing the impacts of microgrids, consisting of PV systems and BESS, on the reliability indices of distribution systems, considering several penetration levels of these technologies. Additionally, new specific indices for microgrids are developed to ensure adequate sensitivity to variations in system reliability.

Chapter 1 delineated the motivations and contributions of this dissertation. The state of the art showed the necessity for research investigating the correlation between varying penetration levels of integration of PV and BESS within microgrids, and their effects on assessing the reliability of distribution networks. In this context, for different operational scenarios, encompassing both normal operation and operation under fault conditions, a method with a stochastic approach was used to consider the variability of DERs and the time-varying islanding operation, thereby enabling the energy supply areas of microgrids in isolated mode to be variable over time.

Chapter 2 outlines the main impacts of DERs on the reliability of distribution networks, detailing the indicators employed in this study.

Chapter 3 presented, in three stages, the method to identify the technical impacts of integrating of microgrids with PV generation and BESS on the reliability of distribution systems. The first stage validated the developed code. The second defined the case studies and the operation strategy of the simulated microgrids. In the last stage, stochastic and grid configuration techniques were used to allow the islanded operation of microgrids, assessing the technical impacts and identifying scenarios that provide the highest benefits for system reliability.

Chapter 4 describes the resources and approaches adopted in the study, detailing the simulated and data used, and structuring the results chapter.

In Chapter 5, the methodology was initially applied to a test system to validate the method and then to a real Brazilian distribution system, simulating the insertion of microgrids. The code validation results revealed a maximum error of -4.10%, demonstrating the code's robustness and reliability. In the context of probabilistic simulations, such as Monte Carlo, this error value is considered low, particularly given the inherent uncertainties associated with the method. Furthermore, the inclusion of new variables in the model without a significant increase in error reinforces the model's effectiveness in reflecting the changes associated with the insertion of microgrids.

The case study results show that all scenarios proposed lead to results surpassing the baseline case. The SAIFI, SAIDI and CAIDI indexes exhibited analogous behavior, with a non-linear behavior for the CAIDI index. In scenarios with only the insertion of PV system, the benefits in reliability, when varying the penetration level, are minimal for the microgrids and the complete feeder due to the variation in solar irradiation throughout the day. On the other hand, the insertion of BESS demonstrates clear benefits in reliability. Varying penetration of BESS influences the battery performance by ensuring a high and stable state of charge (SoC), which is crucial for minimizing instabilities and enhancing the distribution system's reliability in the context of PV integration.

Significant variability is observed in situations with minimal BESS integration, highlighting the essential function of storage systems in mitigating fluctuations during microgrid failures conditions. These scenarios typically exhibit more pronounced peaks, indicating elevated PV generation that cannot be efficiently used without BESS support. Nevertheless, for penetrations exceeding 50%, there is minimal further variation in stability, due to the stabilization of the SoC.

The indices that assess the microgrid performance during time-varying islanding operations indicate an enhancement in the utilization of loads and available DERs during failure scenarios, with negligible additional benefits of BESS at elevated penetration levels. The impacts diminish as the system expands, which can be observed in both the microgrid and the complete feeder.

In general, the proposed method could adjust to modifications in the system and microgrid operation conditions while reducing or eliminating disruptions for customers. The results underscore the necessity of coordinating the growth of DERs with a strategy that enhances system optimization and stability, particularly in light of the significant impact of storage systems.

Ultimately, it underscores the necessity for innovative electricity market design and tailored regulations that suit the unique characteristics of microgrids and the expansion of DERs, since the primary characteristic of microgrids technology is not adequately represented in financial metrics: resiliency. Without a definitive understanding of the benefits for the community and the distribution infrastructure, the chaotic expansion of DERs centered on personal interests may lead to a suboptimal and more unstable system, exacerbating challenges.

6.1 RECOMMENDATIONS FOR FUTURE WORK

- Perform power flow analysis to consider transient stability limits;
- Consider the islanded operation of microgrids in grids with complex protection devices behavior;
- Consider temporary faults;
- Conduct an economic impact analysis of the integration of DERs, evaluating compensation for violations of the limits of continuity indexes;
- Contemplate the incorporation of additional renewable energy sources and new technologies, including electric vehicles (EVs) and demand response (DR);
- Examine the intersection of multiple microgrids concerning system reliability;
- Formulate a strategy to optimize the efficiency of DERs utilization, focusing on determining the optimal dimensions and placement of DERs within microgrids;
- Improve the established methodology for mesh network topologies;
- Enhance the depiction of the stochastic characteristics of DERs;
- Examine DERs deterioration and failure;
- Utilize the Weibull distribution to model the failure rates of system equipment as time-dependent variables;
- Investigate the impacts of various control strategies for DERs.

6.2 PUBLISHED WORKS

This article, presented at a conference, was prepared to convey the research's preliminary findings.

R. P. Gomes, P. C. Cordeiro Vieira, E. G. Domingues and A. L. F. Filho, "**Analysis of the Impact of Integrating Photovoltaic Solar Generation on the Reliability of Distribution Systems**,"2023 Workshop on Communication Networks and Power Systems (WCNPS), Brasilia, Brazil, 2023, pp. 1-7, doi: 10.1109/WCNPS60622.2023.10345158. keywords: Photovoltaic systems;Monte Carlo methods;Power transmission lines;Estimation;Transformers;Frequency estimation;Power system reliability;Distribution system reliability;Sequential Monte Carlo Simulation;PV power integration,

REFERENCES

ABDELSAMAD, A.; LUBKEMAN, D. Sequential monte carlo reliability analysis for economical high-renewable microgrids. In: *2020 IEEE/PES Transmission and Distribution Conference and Exposition (TD)*. [S.l.: s.n.], 2020. p. 1–5. Cited in page 5.

AGAJIE, T. F.; KHAN, B.; GUERRERO, J. M.; MAHELA, O. prakash. Reliability enhancement and voltage profile improvement of distribution network using optimal capacity allocation and placement of distributed energy resources. *Computers Electrical Engineering*, v. 93, p. 107295, 2021. ISSN 0045-7906. Disponível em: <https://www.sciencedirect.com/science/article/pii/S0045790621002755>. Cited in page 7.

AHMAD, S.; SHAFIULLAH, M.; AHMED, C. B.; ALOWAIFEER, M. A review of microgrid energy management and control strategies. *IEEE Access*, v. 11, p. 21729–21757, 2023. Cited 5 times in pages 1, 2, 14, 15, and 28.

ALLAN, R. Power system reliability assessment—a conceptual and historical review. *Reliability Engineering System Safety*, v. 46, n. 1, p. 3–13, 1994. ISSN 0951-8320. Special Issue On Power System Reliability. Disponível em: <https://www.sciencedirect.com/science/article/pii/0951832094900434>. Cited 2 times in pages 16 and 17.

ALLAN, R.; BILLINTON, R.; SJARIEF, I.; GOEL, L.; SO, K. A reliability test system for educational purposes-basic distribution system data and results. *IEEE Transactions on Power Systems*, v. 6, n. 2, p. 813–820, 1991. Cited in page 77.

AMLEH, N.; AL-MUHAINI, M.; DJOKIC, S. Smart restoration for improved reliability of microgrids with renewable energy sources. In: *2018 IEEE PES Innovative Smart Grid Technologies Conference Europe (ISGT-Europe)*. [S.l.: s.n.], 2018. p. 1–6. Cited in page 31.

ANAND, M.; BAGEN, B.; RAJAPAKSE, A. Reliability oriented distribution system analysis considering electric vehicles and hybrid energy resources. *International Journal of Electrical Power Energy Systems*, v. 137, p. 107500, 2022. ISSN 0142-0615. Disponível em: <https://www.sciencedirect.com/science/article/pii/S0142061521007390>. Cited in page 5.

BACHA, B.; GHODBANE, H.; DAHMANI, H.; BETKA, A.; TOUMI, A.; CHOUDER, A. Optimal sizing of a hybrid microgrid system using solar, wind, diesel, and battery energy storage to alleviate energy poverty in a rural area of biskra, algeria. *Journal of Energy Storage*, v. 84, p. 110651, 2024. ISSN 2352-152X. Disponível em: <https://www.sciencedirect.com/science/article/pii/S2352152X24002354>. Cited in page 39.

BAPTISTA, D. F. F. *Direito da energia elétrica: uma proposta de regulação para microrredes*. Tese (Tese (doutorado)) — Universidade Estadual de Campinas (UNICAMP), Faculdade de Engenharia Elétrica e de Computação, Campinas, SP, 2024. 1 recurso online (303 p.). Disponível em: <https://hdl.handle.net/20.500.12733/20342>. Cited in page 2.

BILLINTON, R.; ALLAN, R. Power-system reliability in perspective. *Electronics and Power*, v. 30, n. 3, p. 231–236, 1984. Cited in page 16.

BILLINTON, R.; ALLAN, R. N. *Reliability Evaluation of Power Systems*. 1. ed. Springer New York, NY, 1996. Published: 31 August 1996. ISBN 978-0-306-45259-8. Disponível em: <https://doi.org/10.1007/978-1-4899-1860-4>. Cited 4 times in pages vii, 77, 79, and 80.

BILLINTON, R.; JONNAVITHULA, S. A test system for teaching overall power system reliability assessment. *IEEE Transactions on Power Systems*, v. 11, n. 4, p. 1670–1676, 1996. Cited 2 times in pages 17 and 70.

BILLINTON, R.; WANG, P. A generalized method for distribution system reliability evaluation. In: *IEEE WESCANEX 95. Communications, Power, and Computing. Conference Proceedings*. [S.l.: s.n.], 1995. v. 2, p. 349–354 vol.2. Cited in page 17.

CABALLERO-PEñA, J.; CADENA-ZARATE, C.; PARRADO-DUQUE, A.; OSMA-PINTO, G. Distributed energy resources on distribution networks: A systematic review of modelling, simulation, metrics, and impacts. *International Journal of Electrical Power Energy Systems*, v. 138, p. 107900, 2022. ISSN 0142-0615. Disponível em: <https://www.sciencedirect.com/science/article/pii/S0142061521011133>. Cited in page 17.

CALADO, D. E. D. e. a. *Representação de curto-circuito probabilístico na avaliação da confiabilidade de sistemas de distribuição*. Tese (Doutorado) — Universidade Federal de Santa Catarina (UFSC), 2015. Cited in page 20.

CAMARGO, C. C. B. Confiabilidade aplicada a sistemas de potência elétrica. *LTC Editora Ltda*, 1981. Cited in page 16.

COSTA, A. S. *Modelagem em Tempo Real de Sistemas Elétricos de Potência*. [S.l.]: Universidade Federal de Santa Catarina, 2019. Configurador de Redes. Cited in page 59.

EKLUND, M.; KHALILPOUR, K.; VOINOV, A.; HOSSAIN, M. Understanding the community in community microgrids: A conceptual framework for better decision-making. *Energy Research Social Science*, v. 104, p. 103260, 2023. ISSN 2214-6296. Disponível em: <https://www.sciencedirect.com/science/article/pii/S2214629623003201>. Cited 2 times in pages 15 and 36.

ELIZONDO, G.; POUDINEH, R. *Harnessing the power of distributed energy resources in developing countries: What can be learned from the experiences of global leaders?* Oxford, 2023. Disponível em: <http://hdl.handle.net/10419/280133>. Cited 7 times in pages 1, 10, 11, 12, 18, 25, and 29.

Empresa de Pesquisa Energética (EPE). *Balanço Energético Nacional (BEN) 2024: Ano base 2023*. 2024. Acesso em nov/2024. Disponível em: <https://ben.epe.gov.br>. Cited in page 2.

(EPE), E. de P. E. *Recursos Energéticos Distribuídos*. Rio de Janeiro, 2019. 33 p. Disponível em: <https://www.epe.gov.br/sites-pt/publicacoes-dados-abertos/publicacoes/PublicacoesArquivos/publicacao-227/topico-457/GT%20PNE%20-%20RED%20-%20RelatÃşrio%20Final.pdf>. Cited in page 10.

FAN, Z.; WAN, Z.; GAO, L.; XIONG, Y.; SONG, G. A multi-objective optimal configuration method for microgrids considering zero-carbon operation. *IEEE Access*, v. 11, p. 87366–87379, 2023. Cited in page 28.

FOSE, N.; SINGH, A. R.; KRISHNAMURTHY, S.; RATSHITANGA, M.; MOODLEY, P. Empowering distribution system operators: A review of distributed energy resource forecasting techniques. *Heliyon*, v. 10, n. 15, p. e34800, 2024. ISSN 2405-8440. Disponível em: <https://www.sciencedirect.com/science/article/pii/S2405844024108316>. Cited in page 13.

FUSHENG, L.; RUISHENG, L.; FENGQUAN, Z. Chapter 1 - overview of microgrid. In: FUSHENG, L.; RUISHENG, L.; FENGQUAN, Z. (Ed.). *Microgrid Technology and Engineering Application*. Oxford: Academic Press, 2016. p. 1–10. ISBN 978-0-12-803598-6. Disponível em: <https://www.sciencedirect.com/science/article/pii/B9780128035986000012>. Cited in page 1.

GHOLAMI, M.; MUYEEN, S.; MOUSAVI, S. A. Development of new reliability metrics for microgrids: Integrating renewable energy sources and battery energy storage system. *Energy Reports*, v. 10, p. 2251–2259, 2023. ISSN 2352-4847. Disponível em: <https://www.sciencedirect.com/science/article/pii/S2352484723012763>. Cited 3 times in pages 6, 14, and 30.

GILMAN, P.; DOBOS, A.; DIORIO, N.; FREEMAN, J.; JANZOU, S.; RYBERG, D. Sam photovoltaic model technical reference update. *NREL: Golden, CO, USA*, 2018. Cited in page 13.

GONEN, T. *Electric power distribution engineering*. [S.l.]: CRC press, 2015. Cited 2 times in pages 27 and 41.

IEA. *Unlocking the Potential of Distributed Energy Resources*. Paris, 2022. <https://www.iea.org/reports/unlocking-the-potential-of-distributed-energy-resources>. Licence: CC BY 4.0. Cited 5 times in pages 10, 11, 12, 13, and 18.

International Energy Agency. *Unlocking the Potential of Distributed Energy Resources*. Paris: IEA, 2022. Licence: CC BY 4.0. Disponível em: <https://www.iea.org/reports/unlocking-the-potential-of-distributed-energy-resources>. Cited in page 1.

International Energy Agency. *World Energy Outlook 2024*. Paris: IEA, 2024. Licence: CC BY 4.0 (report); CC BY NC SA 4.0 (Annex A). Disponível em: <https://www.iea.org/reports/world-energy-outlook-2024>. Cited in page 2.

International Energy Agency (IEA). *Renewables 2024*. 2024. <https://www.iea.org/reports/renewables-2024>. IEA, Paris. Licence: CC BY 4.0. Cited in page 1.

ISLAM, K.; KIM, D.; ABU-SIADA, A. A review on adaptive power system protection schemes for future smart and micro grids, challenges and opportunities. *Electric Power Systems Research*, v. 230, p. 110241, 2024. ISSN 0378-7796. Disponível em: <https://www.sciencedirect.com/science/article/pii/S0378779624001299>. Cited in page 2.

LI, W. *et al. Reliability assessment of electric power systems using Monte Carlo methods*. [S.l.]: Springer Science & Business Media, 2013. Cited 7 times in pages 16, 17, 19, 20, 21, 22, and 74.

LOPEZ-PRADO, J. L.; VÉLEZ, J. I.; GARCIA-LLINAS, G. A. Reliability evaluation in distribution networks with microgrids: Review and classification of the literature. *Energies*, MDPI, v. 13, n. 23, p. 6189, 2020. Cited 2 times in pages 29 and 30.

MEERA, P.; HEMAMALINI, S. Reliability assessment and enhancement of distribution networks integrated with renewable distributed generators: A review. *Sustainable Energy Technologies and Assessments*, v. 54, p. 102812, 2022. ISSN 2213-1388. Disponível em: <https://www.sciencedirect.com/science/article/pii/S2213138822008608>. Cited in page 30.

NARANG, D.; GONZALEZ, S.; INGRAM, M.; ROPP, M. *Overview of Functional Technical Requirements for Intentional Islands*. [S.l.], 2022. Cited in page 10.

OLIVEIRA, G. A. *Microrredes em mercados de energia elétrica*. Tese (Doutorado) — Universidade Federal de Santa Catarina, Florianópolis, 2017. Cited in page 27.

PALIWAL, P.; PATIDAR, N. P.; NEMA, R. K. Probabilistic indices for analysing the impact of penetration of distributed energy resources on system reliability. *IET Renewable Power Generation*, v. 14, n. 12, p. 2154–2165, 2020. Disponível em: <https://ietresearch.onlinelibrary.wiley.com/doi/abs/10.1049/iet-rpg.2019.1214>. Cited in page 42.

PARHIZI, S.; LOTFI, H.; KHODAEI, A.; BAHRAMIRAD, S. State of the art in research on microgrids: A review. *IEEE Access*, v. 3, p. 890–925, 2015. Cited in page 28.

PEYGHAMI, S.; PALENSKY, P.; BLAABJERG, F. An overview on the reliability of modern power electronic based power systems. *IEEE Open Journal of Power Electronics*, v. 1, p. 34–50, 2020. Cited in page 16.

REN, Y.; CUI, B.; FENG, Q.; YANG, D.; FAN, D.; SUN, B.; LI, M. A reliability evaluation method for radial multi-microgrid systems considering distribution network transmission capacity. *Computers Industrial Engineering*, v. 139, p. 106145, 2020. ISSN 0360-8352. Disponível em: <https://www.sciencedirect.com/science/article/pii/S036083521930614X>. Cited in page 2.

ROCHA, L. F. *AVALIAÇÃO PROBABILÍSTICA DA CONFIABILIDADE DE SISTEMAS DE DISTRIBUIÇÃO INCLUINDO ASPECTOS DA DINÂMICA DO ILHAMENTO*. Tese (Doutorado) — Universidade Federal do Rio de Janeiro, 2014. Cited in page 18.

SAEED, M. H.; FANGZONG, W.; KALWAR, B. A.; IQBAL, S. A review on microgrids' challenges perspectives. *IEEE Access*, v. 9, p. 166502–166517, 2021. Cited 2 times in pages 12 and 36.

SOUSA, R. S. de; MARTINS, C. C.; SPERANDIO, M. Distribution system reliability assessment using sequential monte carlo simulation. In: *2019 IEEE PES Innovative Smart Grid Technologies Conference - Latin America (ISGT Latin America)*. [S.l.: s.n.], 2019. p. 1–6. Cited in page 21.

STECANELLA, P. A. J. *et al.* Metodologia para a determinação dos impactos técnicos e financeiros provocados pela instalação de geração distribuída fotovoltaica em um sistema de distribuição. Instituição extra IF Goiano, 2020. Cited in page 38.

SU, S.; HU, Y.; HE, L.; YAMASHITA, K.; WANG, S. An assessment procedure of distribution network reliability considering photovoltaic power integration. *IEEE Access*, v. 7, p. 60171–60185, 2019. Cited 2 times in pages 5 and 34.

TORRES, P. F.; PINHO, J. T.; ZILLES, R. Allocation of microgrid-forming resources for distribution systems reliability improvement. *International Journal of Electrical Power Energy Systems*, v. 162, p. 110285, 2024. ISSN 0142-0615. Disponível em: <https://www.sciencedirect.com/science/article/pii/S0142061524005076>. Cited in page 2.

UDDIN, M.; MO, H.; DONG, D.; ELSAWAH, S.; ZHU, J.; GUERRERO, J. M. Microgrids: A review, outstanding issues and future trends. *Energy Strategy Reviews*, v. 49, p. 101127, 2023. ISSN 2211-467X. Disponível em: <https://www.sciencedirect.com/science/article/pii/S2211467X23000779>. Cited 5 times in pages 1, 2, 15, 18, and 36.

WANG, P.; BILLINTON, R. Time sequential distribution system reliability worth analysis considering time varying load and cost models. *IEEE Transactions on Power Delivery*, v. 14, n. 3, p. 1046–1051, 1999. Cited in page 74.

XIAO, L.; MUTTAQI, K. M.; AGALGAONKAR, A. P. Reliability assessment of modern distribution networks embedded with renewable and distributed resources. *Electric Power Systems Research*, v. 212, p. 108374, 2022. ISSN 0378-7796. Disponível em: <https://www.sciencedirect.com/science/article/pii/S0378779622005387>. Cited in page 7.

ZINAMAN, O.; ETO, J.; GARCIA, B.; JOO, J.-Y.; JEFFERS, R.; SCHNEIDER, K. Other, *White Paper: Enabling Regulatory and Business Models for Broad Microgrid Deployment*. 2022. Cited 4 times in pages 1, 2, 14, and 15.

APÊNDICE A

DATA OF THE BRAZILIAN DISTRIBUTION NETWORK

The length of the feeder sections is presented in Table A.1. The load data is depicted in Table A.2. The peak load data for each load point was collected using total demand (kVa) and a power factor of 0,92. For loads whose total demand data were not available, the average demand per customer was calculated and multiplied by the number of customers. The average load per load point was determined by using the ratio obtained from the system validation test system in this study, the RBTS Bus 6. The mean load for residential loads was 56% of the peak load, while for commercial loads, it was 55%.

Table A.1: Section lengths of the Brazilian distribution network.

Line Number	Length (km)	Line Number	Length (km)
1	0.7927	60, 204	0.0469
2, 18, 25	0.0332	63, 67, 72, 129, 169, 171, 193, 203	0.0370
3	0.5742	66	0.0408
4, 47, 49, 52, 55, 79, 104, 170	0.0243	69	0.0839
5	0.0818	70, 125, 191	0.0316
6, 8, 12, 15, 17, 22, 26, 30, 34, 36, 38, 42, 48, 50, 54, 59, 61, 68, 71, 73, 75, 77, 80, 82, 84, 86, 89, 91, 93, 95, 97, 100, 102, 110, 112, 114, 116, 119, 123, 130, 132, 134, 136, 139, 142, 144, 146, 149, 151, 153, 156, 158, 161, 163, 166, 168, 172, 174, 178, 180, 183, 178, 189, 192, 194, 196, 198, 200, 205, 208, 210	0.0020	76, 109, 143	0.0523
7	0.1551	83	0.0539
9	0.1677	85	0.0797
10, 96, 126, 128	0.0099	87, 120	0.0375
11	0.0776	88, 106	0.0445
13	0.0222	90	0.0573
14	0.0886	94, 98	0.1046
16	0.0787	99, 115, 164	0.0684
19	0.0706	101, 165	0.0518
20, 43, 64, 65, 74, 81, 92, 113, 148, 152, 157, 188, 207	0.0297	103	0.0770
21	0.0296	117	0.0728
23	0.0665	118	0.0971
24, 51, 53, 62, 70, 121, 122, 135, 186	0.0226	124	0.0782
27	0.0443	131	0.0400
28	0.0395	140	0.0757
29, 167	0.0893	150, 197	0.0740
31	0.0996	154	0.0391
32, 107, 108	0.0111	155	0.0601
33	0.0697	159	0.1129
35	0.0761	160, 177	0.0613
37, 145, 147, 181, 190	0.0387	162	0.1407
39	0.0832	173	0.0966
40, 56	0.0198	176, 184	0.0341
41, 133, 138	0.0396	179	0.1152
44, 127, 141, 175, 185, 201, 202	0.0148	182	0.0980
45	0.0485	195	0.0679
46	0.1655	199	0.1110
57	0.0535	206	0.0815
58, 111, 137	0.0667	209	0.0453

Table A.2: Load data of the Brazilian distribution network.

Load	Number of Consumers	Peak Power (MW)	Customer Type	Load	Number of Consumers	Peak Power (MW)	Customer Type	Load	Number of Consumers	Peak Power (MW)	Customer Type
1	1	0.0046	Public	32	85	0.0394	Public	63	84	0.0344	Residential
2	1	0.0429	Commercial	33	150	0.0742	Residential	64	136	0.0694	Residential
3	41	0.0358	Commercial	34	96	0.0461	Residential	65	83	0.0462	Residential
4	27	0.0503	Commercial	35	117	0.0579	Residential	66	110	0.0484	Residential
5	1	0.0039	Public	36	22	0.0132	Residential	67	118	0.0574	Residential
6	78	0.0349	Commercial	37	49	0.0290	Residential	68	61	0.0413	Residential
7	118	0.0510	Commercial	38	73	0.0557	Residential	69	84	0.0455	Residential
8	7	0.0057	Commercial	39	44	0.0268	Commercial	70	28	0.0262	Residential
9	1	0.0150	Commercial	40	285	1.0376	Residential	71	49	0.0260	Residential
10	104	0.0327	Commercial	41	119	0.0569	Residential	72	22	0.0176	Commercial
11	1	0.0034	Commercial	42	46	0.0353	Commercial	73	83	0.0385	Commercial
12	131	0.0482	Commercial	43	108	0.0326	Residential	74	109	0.0533	Residential
13	1	0.0586	Commercial	44	60	0.0577	Commercial	75	128	0.4776	Residential
14	65	0.0347	Commercial	45	85	0.0560	Residential	76	125	0.0478	Residential
15	218	0.1442	Residential	46	153	0.0889	Residential	77	106	0.0460	Residential
16	89	0.0634	Residential	47	12	0.0038	Residential	78	26	0.0927	Residential
17	409	1.3964	Residential	48	57	0.0355	Residential	79	53	0.0369	Residential
18	108	0.3709	Residential	49	16	0.0326	Commercial	80	69	0.0373	Commercial
19	1	0.0073	Public	50	94	0.0457	Residential	81	94	0.0584	Residential
20	105	0.0658	Residential	51	33	0.0203	Commercial	82	1	0.0246	Commercial
21	1	0.0457	Commercial	52	72	0.0415	Residential	83	43	0.0390	Commercial
22	53	0.1841	Residential	53	160	0.0983	Residential	84	47	0.0201	Residential
23	48	0.1687	Residential	54	1	0.0334	Residential	85	84	0.0426	Residential
24	27	0.0960	Residential	55	90	0.0443	Commercial	86	133	0.0682	Residential
25	39	0.0265	Commercial	56	95	0.0334	Commercial	87	163	0.0970	Residential
26	1	0.0207	Residential	57	184	0.6777	Residential	88	59	0.0265	Residential
27	68	0.0415	Residential	58	20	0.0251	Commercial	89	72	0.0468	Residential
28	151	0.0900	Residential	59	26	0.0158	Commercial	90	97	0.0301	Residential
29	1	0.0738	Residential	60	99	0.0536	Residential	91	155	0.0654	Residential
30	54	0.1941	Residential	61	60	0.0323	Commercial	92	77	0.0391	Residential
31	35	0.0210	Commercial	62	104	0.0653	Commercial	93	27	0.0131	Residential

APÊNDICE B

SIMULATION PARAMETERS

Table B.1 displays the operational parameters of the FV system with BES used in the simulation of the presented approach, applied to their respective operational strategies.

Table B.1: Simulation Parameters.

PV System	
System Efficiency η [%]	20
Factor that Models Electrical Losses F[%]	92
Temperature Coefficient γ [%/°C]	-0.35
Module Reference Temperature $T_{c,ref}(t)$ [°C]	25
a	-3.56
b	-0.075
ΔT	3
Battery Energy Storage	
Minimum Storage Capacity [%]	20
Initial Energy Stored in the BES	100
Efficiency of Charging η^{c}_{BES} [%]	90
Efficiency of Discharging η^{d}_{BES} [%]	90

APÊNDICE C

EXAMPLE OF APPLICATION OF THE STATE ASSESSMENT PROCEDURE

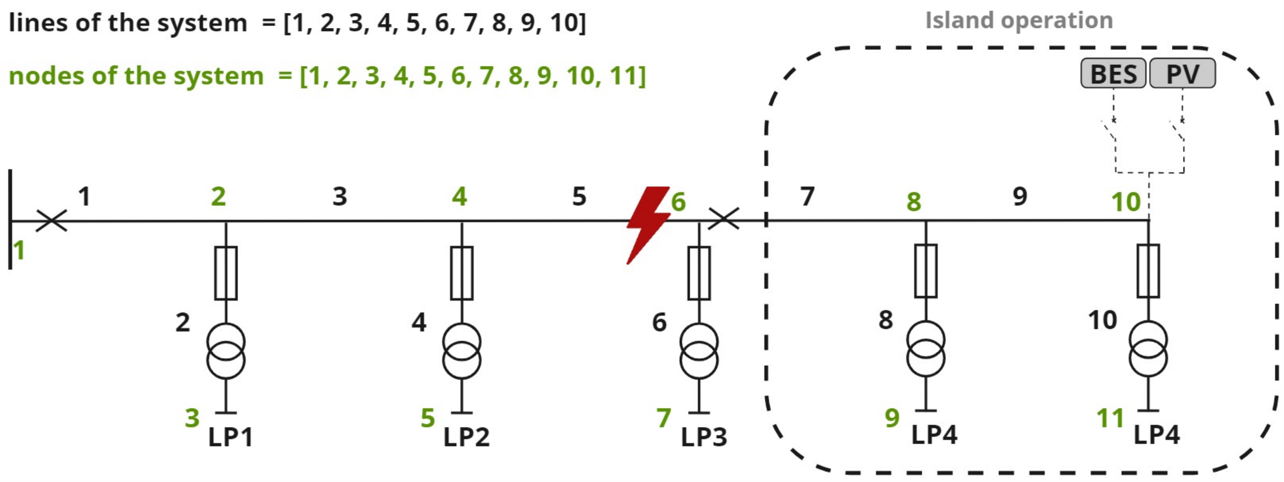

Figure C.1: Illustrative example system utilized to demonstrate the application of the state assessment procedure. Source: Own authorship.

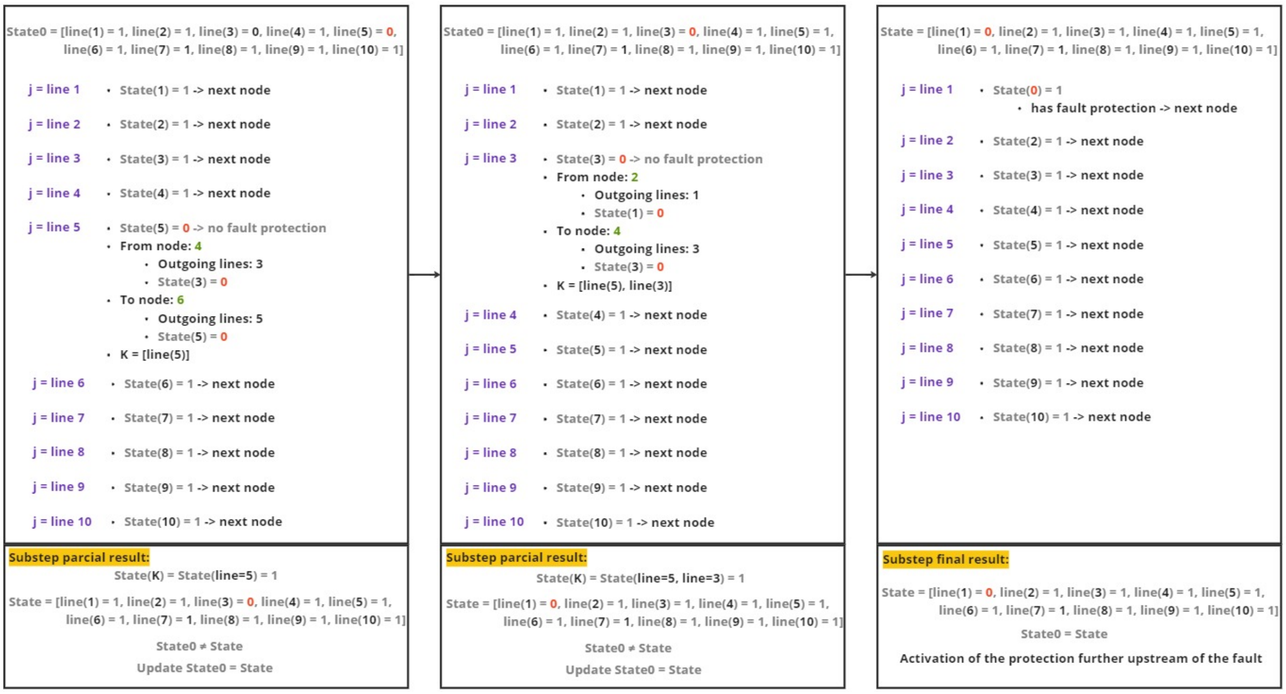

Figure C.2: Application example: Procedure of activation of the protection further upstream of the fault. Source: Own authorship.

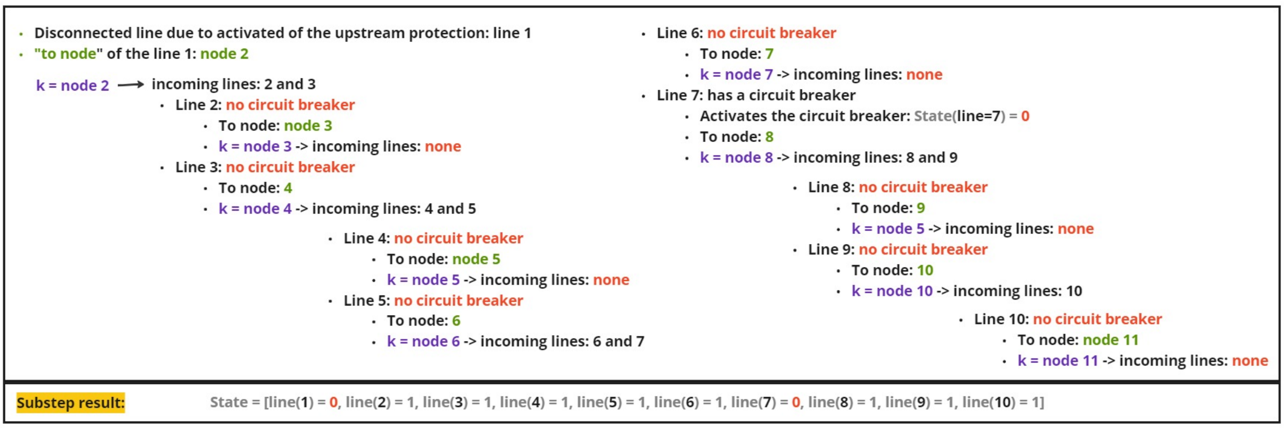

Figure C.3: Application example: Procedure of activation of the protection further downstream of the fault for island operation. Source: Own authorship.

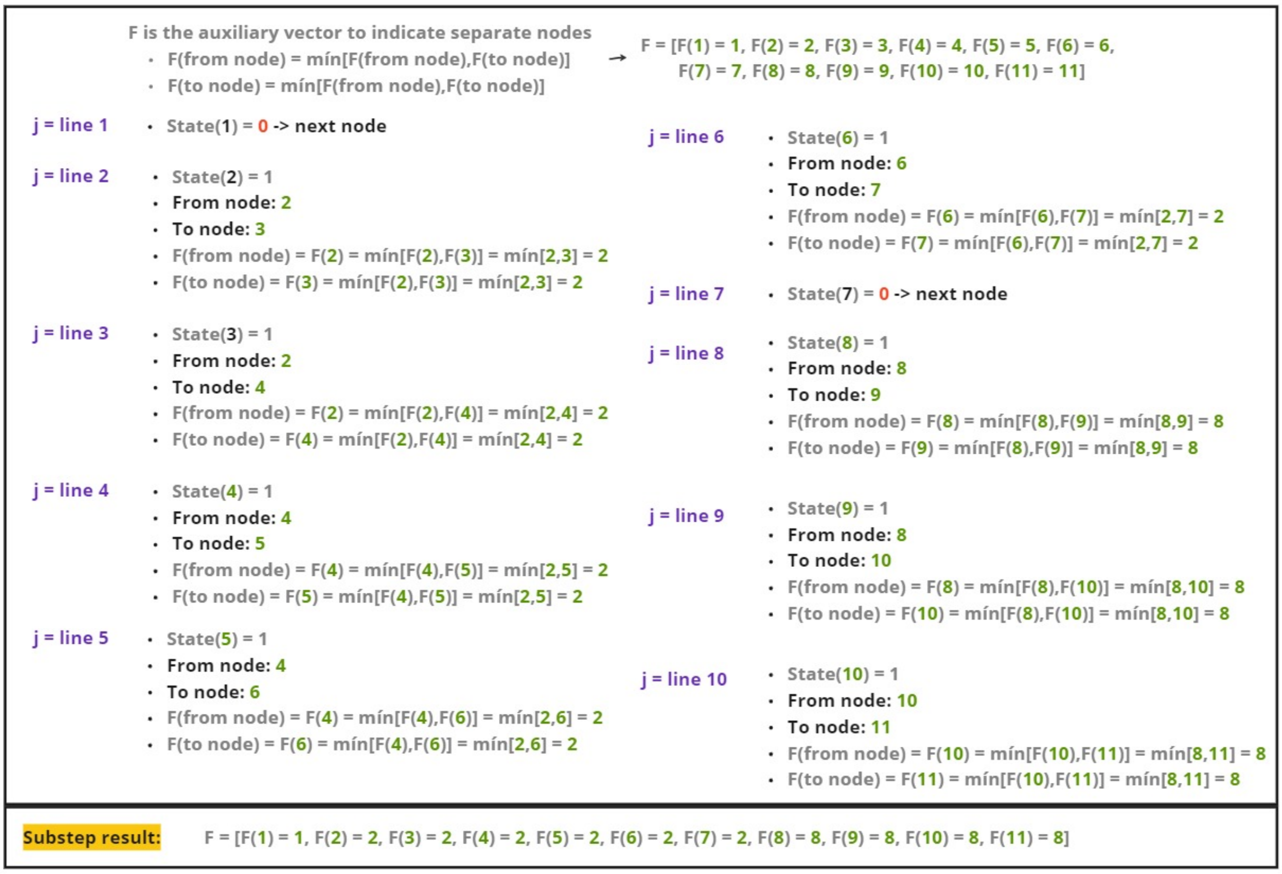

Figure C.4: Application example: Procedure of the topology processor. Source: Own authorship.

APÊNDICE D

SIMULATION RESULTS TABLES

D.1 SAIFI

Table D.1: Impact of BESS and PV penetration on SAIFI (oc./year) indice for the Microgrid 1 from the implementation of Microgrid 1. Source: Own authorship.

Case Studies		**BESS-pen**					
		0%	**10%**	**25%**	**50%**	**75%**	**100%**
PV-pen	**0%**	0.1778	-	-	-	-	-
	10%	0.1813	0.1568	-	-	-	-
	25%	0.1813	0.1372	0.0923	-	-	-
	50%	0.1699	0.1287	0.0737	0.0318	-	-
	75%	0.1634	0.1238	0.0676	0.0298	0.0249	-
	100%	0.1576	0.1221	0.0655	0.0288	0.0240	0.0240

Table D.2: Impact of BESS and PV penetration on SAIFI (oc./year) indice for the complete feeder from the implementation of Microgrid 1. Source: Own authorship.

Case Studies		**BESS-pen**					
		0%	**10%**	**25%**	**50%**	**75%**	**100%**
PV-pen	**0%**	0.3056	-	-	-	-	-
	10%	0.2836	0.2823	-	-	-	-
	25%	0.2836	0.2813	0.2790	-	-	-
	50%	0.2828	0.2807	0.2779	0.2755	-	-
	75%	0.2824	0.2804	0.2776	0.2754	0.2752	-
	100%	0.2821	0.2803	0.2775	0.2754	0.2751	0.2751

Table D.3: Impact of BESS and PV penetration on SAIFI (oc./year) indice for the Microgrid 2 from the implementation of Microgrid 2. Source: Own authorship.

Case Studies		**BESS-pen**					
		0%	**10%**	**25%**	**50%**	**75%**	**100%**
PV-pen	**0%**	0.4054	-	-	-	-	-
	10%	0.2491	0.2322	-	-	-	-
	25%	0.2510	0.2164	0.1738	-	-	-
	50%	0.2488	0.2078	0.1595	0.1208	-	-
	75%	0.2462	0.2032	0.1547	0.1190	0.1144	-
	100%	0.2418	0.2006	0.1539	0.1180	0.1139	0.1139

Table D.4: Impact of BESS and PV penetration on SAIFI (oc./year) indice for the complete feeder from the implementation of Microgrid 2. Source: Own authorship.

Case Studies		**BESS-pen**					
		0%	**10%**	**25%**	**50%**	**75%**	**100%**
PV-pen	**0%**	0.3056	-	-	-	-	-
	10%	0.2337	0.2293	-	-	-	-
	25%	0.2343	0.2247	0.2130	-	-	-
	50%	0.2334	0.2223	0.2092	0.1976	-	-
	75%	0.2329	0.2211	0.2071	0.1977	0.1966	-
	100%	0.2314	0.2204	0.2077	0.1978	0.1964	0.1964

D.2 SAIDI

Table D.5: Impact of BESS and PV penetration on SAIDI (h/year) indice for the Microgrid 1 from the implementation of Microgrid 1. Source: Own authorship.

Case Studies		**BESS-pen**					
		0%	**10%**	**25%**	**50%**	**75%**	**100%**
PV-pen	**0%**	0.9097	-	-	-	-	-
	10%	0.8526	0.7307	-	-	-	-
	25%	0.8526	0.5947	0.4060	-	-	-
	50%	0.6778	0.5265	0.2971	0.1467	-	-
	75%	0.6325	0.4989	0.2696	0.1344	0.1189	-
	100%	0.6094	0.4860	0.2572	0.1274	0.1174	0.1174

Table D.6: Impact of BESS and PV penetration on SAIDI (h/year) indice for the complete feeder from the implementation of Microgrid 1. Source: Own authorship.

Case Studies		**BESS-pen**					
		0%	**10%**	**25%**	**50%**	**75%**	**100%**
PV-pen	**0%**	1.5004	-	-	-	-	-
	10%	1.3913	1.3851	-	-	-	-
	25%	1.3913	1.3781	1.3685	-	-	-
	50%	1.3844	1.3767	1.3651	1.3563	-	-
	75%	1.3821	1.3753	1.3637	1.3561	1.3553	-
	100%	1.3810	1.3747	1.3630	1.3557	1.3552	1.3552

Table D.7: Impact of BESS and PV penetration on SAIDI (h/year) indice for the Microgrid 2 from the implementation of Microgrid 2. Source: Own authorship.

Case Studies		**BESS-pen**					
		0%	**10%**	**25%**	**50%**	**75%**	**100%**
PV-pen	**0%**	1.9635	-	-	-	-	-
	10%	1.1639	1.0912	-	-	-	-
	25%	1.1454	0.9816	0.7879	-	-	-
	50%	1.0628	0.9037	0.6862	0.5376	-	-
	75%	1.0151	0.8734	0.6620	0.5262	0.5140	-
	100%	0.9822	0.8580	0.6500	0.5219	0.5130	0.5130

Table D.8: Impact of BESS and PV penetration on SAIDI (h/year) indice for the complete feeder from the implementation of Microgrid 2. Source: Own authorship.

Case Studies		**BESS-pen**					
		0%	**10%**	**25%**	**50%**	**75%**	**100%**
PV-pen	**0%**	1.5004	-	-	-	-	-
	10%	1.1318	1.1141	-	-	-	-
	25%	1.1261	1.0832	1.0251	-	-	-
	50%	1.1017	1.0617	0.9982	0.9521	-	-
	75%	1.0882	1.0552	0.9869	0.9551	0.9531	-
	100%	1.0791	1.0509	0.9893	0.9556	0.9528	0.9528

D.3 CAIDI

Table D.9: Impact of BESS and PV penetration on CAIDI (h/oc.) indice for the Microgrid 1 from the implementation of Microgrid 1. Source: Own authorship.

Case Studies		**BESS-pen**					
		0%	**10%**	**25%**	**50%**	**75%**	**100%**
PV-pen	**0%**	5.1173	-	-	-	-	-
	10%	4.7029	4.6592	-	-	-	-
	25%	4.7029	4.3344	4.3982	-	-	-
	50%	3.9903	4.0910	4.0292	4.6072	-	-
	75%	3.8704	4.0302	3.9901	4.5091	4.7665	-
	100%	3.8656	3.9793	3.9268	4.4284	4.8877	4.8877

Table D.10: Impact of BESS and PV penetration on CAIDI (h/oc.) indice for the complete feeder from the implementation of Microgrid 1. Source: Own authorship.

Case Studies		**BESS-pen**					
		0%	**10%**	**25%**	**50%**	**75%**	**100%**
PV-pen	**0%**	4.9092	-	-	-	-	-
	10%	4.9064	4.9061	-	-	-	-
	25%	4.9064	4.8989	4.9046	-	-	-
	50%	4.8960	4.9052	4.9125	4.9237	-	-
	75%	4.8936	4.9045	4.9130	4.9235	4.9251	-
	100%	4.8945	4.9037	4.9126	4.9232	4.9257	4.9257

Table D.11: Impact of BESS and PV penetration on CAIDI (h/oc.) indice for the Microgrid 2 from the implementation of Microgrid 2. Source: Own authorship.

Case Studies		**BESS-pen**					
		0%	**10%**	**25%**	**50%**	**75%**	**100%**
PV-pen	**0%**	4.8430	-	-	-	-	-
	10%	4.6725	4.6994	-	-	-	-
	25%	4.5627	4.5361	4.5324	-	-	-
	50%	4.2718	4.3492	4.3032	4.4510	-	-
	75%	4.1230	4.2985	4.2803	4.4203	4.4944	-
	100%	4.0620	4.2775	4.2231	4.4246	4.5048	4.5048

Table D.12: Impact of BESS and PV penetration on CAIDI (h/oc.) indice for the complete feeder from the implementation of Microgrid 2. Source: Own authorship.

Case Studies		**BESS-pen**					
		0%	**10%**	**25%**	**50%**	**75%**	**100%**
PV-pen	**0%**	4.9092	-	-	-	-	-
	10%	4.8420	4.8594	-	-	-	-
	25%	4.8057	4.8211	4.8136	-	-	-
	50%	4.7204	4.7753	4.7727	4.8186	-	-
	75%	4.6731	4.7724	4.7660	4.8299	4.8485	-
	100%	4.6629	4.7686	4.7640	4.8305	4.8504	4.8504

D.4 ENS

Table D.13: Impact of BESS and PV penetration on ENS (MWh/year) indice for the Microgrid 1 from the implementation of Microgrid 1. Source: Own authorship.

Case Studies		**BESS-pen**					
		0%	**10%**	**25%**	**50%**	**75%**	**100%**
PV-pen	**0%**	0.1237	-	-	-	-	-
	10%	0.1164	0.1008	-	-	-	-
	25%	0.1164	0.0831	0.0569	-	-	-
	50%	0.0955	0.0736	0.0418	0.0205	-	-
	75%	0.0892	0.0693	0.0379	0.0186	0.0163	-
	100%	0.0854	0.0673	0.0361	0.0178	0.0161	0.0161

Table D.14: Impact of BESS and PV penetration on ENS (MWh/year) indice for the complete feeder from the implementation of Microgrid 1. Source: Own authorship.

Case Studies		**BESS-pen**					
		0%	**10%**	**25%**	**50%**	**75%**	**100%**
PV-pen	**0%**	7.1160	-	-	-	-	-
	10%	6.5347	6.5192	-	-	-	-
	25%	6.5347	6.5015	6.4752	-	-	-
	50%	6.5230	6.5011	6.4693	6.4419	-	-
	75%	6.5167	6.4968	6.4654	6.4405	6.4382	-
	100%	6.5129	6.4948	6.4636	6.4396	6.4379	6.4379

Table D.15: Impact of BESS and PV penetration on ENS (MWh/year) indice for the Microgrid 2 from the implementation of Microgrid 2. Source: Own authorship.

Case Studies		**BESS-pen**					
		0%	**10%**	**25%**	**50%**	**75%**	**100%**
PV-pen	**0%**	1.9656	-	-	-	-	-
	10%	1.3563	1.2565	-	-	-	-
	25%	1.3252	1.1080	0.8639	-	-	-
	50%	1.2161	1.0097	0.7325	0.5441	-	-
	75%	1.1542	0.9724	0.7028	0.5304	0.5148	-
	100%	1.1131	0.9532	0.6873	0.5247	0.5135	0.5135

Table D.16: Impact of BESS and PV penetration on ENS (MWh/year) indice for the complete feeder from the implementation of Microgrid 2. Source: Own authorship.

Case Studies		**BESS-pen**					
		0%	**10%**	**25%**	**50%**	**75%**	**100%**
PV-pen	**0%**	7.1160	-	-	-	-	-
	10%	5.9198	5.8358	-	-	-	-
	25%	5.8867	5.6879	5.4241	-	-	-
	50%	5.7682	5.5913	5.3024	5.0863	-	-
	75%	5.7057	5.5645	5.2450	5.1085	5.0997	-
	100%	5.6652	5.5454	5.2635	5.1114	5.0984	5.0984

APÊNDICE E

SIMULATION TIMES

The values of the simulation times for each combination of PV (PV-pen) and BESS (BESS-pen) penetration across each microgrid are expressed in minutes, representing the time required for each simulation performed in the study.

The simulation times for two microgrids were analyzed and totaled. For the first microgrid, the simulations accumulated a total of 19 hours, while for the second microgrid, they amounted to 18 hours. This results in a combined simulation time of 37 hours across all scenarios, reflecting the computational effort required to evaluate the performance of both systems under varying configurations of PV and BESS penetration.

Table E.1: Simulation time (in minutes) for each case study of Microgrid 1. Source: Own authorship.

Case Studies		**BESS-pen**					
		0%	**10%**	**25%**	**50%**	**75%**	**100%**
PV-pen	**0%**	53.22	Impractical case	Impractical case	Impractical case	Impractical case	Impractical case
	10%	48.29	48.19	Impractical case	Impractical case	Impractical case	Impractical case
	25%	47.28	47.09	61.49	Impractical case	Impractical case	Impractical case
	50%	45.6	39.4	52.63	52.9	Impractical case	Impractical case
	75%	47.51	46.44	74.96	52.46	71.3	Impractical case
	100%	37.72	38.38	145.36	50.01	52.55	48.29

Table E.2: Simulation time (in minutes) for each case study of Microgrid 2. Source: Own authorship.

Case Studies		**BESS-pen**					
		0%	**10%**	**25%**	**50%**	**75%**	**100%**
PV-pen	**0%**	53.22	Impractical case	Impractical case	Impractical case	Impractical case	Impractical case
	10%	50.05	54.51	Impractical case	Impractical case	Impractical case	Impractical case
	25%	52.62	62.16	54.66	Impractical case	Impractical case	Impractical case
	50%	54.07	49.09	53.36	53.43	Impractical case	Impractical case
	75%	53.21	56.09	52.94	55.71	52.61	Impractical case
	100%	52.81	55.00	51.41	53.00	52.30	40.80